ÅBO AKADEMI

INSTITUTIONEN FÖR KEMITEKNIK

DEPARTMENT OF CHEMICAL ENGINEERING

Processkemiska centret

Process Chemistry Centre

REPORT 12-01

Enzyme Electrode Configurations: for Application in Biofuel Cells

Xiaoju Wang

Academic Dissertation

Laboratory of Inorganic Chemistry

Enzyme Electrode Configurations: for Application in Biofuel Cells

Xiaoju Wang

Academic Dissertation

Laboratory of Inorganic Chemistry
Process Chemistry Centre
Department of Chemical Engineering
Åbo Akademi University

Åbo 2012

Supervisors

Dr. Mikael Bergelin
Laboratory of Inorganic Chemistry
Process Chemistry Centre,
Åbo Akademi University
Åbo, Finland

Docent Johan Bobacka
Laboratory of Analytical Chemistry
Process Chemistry Centre,
Åbo Akademi University
Åbo, Finland

Professor Mikko Hupa
Laboratory of Inorganic Chemistry
Process Chemistry Centre,
Åbo Akademi University
Åbo, Finland

Reviewer

Professor Anthony P. F. Turner
Biosensors & Bioelectronics Centre
IFM-Linköping University
Linköping, Sweden

Reviewer and Opponent

Professor Shelley D. Minteer
Department of Chemistry
The University of Utah
Salt Lake City, Utah, USA

ISSN 159-8205
ISBN 978-952-12-2703-5 (hard copy)
ISBN 978-952-12-2704-2 (pdf)
Painosalama Oy
Åbo, Finland, 2012

‘路漫漫其修远兮，
吾将上下而求索。’

Although the road is endless and faraway,
I still want to pursue the truth in the world.

- 屈原: «离骚»

PREFACE

The research presented in this thesis was carried out at the Laboratory of Inorganic Chemistry at Åbo Akademi University as a part of the activities of the Process Chemistry Center during the year of 2007-2011. Funding for the doctoral activity was provided by Graduate School of Chemical Engineering (GSCE), Finnish Funding Agency for Technology and Innovation (Tekes, PEPSIC and PEPScond projects), European Union Sixth Framework Programme (BIO-MEDNANO, STRP 017350), as well as the Rector of Åbo Akademi University. Furthermore, I would like to acknowledge Stiftelsens för Åbo Akademi forskningsinstitut and GSCE for financially supporting my conference trips and research visits.

To attain a doctoral degree has been a goal that I have been striving for since the year of 2005 when I finished my master study in China. However, this thesis never came into true without the support, encouragement, and contributions from my supervisors. I would like to express my deepest gratitude to Dr. Mikael Bergelin, for your inspiring talk about BFCs on the first time when we met and supporting me to do research in this interesting and cutting-edge field. Micki, your support and encouragement with open-minded scientific attitude through these years have made it possible for Xiaoju to grow as a scientist and to complete this work successfully. I highly value the discussions with you concerning on the fundamentals of electrochemistry and the complex nature of material science. Thanks for reading through and giving comments on my papers and thesis and for being patient on waiting for me to grow in science! I would like to thank Docent Johan Bobacka for his support on brain-storming the research ideas and reading through all my works. Johan, thank you for letting me in and talk every time when I just popped up in front of the door! I would also like to express my gratitude to Professor Mikko Hupa for giving me the opportunity to perform my doctoral studies at the Laboratory of Inorganic Chemistry.

During these years, I am happy to have the privilege to get to know a number of people who share my interest in electrobiocatalysis of enzymes. Dr. Maria Smolander and Dr. Harry Boer at VTT Technical Research center of Finland (Espoo) are acknowledged for their help to arrange the possibility in VTT to work on the carbodiimide chemistry of protein. Professor Franco Mazzei is acknowledged for accepting me for the research visit in Sapienza University of Rome. Dr. Marco Frasconi, thanks for all the inspiring and insightful discussions on the electron transfer processes. Marco, of course, that is not all I want to say 'thanks' to you (E'un piacere averti conosciuto). I highly appreciate and value the half a year time that I spent in Lund with Professor Lo Gorton's group. Lo, thanks for being kind to me, listening to what I was looking for at that time, and all the help and scientific guide on the work we made together. My coauthors, Dr. Sergey Shleev, Roberto Ortiz, Magnus Falk, and Muammad Nadeem Zafar, are acknowledged for their cooperation and contributions on our joint papers.

Working at the Laboratory of Inorganic Chemistry has been a true pleasure thanks to the great atmosphere and colleagues here. I would like to especially thank to our present and former colleagues in our electrochemistry group and within the projects: Docent Tomasz Sokalski, Dr. Rose-Marie Latonen, Dr. Pia Sjöberg-Eerola, Jan-Erik Eriksson, Max Johansson, and Nianxing Wang. Thanks for all of your contributions at any aspect into my thesis. Furthermore, my great girls at OOK, Dori, my sweetie, one of the greatest things during my years in Finland that I have had the company of yours in our room through this study, all the tears and laughter, I have you to shear with! Pati, thanks for the unforgettable exploration together to Salsa and all those heart-to-heart conversations on any possible topics! Suski, thanks for being a great friend and all the happy partying time together!

在写下这扉页的时刻，我在图尔库城共同学习和生活的中国朋友们，苏萍，涛涛和德德，娜娜，张迪和端木，婷婷，炳之，……，谢谢那些与你们一起度过的快乐时光！你们是图尔库漫长的冬日里有着的温暖和光亮:-)!

在最后，但最重要的是，我要感谢爸爸妈妈对女儿无条件的爱与支持，很开心成为你们的骄傲; 林林，谢谢你，陪伴我在这里与我一起走过！谢谢你的包容与支持和那些带给我生命中的喜悦与幸福……！

Xiaoju

In Åbo, on a sunny and lovely day in October,

ABSTRACT

The conducting polymer, poly(3,4-ethylenedioxythiophene) (PEDOT) film is a suitable matrix material for the enzymes, due to its outstanding properties, specifically, high electrical conductivity and excellent inherent environmental stability. The counter ions for PEDOT have a significant effect on the structural features and morphology of the polymer film produced by electropolymerization. Different carbon-based materials, ranging from paper-like carbon ink paper or carbon paper to reticulated vitreous carbon foam (RVC foam), were explored as substrate materials for PEDOT film generation by electropolymerization. The immobilization of *Trametes hirsuta* laccase (*Th*L) in the PEDOT film was facilitated via *in situ* entrapment during electropolymerization. When 2,2'-azinobis(3-ethylbenzothiazoline-6-sulfonate) ($ABTS^{2-}$) was used as the mediator, the immobilized *Th*L exhibited catalytic activity for the reduction of O_2 to water. The amount of *Th*L in the PEDOT matrix is tunable by controlling the manufacturing parameters, including the charge density used for the electropolymerization of the EDOT monomer and the *Th*L concentration in the electropolymerization electrolyte. The use of a porous material, e.g., RVC foam, as the PEDOT supporting template was tested to improve the current density per unit area/volume generated by biocathodes. These RVC foam-based biocathodes produced a large current density, reaching 1 mA/cm^3 at 0.45 V when 19.5 μg/ml of *Th*L was used in the electropolymerization electrolyte.

In addition, direct electron transfer (DET) type biocatalysis was accomplished for *Th*L by immobilizing *Th*L into a fine-tuned dual-layer-architecture of PEDOT films. In a PEDOT-NO_3/*Th*L/PEDOT-PSS enzyme electrode, the reduction of O_2 to water was catalyzed by *Th*L with the T1 Cu site as the primary electron acceptor. The fabrication parameters included different combinations of PEDOT films, *Th*L loadings, and thicknesses of both PEDOT layers; their effects on the electrode performance were then investigated. It is proposed that the π-π interaction between the PSS^- and the hydrophobic substrate-binding pocket in the vicinity of the T1 Cu site results in a favorable location of the conducting polymer chain of PEDOT-PSS close to the T1 Cu site and thus facilitates the DET of *Th*L within this particular architecture.

The flavin adenine dinucleotide (FAD)-dependent glucose dehydrogenase from *Glomerella cingulata (Gc*GDH) and cellobiose dehydrogense from *Corynascus thermophuilus* (*Ct*CDH) have been studied to construct different enzyme electrode configurations as bioanodes towards biofuel cell applications. For *Gc*GDH, six Os-containing polymers, whose redox potentials range across a broad potential window between +15 and +489 mV *vs*. NHE, were used to 'wire' the *Gc*GDH on the graphite electrodes to catalyze the oxidation of glucose. The ratio of *Gc*GDH:Os-polymer in the overall loading onto the electrode surface significantly affected the catalytic performance of the enzyme electrode on the glucose oxidation. Both the Os-polymer and the *Gc*GDH:Os-polymer ratio were optimized for obtaining the maximum current density; a high current density of 493 $\mu A/cm^2$ for 30 mM glucose was produced by a *Gc*GDH/Os *c* modified electrode. DET type biocatalysis of *Ct*CDH on lactose (and glucose) oxidation was accomplished on Au nanoparticle (AuNP) structured electrode. The haem site in the *Ct*CDH enzyme functions as a 'built-in' mediator for communicating the electron transfer between the FAD site and the AuNP surface. The redox potential of the haem site in *Ct*CDH was determined to be $E_{1/2}' = -122$ *mV vs.* Ag/AgCl/KCl(s) (75 mV *vs*. NHE). The *Ct*CDH/AuNP/Au bioanode can generate a maximum current response for lactose with I_{max} = 43.3±1.5 ($\mu A/cm^2$) or for glucose with I_{max} = 31.2±2.3 ($\mu A/cm^2$). The DET type biocatalysis of *Ct*CDH works most efficiently in a more neutral pH range (pH = 7.0 to 8.5).

An enzyme electrode *Ct*CDH/AuNP/Au used as a bioanode was coupled with a *Myrothecium verrucaria* bilirubin oxidase (*Mv*BOD) enzyme electrode *Mv*BOD/AuNP/Au as a biocathode to fabricate a one-compartment, implantable BFC. The best performance characteristics of this mediator- and membrane-less BFC were obtained in a pH = 7.4 phosphate buffer containing 5 mM lactose, showing an open circuit voltage (OCV) of 0.68 V and a maximum power density of 15 $\mu W/cm^2$ at an operating cell voltage of 0.52 V. The corresponding values measured in human blood were 0.65 V and 3 $\mu W/cm^2$ at an operating cell voltage of 0.45 V.

SVENSK SAMMANFATTNING

Den ledande polymeren poly(3,4-etyldioxytiofen) (PEDOT) är ett passande matrismaterial för enzymer p.g.a. sina speciella egenskaper, i synnerhet dess höga elektriska ledningsförmåga och utmärkta kemiska stabilitet. De för PEDOT använda motjonerna har en signifikant inverkan på strukturen och morfologin hos den elektropolymeriserade polymerfilmen. Olika kolbaserade material, sträckande från ett med elektriskt ledande kolbläck impregnerat pappersmaterial eller kolfiberpapper till poröst/retikulerat vitröst kolskum (RVC-skum), prövades som substratmaterial för PEDOT-filmens bildning via elektropolymerisation. Immobiliseringen av *Trametes hirsuta*-lackas (*Th*L) i PEDOT-filmen uppnåddes genom *in-situ*-inneslutning under elektropolymeriseringsprocessens gång. När 2,2'-azinobis(3-etylbenzotiazolin-6-sulfonat) ($ABTS^{2-}$) användes som mediator, visade den immobiliserade *Trametes hirsuta*-lackasen katalytisk aktivitet med avseende på reduktionen av O_2 till vatten. *Th*L-halten i den färdiga polymerfilmen kan regleras genom att variera polymerisationsparametrarna, speciellt den använda laddningstätheten under elektropolymerisationen av EDOT-monomeren samt koncentrationen av *Th*L i polymeriseringselektrolyten. Användningen av porösa material, som t.ex. RVC-skum, som substrat för PEDOT undersöktes med avsikt att förbättra den, för elektroden per enhetsareal/-volym, genererade strömtätheten. Dessa RVC-skum baserade biokatoder uppvisade en hög katodisk öppenkretspotential och genererade en hög strömtäthet, vilken uppnådde 1 mA/cm^3 vid 0.45V när halten av *Th*L-enzym i polymeringselektrolyten var 19.5 µg/ml.

Vidare, biokatalys som utnyttjar direkt elektronöverföring (DET) uppnåddes för *Th*L genom immobilisering av enzymet i noga avstämda tvålagerkonfigurationer av PEDOT-filmer. I en PEDOT-NO_3/*Th*L/PEDOT-PSS-enzymelektrod katalyserades reduktionen av O_2 till vatten med enzymets T1 Cu-atomposition som primär elektronacceptor. De olika framställningsparametrarna omfattade olika kombinationer av PEDOT-filmer, olika *Th*L-halter samt olika PEDOT-filmtjocklekar, och deras inverkan på elektrodprestandan undersöktes. Det har föreslagits att π-π-interaktionen mellan PSS^--motjonen och den hydrofoba bindningsfickan hos substratet i närheten av T1 Cu-atompositionen resulterar i en fördelaktig position hos den ledande PEDOT-PSS-polymerkedjan, och därmed befrämjar DET hos *Th*L i denna specifika polymerstruktur.

Flavin-adenin-dinukleotidberoende (FAD) glukosdehydrogenas från *Glomerella cingulata* (*Gc*GDH) och cellobiosdehydrogenas från *Corynascus thermophuilus* (*Ct*CDH) studerades med avsikt att konstruera olika enzymelektrodkonfigurationer för bioanoder i biobränslecellapplikationer. För *Gc*GDH, 6 Os-innehållande polymerer, vilkas redoxpotentialer sträcker sig över ett brett potentialområde mellan +15 och +489 mV med avseende på NHE, användes för att uppnå en elektronisk koppling mellan enzymet på grafitelektroder för oxideringen av glukos. Den enzymatiska aktiviteten för glukosoxidation påverkades starkt av förhållandet *Gc*GDH/Os-polymer i den sammansatta elektrodkompositionen. Både Os-polymeren och *Gc*GDH/Os-polymerförhållandet optimerades med avseende på den maximala strömtätheten, vilken uppnåddes som 493 $\mu A/cm^2$ för en 30 mM lösning av glukos. DET-typs biokatalys för *Ct*CDH uppnåddes även för oxidationen av laktos (samt glukos) på elektroder med ytstrukturer av guld-nanopartiklar (AuNP). *Haem*-gruppen i *Ct*CDH-enzymet fungerar som en "inbyggd" mediator för elektronöverföringen mellan FAD-gruppen och elektrodens AuNP-yta. *Haem*-gruppens redoxpotential i *Ct*CDH uppmättes till $E_{1/2}' = -122$ *mV vs.* Ag/AgCl/KCl(s) (75 mV *vs*. NHE). *Ct*CDH/AuNP/Au-bioanoden kan generera en maximal strömrespons för laktos som I_{max} = 43.3±1.5 ($\mu A/cm^2$) samt för glukos som I_{max} = 31.2±2.3 ($\mu A/cm^2$). Biokatalysen för DET-typs *Ct*CDH fungerar effektivast vid neutrala pH-värden (pH = 7.0 – 8.5).

En *Ct*CDH/AuNP/Au-enzymanod kopplades ihop med en *Myrothecium verrucaria* bilirubinoxidas (*Mv*BOD) enzymelektrod av typen *Mv*BOD/AuNP/Au som biokatod för att framställa en inplanterbar biobränslecell där samtliga komponenter delar samma cellvolym. För denna mediator-, separator- och membranlösa biobränslecell uppmättes i en pH=7.4 fosfatbufferlösning innehållande 5 mM laktos en öppenkretspotential (OCV) på 0.68V samt en maximal effekttäthet på 15 $\mu W/cm^2$ vid en operativ spänning på 0.52V. Motsvarande värden för människoblod var OCV=0.65V samt 3 $\mu W/cm^2$ vid 0.45V.

List of Publications

This thesis is based on the following papers, which will be referred to in the text by their Roman numerals. The papers are appended at the end of the thesis.

I. Wang, X., Sjöberg-Eerola, P., Eriksson, J.-E., Bobacka, J., & Bergelin M., The effect of counter ions and substrate material on the growth and morphology of poly(3,4-ethylenedioxythiophene) films: Towards the application of enzyme electrode construction in biofuel cell. ***Synth. Met.*** (**2010**) 160, 1373-1381.

II. Wang, X., Sjöberg-Eerola, P., Immonen, K., Bobacka, J., & Bergelin, M., Immobilization of *Trametes hirsuta* laccase into poly(3,4-ethylenedioxythiophene) and polyaniline polymer-matrices. ***J. Power Sources*** (**2011**)196, 4957-4964.

III. Wang, X., Latonen, R.-M., Sjöberg-Eerola, P., Eriksson, J.-E., Bobacka, J., Boer, H., & Bergelin, M., Direct electron transfer of *Trametes hirsuta* laccase in a dual-layer-architecture of poly(3,4-ethylenedioxythiophene) films. ***J. Phys. Chem. C*** (**2011**)115, 5919-5929.

IV. Zafar, M. N., Wang, X., Sygmund, C., Ludwig, R., Leech, D., & Gorton, L., Electron transfer studies with a new FAD-dependent glucose dehydrogenase and osmium polymers of different redox potentials. ***Anal. Chem.*** (**2012**) 84, 334-341.

V. Wang, X., Falk, M., Ortiz, R., Bobacka, J., Ludwig, R., Bergelin, M., Gorton, L., & Shleev, S., Mediatorless sugar/oxygen enzymatic fuel cells based on gold nanoparticle-modified electrodes. ***Biosens. Bioelectron.*** (**2012**) 31, 219-225.

Contributions of the Author

Paper I. The author performed all the experimental work, evaluated the results, and wrote the manuscript.

Paper II. The author planned and performed all the experimental work, evaluated the results, and co-wrote the manuscript with Pia Sjöberg-Eerola.

Paper II. The author planned and performed all the experimental work, evaluated the results, and wrote the manuscript.

Paper IV. The author partially performed the experimental work. The author participated in the writing of manuscript by drafting the results and discussion section. This paper is also presented in the Muhammad Nadeem Zafar's Ph.D. thesis, with the title of '2nd and 3rd generation electrodes for biosensors and biofuel cells' (Lund University, Sweden, 2011).

Paper V. The author carried out the electrochemical measurements for the bioanode and performed the biofuel cell measurements together with Magnus Falk. The author participated in the data processing and analysis, and drafted the first version of the manuscript. It was then completed with the contributions from the co-authors Magnus Falk and Sergey Shleev.

Table of Contents

Abbreviations

ABTS	2,2'-azinobis(3-ethylbenzothiazoline-6-sulfonate)
AuNPs	Au-nanoparticles
BFC	Biological fuel cell
BOD	Bilirubin oxidase
CA	Chronoamperometry
CDH	Cellobiose dehydrogenase
CE	Counter electrode
CNTs	Carbon nanotubes
*Ct*CDH	*Corynascus thermophuilus* cellobiose dehydrogenase
CV	Cyclic voltammogram
CYT_{cdh}	Cytochrome domain in cellobiose dehydrogenase
DET	Direct electron transfer
DH_{cdh}	Flavodehydrogenase domain in cellobiose dehydrogenase
EDOT	3,4-ethylenedioxythiophene
EDXA	Energy Dispersive X-ray Analysis
FAD	Flavin adenine dinucleotide
FIA	Flow injection analysis
GC	Glassy carbon
*Gc*GDH	*Glomerella cingulata* glucose dehydrogenase
GDH	Glucose dehydrogenase
GOx	Glucose oxidase
ITO	Indium-tin-oxide
LSV	Linear sweep voltammetry
MET	Mediated electron transfer
*Mv*BOD	*Myrothecium verrucaria* bilirubin oxidase
MWCNTs	Multi-walled carbon nanotubes
NADP	Nicotinamide adenine dinucleotide phosphate
OCV	Open circuit voltage

PANI	Polyaniline
PEDOT	Poly(3,4-ethylenedioxythiophene)
PEGDGE	Poly(ethylene glycol) diglycidyl ether
PPy	Polypyrrole
PQQ	Pyrroloquinoline quinone
PSS^-	Poly(styrene sulfonate)
PVI	Poly(1-vinylimidazole)
PVP	Polyvinylpyrrolidone
RDE	Rotating disk electrode
RE	Reference electrode
RVC foam	Reticulated vitreous carbon foam
SAM	Self-assembled monolayer
SEM	Scanning electron microscopy
SWCNTs	Single-walled carbon nanotubes
*Th*L	*Trametes hirsuta* laccase
*Tv*L	*Trametes versicolor* laccase
WE	Working electrode

1. Objectives

Nowadays, when fossil fuel depletion and global climate change threaten our existence and future, extensive research has been devoted on finding alternative energy resources and developing more efficient and environmentally friendly processes for energy storage and conversion. The current work focuses on enzymatic biological fuel cells (BFCs), which are designed to convert the chemical energy of the fuel into electricity in a green and biocompatible manner. The objectives are: to achieve a better understanding of the interplays of the enzymatic biocatalysis of the anodic or cathodic electrode reactions, and to design new enzyme electrode configurations for BFCs by addressing the major challenges in BFC research, which involve enhancing power output and operational stability, to bring BFCs closer to the requirements of the promised applications.

This work was part of the European Union Sixth Framework Programme project BIO-MEDNANO: *Integrating enzymes, mediators and nanostructures to provide bio-powered bio-electrochemical sensing systems* (STRP 017350); the Finnish-Tekes projects PEPSIC: *Printed Enzymatic Power Source with an Integrated Capacitor* (1681/31/07); and *PEPScond: Printed Enzymatic Power Supply with Embedded Capacitor on Next generation Devices* (40109/10). These multidisciplinary projects explored the frontiers of knowledge about enzymes, mediators, surfaces, and immobilization strategies, with the aim of improving enzymatic electron transfer reactions for use in integrated bio-powered electronics for diagnostic and healthcare applications. The objectives of the current sub-project were to optimize electrode materials to achieve improved electron transfer systems and to maximize the enzyme loading and activity on the electrode surface; and to create novel electrodes, with improved electrochemical transduction system performance. In the current thesis, **Papers I to III**, dealing with different immobilization strategies for laccase immobilization in biocathode construction, were resulted from the project work.

In 2010, the author was a visiting researcher in Professor Lo Gorton's group at Lund University, Sweden. The work performed there focused on developing new enzyme electrode configurations for bioanode construction (**Papers IV and V**) and on developing an implantable, one-compartment BFC as a demonstration for the full BFC setup (**Paper V**).

2. Background

Section 2.1 presents a general introduction to the concept of the BFC, its development along the historical line, and its applications as power sources. Section 2.2 to 2.5 provide a more detailed discussion of the critical issues involved in the construction of enzyme electrodes for BFCs including biocatalysts, enzyme catalysis, electron transfer, and enzyme electrode configuration.

2.1 BFCs

BFCs are energy conversion devices that utilize biocatalysts (either complete living cells or enzymes) to convert the chemical energy of a fuel into electrical energy. They are also a special class of fuel cells, in which the biocatalysts are employed to catalyze the electrode reactions instead of the metallic inorganic catalysts used in conventional polymer electrolyte membrane fuel cells. There are different types of BFCs, defined by the type of biocatalyst. Microbial BFCs use living cells to catalyze the electrode reactions of the fuel and the oxidant, whereas enzymatic BFCs use enzymes for this purpose. Microbial BFCs typically have long lifetimes (up to several years) and are capable of completely oxidizing the fuels; however, they usually produced low power density owing to slow transport across cellular membranes. In contrast, enzymatic BFCs typically have power densities orders of magnitude higher, but can only partially oxidize the fuel and have limited lifetimes owing to the fragile nature of the enzymes (Cooney et al., 2008; Minteer et al., 2007). The current work focuses mainly on enzymatic BFCs. Hereby, BFCs refer to enzymatic BFCs in this thesis.

A conventional BFC configuration is illustrated in Fig. 2.1. Like any galvanic cell, a BFC consists of an anodic compartment and a cathodic compartment. In the anodic compartment, the substrate specific to the anodic enzyme is fed in as the fuel and is oxidized to the corresponding oxidized form of the substrate. In the cathodic compartment, O_2 or H_2O_2 is taken as the oxidant and reduced to the end product, H_2O. The electrode reactions, both the oxidation of the fuel and the reduction of the O_2, are catalyzed by the enzymes integrated into the anodic or cathodic enzyme electrode. It is important to note that a separation membrane (e.g., a size exclusion membrane, as shown in Fig. 2.1) is standard, but if there are selective enzymes on the anode and cathode then the separation membrane is unnecessary. The electrons produced by the oxidation of the fuel are collected by the anode current collector and then flow through the outer circuit to the cathode where they participate in the reduction of oxidant. The fuels that can be used in BFCs diverse from carbohydrates to alcohols, as well as H_2 (as in the conventional fuel cell), depending on the specificity of the anodic enzyme species used in the enzyme electrode configuration. Since biocatalysts mostly prefer ambient temperature and only some thermophilic species can tolerate elevated temperatures, BFCs typically work under more neutral pHs and near room temperature conditions (Barton et al., 2004; Bullen et al., 2006; Cooney et al., 2008).

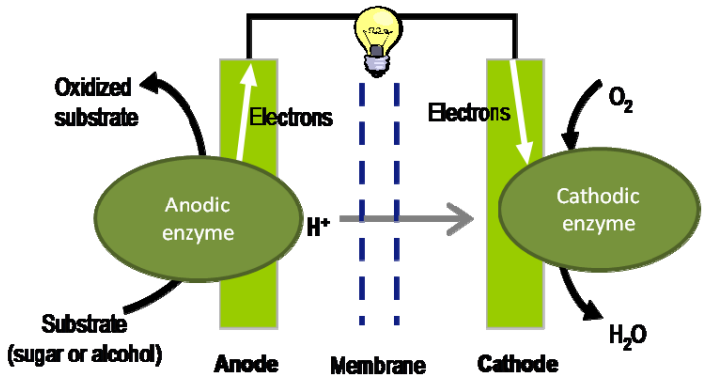

Fig. 2.1. Schematic diagram of a BFC cell configuration

The history of BFCs dates to 1912. The first microbial BFC was demonstrated by Potter, in which the yeast cells were used to oxidize glucose on the anode (Potter, 1912). There was little research interest in BFCs until the 1960s when Kimble proposed using isolated enzymes at electrode surfaces. He and his co-workers were able to generate positive open circuit potentials for the two oxidases in complete BFCs work which initiated this research area called enzymatic BFCs (Yahiro et al., 1964). Fig. 2.2 displays the key chronological landmarks in the development of enzymatic BFCs.

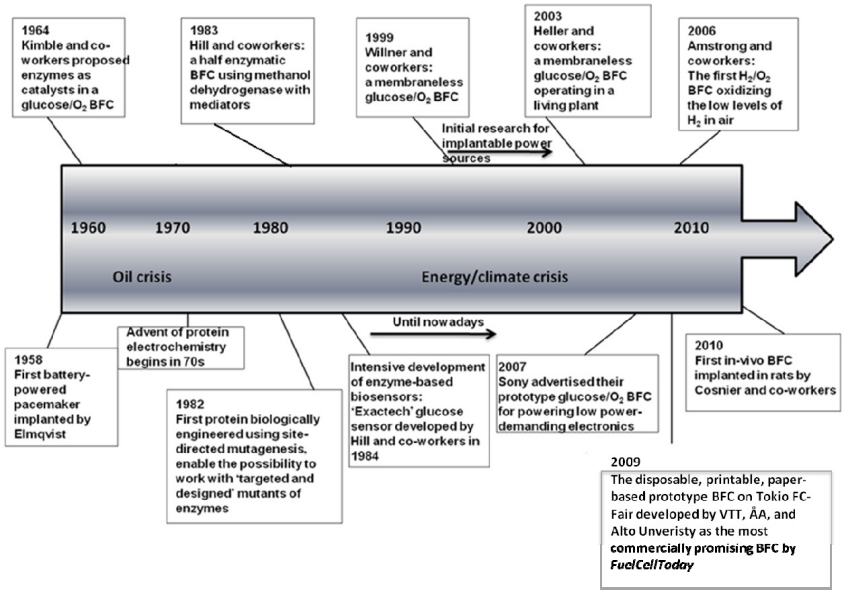

Fig. 2.2. Landmarks in the development of enzymatic BFCs (Cracknell et al., 2008) (Copyright permission with American Chemical Society)

At the beginning of the 1980s, Hill and co-workers reported a half enzymatic methanol-oxidizing BFC that used a diffusive methanol dehydrogenase as the anodic catalyst with diffusive mediator mediating electron transfer to a Pt electrode (Davis et al., 1983). With direct O_2 reduction on the Pt electrode at the cathode, this half enzymatic BFC produced a current density of 30 $\mu A \cdot cm^{-2}$ at an operating voltage of 50 mV.

Throughout the 1980s and 1990s, there was more intense activity devoted to enzyme-based biosensors because of the more obvious market for the rapid analysis of critical analytes, such as glucose, and because low power output was not an issue for such applications (Wang, 2008; Wilson & Hu, 2000). Research on biocatalytically modified electrodes for sensor applications provided a substantial technological underpinning for BFC research. In 1999, Willner and co-workers reported a membraneless BFC with immobilized enzymes as catalysts at both the anode and the cathode (Katz et al., 1999). This BFC was based upon the anodic oxidation of glucose catalyzed by flavin-containing glucose oxidase (GOx), coupled to the cathodic reduction of O_2 by cytochrome *c* oxidase. From then on, the feasibility of a BFC to be simply constructed and to be minimized without the need of a membrane to separate the fuel and the oxidant, has gathered support. Based on these specifications, the enzymatic BFC was conceived as an implantable power source that can operate in biological fluids. Willner and co-coworkers developed elaborate strategies for attaching flavin- or PQQ- dependent enzymes to electrodes, employing covalent attachment of the cofactor, and allowing it to reinsert into the apoenzymes (Willner et al., 1996; Zayats et al., 2005). Armstrong et al. proposed an immobilization strategy for a cathodic enzyme (laccase) based on the affinity concept: the substrate-like electron-conducting functionalities are covalently grafted onto the electrodes, which can enhance the adsorption of laccase on the electrode surface through the specific affinity between the substrate-like functionalities and the substrate binding pocket in the vicinity of the electron relay centre and also orient laccase on the electrode surface via direct electron transfer since the electron tunneling distance is shortened (Blanford et al., 2008). These immobilization strategies grew out of the development of knowledge and techniques development in several fields. They benefited from the study of 'protein film voltammetry' which began in the 1970s (Rusling & Zhang, 2003; Leger & Bertrand, 2008) and from the rapid progress in protein engineering technology for site-direct mutagenesis after 1980s (Stracha & Read, 1999), which improved the understanding of the electrocatalysis mechanism of the redox enzymes and enabled to work with more efficient and specified functionality-directed mutants of enzymes.

A major advance in BFC research was the Os-redox hydrogel enzyme electrode configuration proposed by Heller and co-workers, in which the enzymes (GOx, laccase, or bilirubin oxidase (BOD)) are embedded into the hydrogel formed by a redox polymer to which Os-complexes are attached as the electron mediating component (Mano et al., 2005; Mano et al., 2006; Kang et al., 2006). This design produces a 3D electrode equivalent to a large number of monolayers of electronically coupled enzymes. Another distinguished feature of this enzyme electrode configuration is the co-immobilization of the redox mediating segment in the hydrogel. This type of enzyme electrode facilitates the construction of a miniaturized, membrane-less, one-compartment BFC, which yields electricity in glucose-containing physiological buffers or in living plants (a grape) (Mano et al., 2002; Mano et al., 2003a; Mano et al., 2003b).

In addition to alcohol/sugar-fueled BFCs, there are also H_2-fueled BFC. The H_2-O_2 combination as fuel and oxidant has long been the standard in conventional PEM fuel cells and is featured with attractive characteristics, such as the low reduction potential of H_2, the clean and thorough oxidation to the plain end product H_2O, and the ease of supplying a gaseous fuel. Researchers have explored the feasibility of applying hydrogenase as a replacement for Pt and it has been proposed that the active sites of hydrogenases have activity comparable to that of Pt (Jones et al., 2002; Karyakin et al., 2005). While most hydrogenases are inactivated by traces of O_2, the important discovery of O_2-tolerant hydrogenase from aerobes eliminates this problem (Cracknell et al., 2008). The first membrane-less $H_2|O_2$ BFC based on the oxidation of low level of H_2 in air was demonstrated by Armstrong and co-

workers, it can power a wristwatch (Vincent et al., 2006). This proves that highly active enzymes can extract energy from H_2 and O_2, producing clean water as the ultimate end product.

The possible applications of BFCs fall into three classes: (1) implantable power sources, such as microscale cells implanted in human or animal tissues or larger cells implanted in blood vessels; (2) power derived from ambient fuels or oxidants, mainly plant saps or juices, but extendable to sewage and other waste streams; and (3) power derived from conventional fuels, including H_2, methanol, and higher alcohols (Barton et al., 2004). Classes 1 and 2 are closely related since the reactants available for implantable power, such as blood-borne glucose, lactate, or O_2, are ambient in these specific environments. However, Class 2 ambient-fueled BFCs have more versatile fuel availability, mainly the carbohydrates in the plants or waste-derived. In contrast, Class 3 BFCs have to compete with well-established conventional fuel cell technology.

The implantable power source is the most intuitive application of BFCs. Biocatalysts are physiological species and have evolved to function in complex physiological environments, efficiently catalyzing reactions at physiological pH and temperature that involve fuels and oxidants present in such environments, and most important, producing reaction products that are tolerable to the host organism (Barton et al., 2004). The major advantage of an implantable BFC over a conventional battery is its infinite energy density if energy can be derived from ambient sugars and if the BFC operates in a self-sustaining manner in the host organism. By 2010, Cosnier and co-workers had demonstrated the first *in vivo* functional implantable BFC, which operates in the retroperitoneal space of freely moving rats (Cinquin et al., 2010). This BFC, with 0.133 ml electrodes, produced a peak specific power of 24.4 μW/ml, which exceeds the requirement of a pacemaker.

The use of ambient fuels to generate power is attractive in situations, in which the power requirements of small electronics are distributed, disconnected, and long-term (Barton et al., 2004). The ambient-fueled BFCs find their potential applications as power sources for electronic sensor systems which have to operate remotely or in the presence of biohazards. The principal fuels, used by the ambient BFCs, are the carbohydrates present in plants or in the effluent of human or animal processes (Barton et al., 2004); these include monosaccharides, glucose, fructose, and disaccharide sucrose. Many oxidoreductases have been found to catalyze the oxidation of carbohydrates, such as GOx (EC 1.1.3.4) (Cracknell et al., 2008), glucose dehydrogenase (GDH) (EC 1.1.99.17) (Miyake et al., 2009; Tanne et al., 2010), fructose dehydrogenase (EC 1.1.99.11) (Kamitaka et al., 2007), pyranose oxidase (EC 1.1.3.10) (Odaci et al., 2008), pyranose dehydrogenase (EC 1.1.99.29) (Zafar et al., 2010; Tasca et al., 2010), cellobiose dehydrogenase (CDH) (EC 1.1.99.18) (Ludwig et al., 2010) and other oligosaccharide dehydrogenases (Ruzgas et al., 1996; Tessema et al., 1997). Compared with implantable BFCs, ambient-fueled BFCs can use more versatile fuels and are more flexible in terms of the selection of materials for enzyme electrode construction. Sony is already advertising their 'biobattery', which they first demonstrated in 2007 (Sony Globe, 2011). Using GDH and BOD as biocatalysts with diffusive redox mediators on the anode and cathode compartments, respectively, it can generate a power output of over 70 mW (28 cm^3, 2.5 mW/cm^3) for three cell units in series and is able to operate a memory-type Walkman and a radio-controlled toy car (Sakai et al., 2010). Another notable BFC prototype development is the printable, flexible, and disposable BFCs on paper-substrates. This printed BFC is a miniature power source developed for intelligent packaging by the Finnish-Tekes projects *PEPSIC* (1681/31/07) and *PEPScond* (40109/10). Intelligent packaging refers to packaging for goods such as food and pharmaceuticals, that includes sensors which monitor the

condition of the product (Smolander et al., 2010). This BFC would be printed alongside the sensors on the same piece of paper as it is envisaged in the application. At the present stage of development, it can produce an output of around 50 μW and can drive electronics with lower power demand, e.g., an active radio frequency identification tag or a functional greeting card. Besides intelligent packaging, the other applications being considered for printed BFCs are in the medical sector, where they could be integrated into disposable medical devices requiring portable, long-term power, such as 24 h pulse monitoring or body temperature logging. This printed BFC was selected as one of the more innovative Demos at the 5th Fuel Cell Expo in Tokyo (Butler & Hugh, 2009).

To compete with conventional fuel cell technology, H_2- or alcohol-fueled BFCs have advantageous key properties, including catalytic activity at low temperatures and near-neutral pHs, chemical selectivity, and potentially low-cost production using fermentation and bioseparation technologies. However, the current density (1-10 mA/cm^2) which H_2- or methanol-fueled BFCs can generate at present is still several orders of magnitude lower than that from conventional methanol fuel cells. Because of this constraint, the only major category of conventional applications suitable for this type of BFCs is small fuel cells for portable power (Barton et al., 2004).

The fundamental technical requirements for all three classes of application include high power density and excellent operational stability, which are the main challenges for BFC research. The modest current density generated by the present BFC electrode design is limited mainly by factors related to the physicochemical processes in the BFC, such as the low catalytic efficiency of biocatalysts after immobilization in the electrode structure and the mass transfer issue of the fuel to the active sites of enzymes. The lifetime of a BFC is regulated by several factors. For MET BFCs, the lifetime of the redox mediator is a concern; for most BFCs, the lifetime is determined by stability of the biocatalysts. Typically, BFCs last only a few days (Kim et al., 2006). Immobilization of an enzyme in its preferred environment helps to extend its lifetime (Moore et al., 2004). Therefore, in terms of both the catalytic efficiency and stability of immobilized enzymes, it is important to develop more efficient biocompatible enzyme immobilization techniques for BFC electrode.

To find solutions to these challenges, in the past decade, extensive research has focused on screening more efficient and durable enzymes for bioelectrocatalysis, understanding the interplay of the electrocatalysis reactions, designing novel enzyme electrode configurations by integrating nanostructured conductive materials to enhance the current density output, and engineering prototype BFCs for specified applications to bring them closer to commercialization. More detailed discussions on the specific aspects of BFC research appear in the following chapters.

2.2 Biocatalysts in enzymatic BFCs

This section describes in detail the enzymes used in the BFC cathode and anode as catalysts for the electrode reactions (the oxidation of sugars/or reduction of O_2). The structural features and catalytic properties of the enzymes, including substrate specificity, active sites, and substrate-bind sites, are addressed for each enzyme studied in this thesis.

2.2.1 Biocatalysts for BFC cathodes

The biocatalysts employed in the BFC cathode are enzymes which possess catalytic activity on the reduction of O_2 or H_2O_2 into water. In earlier research, peroxidases were extensively studied to develop biosensors for detection of H_2O_2 and phenolic compounds in

various industrial process fluids (Gorton et al., 1992; Lindgren et al., 2001; Nakabayashi & Yoshikawa, 2000; Serra et al., 2003). For BFCs, peroxidases have also been exploited as biocatalysts when H_2O_2 is used as the oxidant in the biocathode (Jia et al., 2010).

O_2 is more clean and preferable oxidant for BFC design simply due to its more universal presence in the ambient. Blue multicopper oxidases are the most common biocatalysts in O_2-consuming BFC cathodes. Blue multicopper oxidases refer to a class of Cu-containing oxidoreductases which can catalyze the four-electron reduction of O_2 to water without the formation of highly toxic oxygen intermediates, coupled to the one-electron oxidation of a variety of small organic (generally aromatic) or inorganic substrates (Solomon et al., 1996; Nakamura & Go, 2005; Kosman, 2010). The well-defined multicopper oxidases include laccase (Rodgers et al., 2009), BOD (dos Santos et al., 2010), ceruloplasmin (Biellli & Calabrese, 2002), and ascorbate oxidase (Solomon et al., 1996). In research into the construction of BFC cathodes, laccase and BOD are the two most extensively investigated blue multicopper oxidases.

Laccases (*p*-diphenol: dioxygen oxidoreductase, EC 1.10.3.2) catalyze the oxidation of *ortho*- and *para*- diphenols, amino-phenols, polyphenols, polyamines, lignins, and aryl diamines, as well as some inorganic ions coupled to the reduction of O_2 to water (Yaropolov et al., 1994; Solomon et al., 1996). The catalytic sites of laccases consist of four Cu ions, which can be classified in accordance with their spectroscopic characteristics as T1, T2, and T3 sites. A mononuclear T1 Cu is responsible for the blue color of the enzyme with a characteristic absorbance band at a wavelength around 610 nm in the UV-vis spectrum. One T2 Cu and two T3 Cus form a trinuclear cluster site, where oxygen is bound between the two T3 Cu nuclei and reduced to water. The T1 Cu extracts one electron from the electron donor (substrate), followed by a subsequent intramolecular electron transfer *via* a His-Cys-His bridge to the T2-T3 Cu cluster, where the oxygen is reduced to water (Solomon et al., 1996; Shleev et al., 2005).

Laccases are widely distributed in high plants, fungi (ascomycetes and basidiomycetes), and even in some bacteria and insects (Claus, 2004). The enzymatic and physicochemical properties of laccase depend on the original source. The key characteristics of laccase are the standard redox potentials of its redox centres: the T1, T2, T3 sites. The value of the redox potential of the T1 Cu site, which has been determined for a great number of different laccases using potentiometric titration with redox mediators, varies between 430 and 780 mV *vs.* NHE (Shleev et al., 2005). As stated above, the T1 Cu site is the primary active site at which electrons are accepted from the reducing substrates. The catalytic efficiency of laccase is dependent on the redox potential of the T1 Cu site. Laccases are divided into three groups based on the redox potential of the T1 site: low, middle, and high potential laccases. The low potential group includes laccases from trees, e.g., *Rhusvernicifera* whose T1 Cu site has a potential of about 430 mV *vs.* NHE (Reinhammar & Vänngård, 1971). The middle group includes laccases from basidiomycetes like *Myceliophthora thermophila* (Xu et al., 1996), basidiomecete C30 (Klonowska et al., 2002), *Rhizoctonia solany* (Xu et al., 1996), and *Coprinus cinereus* (Schneider et al., 1999), whose T1 Cu sites have a potential ranging from 470 to 710 mV *vs.* NHE. The high potential laccases, produced from *Trametes versicolor*, *Trametes hirsuta*, and *Trametes villosa*, are those whose T1 Cu sites have a potential of about 780 mV *vs.* NHE (Reinhammar 1972; Xu et al., 1996). The high potential laccases are of special interest in biotechnology due to their higher catalytic efficiency; they are especially well suited to use in BFCs. Within this thesis, *Trametes versicolor* laccase *(Tv*L) and *Trametes hirsuta* laccase *(Th*L) are elaborately described.

The *Tv*L is a monomeric protein, organized in three sequentially arranged domains (Fig. 2.3.A). It has dimensions of 65×55×45Å (Piontek et al., 2002). The trinuclear T2/T3 Cu cluster is embedded 12 Å deep from the molecular surface between domains 1 and 3 with both domains providing residues involved in the coordination of the Cu. The oxygen-reducing site at the T2/T3 Cu cluster has access to solvent through two channels, one of which leads to the T3 Cu sites and the other to the T2 Cu site. These solvent channels are well suited to both fast access of O_2 to the trinuclear cluster and subsequently easy release of H_2O. The mononuclear T1 Cu lies embedded in domain 3, about 6.5 Å below the enzyme surface. The T1 Cu is connected to the trinuclear cluster by a His-Cys-His tripeptide, which is highly conserved in the blue multicopper oxidases. For *Tv*L, the closest distance between the T1 and T2/T3 Cus is about 12 Å. Near the T1 Cu site, there is a wide and hydrophobic substrate binding pocket, rich in π electron density, to which a range of substrates can bind and undergo rapid one-electron oxidation to radical products that dissociate before further reaction. Accordingly, the T1 Cu is regarded as the primary electron acceptor site. *Tv*L has a dominating surface distribution of negative charges as in accordance with the acidic PI of about 3.5. The substrate binding pocket is also a small negatively charged cavity, which can stabilize the radical cation products formed during the catalytic cycle (Piontek et al., 2002).

This study uses *Th*L, which is produced by the white rot basidiomecete *Trametes hirsuta*. *Th*L and *Tv*L have a sequence identity of 90%. The main structural features of *Th*L, including the folding pattern (in three domains) and the location of the active sites, are similar to those of *Tv*L. *Th*L is more glycosylated than *Tv*L, having a higher content of sugar residues (Polyakov et al., 2009). The phenylalanine residues are highly conserved in the coordination ligands of the T1 Cu site among the high redox potential laccases, *Tv*L and *Th*L, which suggests that it may act as a binding site for a hydrophobic substrate. The substrate binding pocket has dimensions of 8×10×10 Å. Furthermore, a comparison of the amino acid residues forming the substrate binding pockets shows that the pockets of the high redox potential laccases *Tv*L and *Th*L contain more aromatic residues, about 18 on average, than those of medium redox potential laccases, which contain about 13 aromatic residues (Polyakov et al., 2009).

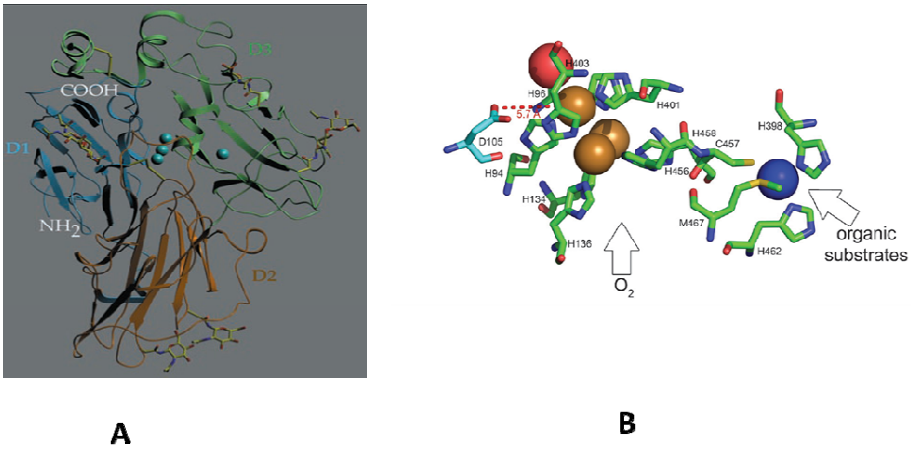

Fig. 2.3. A. Ribbon diagram of *Tv*L. The arrangement of the domain structure is depicted in different color coding (D1-D3). The blue spheres represent Cu ions. Carbohydrates appear as stick models (Piontek et al., 2002). B. 3D representation of the copper binding site of BOD from *Myrothecium verrucaria*. The brown spheres represent the coppers in the T2/T3

trinuclear cluster and the dark blue sphere represents the T1 Cu. The red sphere represents an oxygen species bound to the trinuclear cluster (dos Santos et al., 2010) (Copyright permission with RSC publishing).

Due to its high reactivity at neutral pH, BOD from *Myrothecium verrucaria* has been considered one of the best enzymes for catalyzing the biocathodic reactions in BFCs. In contrast, the high redox potential laccases usually have optimal pHs in acidic range and exhibit a substantial reduction of the catalytic activity at neutral pHs (Shleev et al., 2005). Consequently, BOD is an attractive candidate as a biocathodic enzyme in implantable BFCs.

In vitro, BOD catalyzes the oxidation of bilirubin to biliverdin and then to a purple pigment. In pharmaceutical applications, BOD is used for the diagnostic measurement of the bilirubin concentration in serum (Shimizu et al., 1999). The crystalline structure of BOD has recently been resolved (Mizutani et al., 2010); BOD is a monomeric protein with a molecular mass of 60 kDa. The protein is folded into three domains and contains four copper binding sites, which are the catalytic sites for the binding of oxygen and extraction of electrons from electron donors. The overall structure of the four-copper binding sites is almost identical to that of the other multicopper oxidases (Fig. 2.3.B). Numerous studies have attempted to elucidate the electron transfer mechanism involved in the biocatalysis of O_2 reduction by BOD. The redox potential of the T1 copper site in BOD has been determined in the range of +650 ~ +670 mV *vs.* NHE at pH 7.0. It is generally accepted that, as in laccases, the mononuclear T1 copper is the physiological entry point for electrons, which in turn are transmitted to the trinuclear centre via a highly conserved His-Cys-His bridge across a distance of 13 Å (dos Santos et al., 2010). However, the intermediate states of BOD involved in the catalysis are not completely understood.

2.2.2 Biocatalysts for BFC anode

The biocatalysts employed in BFC anodes are enzymes which possess catalytic activity for the oxidation of sugars such as monosaccharides (e.g., glucose and fructose) and disaccharides (e.g., cellobiose and lactose). A single enzyme is typically used to catalyze the first step of the oxidation of carbohydrates, but several enzymes can be integrated into the electrode configuration to increase the columbic efficiency of the catalysis of sugar oxidation (Tasca et al., 2010). Glucose is the most widely used fuel in BFCs due to its presence in diverse sources. In particular, glucose is the fuel available in physiological fluids for implantable BFCs. In this thesis, GOx (EC 1.1.3.4), GDH (EC 1.1.99.17), and CDH (EC 1.1.99.18) are used as the biocatalysts for BFC anodes.

Currently, GOx and GDH are the biocatalysts most commonly used in BFC anodes; they have been extensively studied in the context of glucose biosensor, which dates back to the 1970s (Clark Jr. & Lyons, 1962; Degani & Heller, 1988; Degani & Heller, 1989). GOx is a flavoenzyme, which catalyzes the oxidation of β-D-glucose to D-glucono-1, 5-lactone with the concurrence of H_2O_2. It is highly specific for β-D-glucose and does not act on α-D-glucose. GOx from *Aspergillus niger* is a homodimeric and structurally rigid glycoprotein with a molecular weight of 146~186 kDa. The protein structure consists of two identical polypeptide chains, each containing noncovalently bound flavin adenine dinucleotide (FAD) as the cofactor, which is localized in a cavity deeper than 13 Å in the apoenzyme (Fig. 2.4) (Hecht & Schomburg, 1993). Native GOx is highly glycosylated, with a carbohydrate content of 16~20%. Glucose binds close to the active site; it is stabilized by hydrogen bonds and hydrophobic interactions with aromatic amino acid residues and FAD (Wohlfahrt et al., 1999). FAD serves as the catalytic site, by accepting the electrons donated by the glucose and being reduced to $FADH_2$. Two protons and two electrons can subsequently be transferred

from GOx to O_2, yielding H_2O_2 and regenerating the oxidized state of GOx. Therefore, O_2 is a competing electron acceptor when GOx is used as the biocatalyst in a BFC anode.

To date, a great number of GDHs have been reported to catalyze the oxidation of glucose, in which a hydroxyl group in the C1 position of D-glucose is oxidized in the presence of an electron acceptor to yield D-glucono-1, 5-lactone. However, depending on the cofactor involved in the catalytic reaction, GDHs can be classified as nicotinamide adenine dinucleotide phosphate (NADP)-dependent, pyrroloquinoline quinone (PQQ)-dependent, or FAD-dependent. FAD-dependent GDHs have been isolated from a limited number of bacterial or fungal strains (Hauge, 1964; Bak, 1967; Matsushita et al., 1980; Sode et al., 1996; Tsujimura et al., 2006). The structural features of these GDHs, such as molecular mass, protein configuration, glycosylation degree, are as diverse as their sources. Despite their great structural diversity, all FAD-dependent GDHs share the characteristics of a high substrate affinity and a high turnover number for glucose. The GDH studied in present work, isolated from the ascomycete fungus *Glomerella cingulata*, is a novel FAD-dependent GDH. This *Glomerella cingulata* glucose dehydrogenase *(Gc*GDH) has the feature of being completely O_2 insensitive, which makes it an attractive anodic enzyme because it can avoid competition of O_2 as the electron acceptor for the reduced $FADH_2$. No crystalline data is available at present for *Gc*GDH.

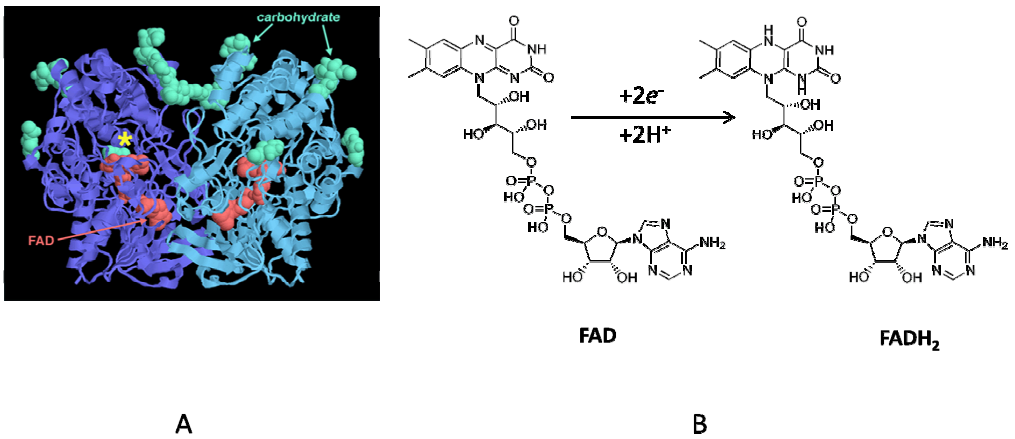

Fig. 2.4. A. 3D structure of GOx. B. Chemical structure of FAD (oxidized form) and $FADH_2$ (reduced form)

CDH is a flavocytochrome (the only known extracellular one) produced by many lignocellulose-degrading fungi; it belongs to the haemoflavoprotein family, which includes flavocytochrome b_2, mandelate dehydrogenase, fumarate dehydrogenase, nitric oxide synthase, and the bacterial cytochrome P-450 (Ludwig et al., 2010; Henriksson et al., 2000). CDHs participate in the degradation of cellulose and lignin (Zamocky et al., 2006). In general, these proteins have a distinct flavodehydrogenase domain (DH_{cdh}) and a cytochrome domain (CYT_{cdh}), which are connected by a flexible peptide linker (Fig. 2.5). Crystallization of the complete flavocytochrome is hindered by the extensive interdomain peptide linker. The crystalline structures of DH_{cdh} and CYT_{cdh} have been determined separately after the cleavage of the two domains (Martin Hallberg et al., 2002). In terms of the tertiary protein structure, the two domains are in close contact, which allows internal electron exchange (Martin Hallberg et al., 2002). The DH_{cdh} contains FAD or 6-hydroxy-FAD moiety (noncovalently) as the prosthetic group. The CYT_{cdh} carries a haem moiety, either *b*- or *c*-type, as the cofactor. CDHs usually have molecular masses of 90~100 KDa, and the glycosylation is around 10%.

The catalytic mechanism of CDHs and the role of CYT_{cdh} are not fully understood at present. In biocatalysis, FAD serves as the catalytic site where the substrate is oxidized. Cellobiose is one of the substrates preferred by CDHs, and DH_{cdh} catalyzes a two-electron oxidation at the anomeric C1 position of cellobiose to yield cellobiono-1,5-lactone. The reduced FAD can then be reoxidized by various electron acceptors, or the electrons can be sequentially transferred to the haem, which in turn donates the electrons directly to the electrode. In addition, CDHs efficiently oxidize cellodextrins, mannodextrins, and lactose to the corresponding lactones at the DH_{cdh} domain, and depending on its origin, they may also oxidize monosaccharides, e.g., glucose.

More than twenty-five species of fungi have been shown to produce CDH (Ludwig et al., 2010). All CDHs belong to two related subgroups: Class I, produced by basidiomycetes; and Class II, produced by ascomycete. Class I CDHs usually have short sequences and exhibit a strong substrate discrimination against glucose and an acidic pH optimum (around 3.5 to 4.0) for efficient internal electron transfer (IET) between the DH_{cdh} domain and the CYT_{cdh} domain. Whereas, some Class II CDHs have more complex sequences, work under neutral or basic conditions, and may have a high turnover number with monosaccharides (e.g., glucose) and oligosaccharides other than cellodextrins and lactose (Zamocky et al., 2006).

This thesis studied *Corynascus thermophuilus* CDH (*Ct*CDH), an ascomycete Class II CDH, which has comparatively high catalytic activity for glucose oxidation at neutral pHs. The ultimate goal was to use it to construct bioanodes for implantable BFCs (Harreither et al., 2011).

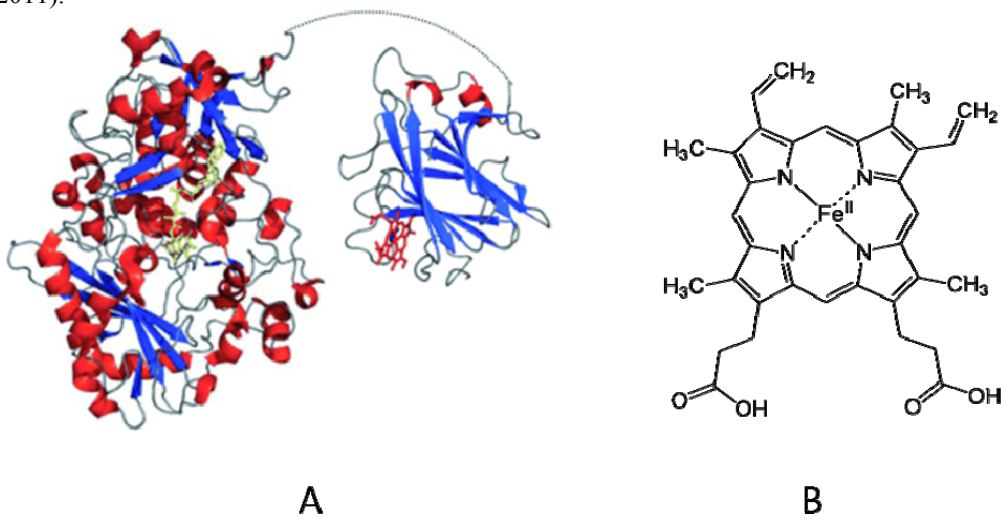

Fig. 2.5. A. Dehydrogenase domain (left) and cytochrome domain (right) of *P. chrysosporium* CHD. The position of the interdomain linker is indicated by the dots. Both domains are turned from their face-to-face position by 45º towards the observer to give a better view of the FAD (yellow) and the haem b (red) (Ludwig et al., 2010) (Copyright permission with John Wiley and Sons). B. Chemical structure of haem b in the cytochrome domain of CDHs.

2.3 Kinetics of enzymatic catalysis

The Michaelis-Menten model describes the kinetics properties of many enzymes (Michaelis & Menten, 1913). It is relevant to situations in which very simple kinetics can be assumed, i.e., there is no intermediate or product inhibition and there is no allostericity or cooperativity. In this model, an enzyme (*E*) combines with a substrate (*S*) to form an enzyme-

substrate complex, which can proceed to form a product (P) or to dissociate into E and S, as shown in the reaction below:

$$E + S \underset{k_{-1}}{\overset{k_{+1}}{\rightleftharpoons}} ES \xrightarrow{k_2} E + P \tag{2.1}$$

The rate of product formation (V_0) is given by the *Michaelis-Menten* equation,

$$V_0 = V_{max} \frac{[S]}{[S] + K_M}, \tag{2.2}$$

where V_{max} is the reaction rate when the enzyme is fully saturated with substrate, and K_M, the Michaelis constant, is the substrate concentration at which the reaction rate is half maximal. Here, V_{max} is equal to the product of k_2 (the k_{cat} turnover number) and the total concentration of the enzyme. The Michaelis constant is related to the reaction constants by $K_M = (k_{-1}+k_2)/k_{+1}$. The enzyme catalytic efficiency can be interpreted as the ratio k_{cat}/K_M.

2.4 Electron transfer in the enzyme electrode configuration

Energy conversion in bioenergetic processes such as respiration and photosynthesis is carried out by a series of proteins and enzymes that form multi-step, long-range electron transfer chains. It is of great importance to elucidate the electron transfer pathway along the protein structure (Bartlett, 2008). When redox enzymes are utilized to convert chemical energy into electricity in BFC, electron transfer between the enzyme active sites and the current collector is a key process and is a crucial determinant of the magnitude of the catalytic current and thus of the overall BFC power output performance. In this section, the electron transfer mechanism is described in terms of Marcus Theory and then the two means of realizing the electron transfer from the enzyme active site to the electrode surface, direct electron transfer (DET) and mediated electron transfer (MET), are discussed respectively for the enzymes investigated in this thesis.

2.4.1 Electron transfer mechanism: Marcus Theory

During an electron transfer reaction, an electron moves from the donor (D) to the acceptor (A).

$$D + A \longrightarrow D^+ + A^-. \tag{2.3}$$

There are several classes of electron transfer reactions, defined by the state of the two redox centres and their connectivity: i) inner-sphere electron transfer (discovered by Henry Taube (Taube et al., 1953), who won the Nobel Prize in 1983), in which the donor and the acceptor are covalently linked during electron transfer; if this bridge is permanent, the electron transfer is termed with intramolecular electron transfer, and if the covalent linkage is transient, the electron transfer is termed with intermolecular electron transfer; ii) outer-sphere electron transfer, in which the chemical moieties remain separate species before, during, and after electron transfer and the electrons hop through space from the donor to the acceptor; outer-sphere electron transfer is by definition intermolecular, and it can occur between different species or between identical chemical species that differ only in their oxidation state (self-exchange); and iii) heterogeneous electron transfer, in which the electrons move across the boundary of two phases, such as liquid-solid interface, during the electrode reaction.

The first generally accepted electron transfer theory was developed by Rudolph A. Marcus (Nobel Prize in 1992); it was elaborated in the 1950s to describe the rate of electron transfer reactions (Marcus, 1956). Originally formulated to accommodate outer-sphere electron transfer reactions, it was then extended for inner-sphere electron transfer reactions and heterogeneous electron transfer (Marcus, 1964; Marcus, 1965; Marcus & Sutin, 1985; Marcus, 1993).

Semi-classical Marcus theory predicts that the electron transfer rate is governed by the thermodynamic driving force of the reaction (ΔG^o), the nuclear reorganization energy (λ), and the electronic coupling (H_{DA}) between the donor (D) and the acceptor (A) at the transition state, as shown in Eq. 2.4:

$$k_{et} = \frac{2\pi}{\hbar} \frac{H_{DA}^2}{\sqrt{4\pi\lambda RT}} e^{-\frac{(\Delta G^\circ + \lambda)^2}{4\lambda RT}}, \quad (2.4)$$

where k_{et} is the DET rate, $\hbar$ is the reduced Planck constant, R is the universal gas constant, and T is the absolute temperature (Marcus & Sutin, 1985). Eq. 2.4 partitions into nuclear (exponential) and electronic (pre-exponential) terms: electron transfer reaches a maximum when the nuclear factor is optimized (i.e., $-\Delta G^\circ = \lambda$), and it depends only on the electronic factor (H_{DA}). To elucidate the parameters involved in Eq. 2.4, a simple model is given in Fig. 2.6, in which the reactant and product energy surfaces are treated as parabolic (Marcus & Sutin, 1985).

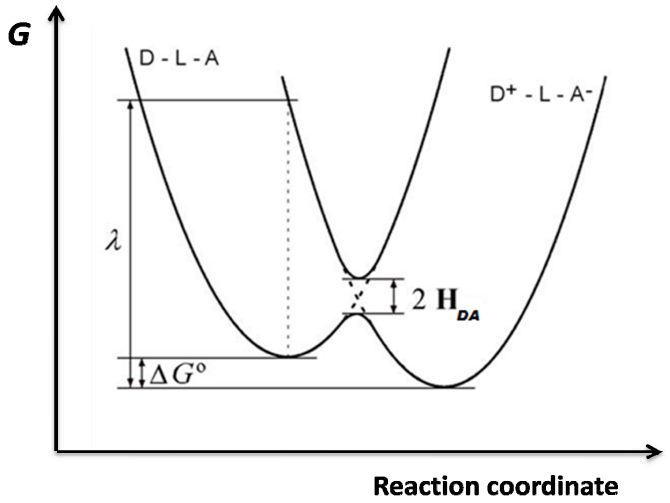

Fig. 2.6. Gibbs free energy curves with the reaction coordinate, showing the states of the reactants and the products. The symbols ΔG^o, λ and H_{DA} represents as they do in Eq. 2.4.

In recent decades, there has been a substantial body of research devoted to studying electron transfer reactions within proteins (Marcus & Sutin, 1985; Moser et al., 1992; Langen et al., 1995; Kuznetsov & Ulstrup, 1999; Gray & Winkler, 2001; Page et al., 2003) and in heterogeneous electron transfer reactions between proteins and electrode surfaces (Leger & Bertrand, 2008; Shleev et al., 2005). Different approaches have been used to predict H_{AD} in proteins. The simplest is the square-barrier model: the protein is regarded as a 'frozen organic

glass' in which H_{DA} decays exponentially as a function of the distance between the donor and the acceptor:

$$H_{DA}^2 = (H_{DA}^0)^2 e^{-\beta(r_{DA} - r_0)}, \quad (2.5)$$

Where H^0_{DA} is the electronic coupling at the van der Waals distance ($r0$) and r_{DA} is the distance between the donor and acceptor (Moser et al., 1992). The exponential attenuation of the overlap in terms of the distance between the donor and acceptor is given by the tunneling parameter β, which depends on the structure of protein in protein, ranging between 0.8 and 1.6 $Å^{-1}$ (Langen et al., 1995; Gary & Winkler, 1996).

Electron tunneling occurs when the potential energy acting on the electron in space between the reacting pair is higher than the energy of the electron in its initial localized site. However, direct electronic coupling between the prosthetic group and the electrode is not easily achieved for many enzymes since the redox centres are often deeply embedded within the protein structure. Different means to realize the electron transfer between the redox centres of enzyme and the electrode surface address either the appropriate protein orientation on the electrode surface to accomplish DET or the use of mediators (electron transfer relays) to facilitate MET.

2.4.2 DET

One of the most intriguing phenomena in bioelectrochemistry, direct electron transfer (DET) between the redox cofactor of a protein and the electrode surface has been the focus of considerable over the past few decades (Guo & Hill, 1991; Gorton et al., 1999; Armstrong, 2002; Shleev et al., 2005; Leger & Bertrand, 2008). Research on the direct electrochemistry of a redox protein at the electrode surface has yielded valuable information about its thermodynamic and kinetic properties, with implications for the catalytic and analytical utilization of proteins (Armstrong, 2002; Leger & Bertrand, 2008). The earliest studies on DET with a redox active protein were published in 1977. Eddowes and Hill (Eddowes & Hill, 1977), using bipyridyl modified gold electrode, Yeh and Kuwana (Yeh & Kuwana, 1977), using tin doped indium oxide electrode, independently showed that cytochrome *c*, exhibits virtually reversible electrochemistry as revealed by cyclic voltammetry. Later, in 1978-79, Russian scientists provided indirect evidence of DET for larger redox proteins with enzyme activity, either with a laccase-modified carbon electrode (Tarasevich et al., 1979) or with a peroxidase-modified carbon electrode (Yaropolov et al., 1979), demonstrating catalytic activity *via* DET in the presence of the substrates O_2 or H_2O_2. Since then, efficient DET reactions with electrodes have been demonstrated for many redox proteins which have no intrinsic catalytic activity but act as electron transfer components in biological pathways (e.g., ferredoxins, flavodoxins, cytochrome c, and azurin) (Guo & Hill, 1991; Bond, 1994; Hill et al., 1996). However, efficient DET reactions with electrodes have been reported for a restricted number of redox enzymes, of which the majority contains redox active metallocentres in their active sites, e.g., haem, iron-sulphur cluster, and copper (Gorton et al., 1999). It is more difficult to achieve DET for a redox enzyme containing a sole organic cofactor (e.g., a flavin or quinone).

There are in principle two experimental approaches to verify whether DET occurs between redox enzymes and electrode surfaces (Shleev et al., 2005):

1. Direct evidence from the observation of independent electrochemical activity of the redox cofactor comprising the active site in the absence of substrate.

2. Indirect evidence from observation of a catalytic response current in the presence of the enzyme substrate.

The literature suggests that the accomplishment of DET of large redox proteins on an electrode surface mainly addresses the favorable orientation of the enzyme on the electrode surface, with the redox centre in close proximity to the conductive electrode surface. This is achieved either *via* specific interactions between the functionalized electrode surface and the protein structure close to the active centre, or by integrating nano-sized conductive material (e.g., metallic nanoparticles) into the enzyme electrode configuration. This material then functions as an electronic conductor projecting into the enzyme, enabling DET (Fig. 2.7A, B, and C).

For blue multicopper oxidases, the realization of DET was reported on an Au electrode surface with the aid of self-assembled monolayers (SAMs) of different types of thiols, which favor the orientation of enzyme by interacting with some protein structure close to the active centres (Shleev et al., 2004; Gupta et al., 2004; Shleev et al., 2006; Pita et al., 2008; Ramirez et al., 2008). These studies provide substantial insight to the electron transfer mechanism for enzymes on the electrode surface. A noteworthy approach, the 'enhanced adsorption' of laccase, was developed by Blanford et al.: polycyclic aromatic amines are chemically grafted onto a carbon electrode surface chosen to mimic the natural organic substrate. There they bind tightly with laccase in an orientation favorable to DET by interacting more closely with the hydrophobic substrate binding pocket in the vicinity of the T1 Cu due to the π-π affinity (Blanford et al., 2008). This concept has also been exploited on other electrode materials, e.g., 1-pyrenebutanoic acid modified MWCNTs (Ramasamy et al., 2010) and anthracene-2-methanethiol modified gold (Thorum et al., 2010). The DET biocatalysis of laccase/BOD can be facilitated by integrating nano-sized conductive materials into the enzyme electrode configuration, such as Au nanoparticles (Rahman et al., 2008; Murata et al., 2009; Dagys et al., 2010) or carbon nanotubes (CNTs) (Zheng et al., 2006; Lim et al., 2007; Zheng et al., 2008; Rubenwolf et al., 2010). These materials interact in closer proximity within the glycoprotein and shorten the electron tunneling distance. The DET type biocatalysis of multicopper oxidases has also been reported for enzyme adsorbed on various carbon-based electrode materials, e.g., pyrolytic graphite (Shleev et al., 2005), spectrographic graphite (Coman et al., 2008; Ramirez et al., 2008), carbon black (Habrioux et al., 2010), carbon aerogel (Kamitaka et al., 2007), and carbon ceramic electrodes (Nogala et al., 2010).

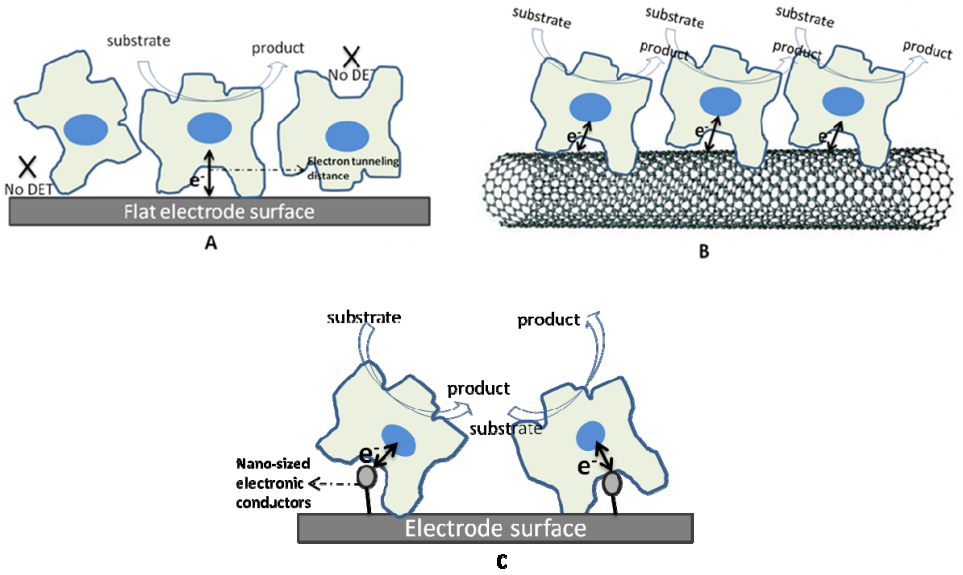

Fig. 2.7. Schematic diagrams of DET from the enzyme active centre to the electrode surface. (A) Electron tunneling with enzyme having a favourable orientation (with small likelihood) on a flat electrode surface; (B) Promoting DET from the enzyme active centre to the electrode surface on a carbon nanotube surface by favouring the appropriate enzyme orientation; (C) Promoting DET from the enzyme active centre to the electrode surface by incorporating nano-sized electronic conductors.

Both GOx and FAD-dependent GDH contain solely the FAD moiety as the cofactor. The DET of these enzymes on the electrode surface is accomplished mainly by using different electrically conductive promoters to reduce the electron tunneling distance from the FAD cofactor to the electrode surface, e.g., metallic nanoparticles (Xiao et al., 2003; Zhao et al., 2006; Zayats et al., 2008), graphene (Kang et al., 2009; Zheng et al., 2010; Zhang et al., 2011), and single- or multi-walled CNTs (Cai & Chen, 2004; Jia et al., 2005). In particular, CNTs have been extensively studied. They have been integrated into various composite materials to promote the DET of GOx on the electrode surface. Examples include CNTs wrapped in polyelectrolytes (Wen et al., 2007), CNTs/chitosan matrix (Zhou et al., 2008), CNTs/silica matrix (Ivnitski et al., 2008), and CNTs/ionic liquid reconstituted cellulose matrix (Wu et al., 2009).

For CDHs, the presence of CYT_{cdh} in the protein structure can facilitate DET from the DH_{cdh} to the electrode surface, where the haem cofactor situated on the surface of CYT_{cdh} can come into close proximity to the FAD cofactor in DH_{cdh} with diffusing further through the flexible linker, accept the electron, and then donate it to the electrode surface. Fig. 2.8 presents a schematic diagram of the DET pathway from the FAD cofactor of CDHs to the electrode surface. To some extent, the CYT_{cdh} can be looked upon as an enzyme itself 'built-in' mediator (Ludwig et al., 2010). The DET type catalysis of CDHs from different origins has been observed on various types of electrode materials, including Au electrodes modified with the SAM of thiols (Lindgren et al., 2000; Stoica et al., 2005), spectrographic graphite (Larsson et al., 2000; Stoica et al., 2006; Harrieither et al., 2007), and single- and multi-walled CNTs (Tasca et al., 2008; Tasca et al., 2009).

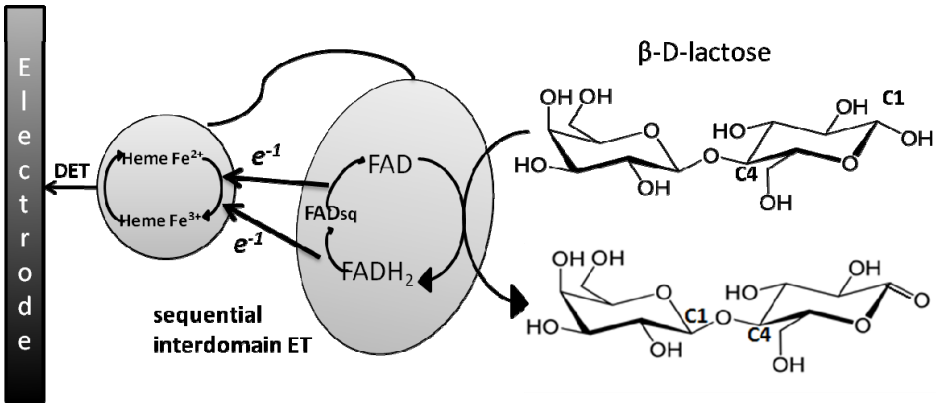

Fig. 2.8. Electron transfer from β-D-lactose *via* CDH to an electrode in the DET mode

To accomplish DET between redox enzymes and the electrode surface is of great significance in the design of BFC. It diminishes the potential loss caused by the mediated component and simplifies the prototype cell design, as no separation membrane is required to prevent the cross-over of the anodic and cathodic mediators if they are in diffusive form. This is crucial for achieving a stable, long-term operation of BFC. However, the main challenges for DET type biocatalysis are the comparatively low catalytic efficiency (low turnover rate) of enzymes undergoing DET and insufficient use of the overall enzyme dosage (the proportion of enzyme molecules with the 'preferred orientation' on an electrode surface for DET is still small). In terms of the power output performance of BFCs, the DET type biocatalysis configuration is typically less competitive than the MET type biocatalysis configuration.

2.4.3 MET

Another approach to facilitate electron transfer in an enzyme electrode is to mediate electron transfer (MET), in which a redox couple is introduced as a mediating component into the electrode configuration to shuttle the electrons between the enzyme active site and the electrode surface. One of the benefits of using redox mediators is the enhanced electron transfer rate between the enzyme active site and the electrode surface; this is because the enzyme molecules do not need to interact directly with the electrode surface. Depending on the enzyme and the reaction conditions, the rate of MET type biocatalysis can be several orders of magnitude greater than that of DET type biocatalysis (Barton et al., 2004). However, since additional electron transfer steps are introduced in MET, two aspects must be considered. One is that the kinetics of MET type biocatalysis has to consider the potential control over the relative concentrations of the oxidized and reduced mediator at the electrode surface, which are also affected by bulk mediator diffusion or mediator self-exchange. The other is the thermodynamic loss caused by the mediating component, which in practice compromises the reversible potential of a mediated biocatalytic electrode as a mixed potential between the redox potential of the enzyme active site and the redox potential of the mediator, but dominated by the mediator couple. By extension, the open circuit voltage (OCV) of a BFC comprising two MET type bioelectrodes is determined primarily by the difference between the redox potentials of the two mediator couples (there is no crossover of mediators taking place between the anodic and cathodic compartments). The potential components for a mediated glucose/O_2 BFC are shown in Fig. 2.9. In principle, the criteria for selecting an appropriate mediator for enzymatic catalysis are the following: the redox chemistry of the

mediator on the electrode has to be reversible; and the redox potential of the mediator should be thermodynamically favored in the electron transfer cycles and preferably sufficiently close to the redox potential of the enzyme active sites to minimize the potential loss caused by employing the mediating component, thus increasing the MET efficiency (Heller, 2003).

The mediator for biocatalysis can be either in a freely diffusional form in the electrolyte or co-immobilized with the enzyme in the enzyme electrode configuration. The expertise acquired from related biosensor research can be usefully applied to mediation for the redox enzymes used as biocatalysts in BFCs.

Among the possible diffusional mediators for cathodic enzymes (e.g., high redox potential laccases and BOD), the most widely used is 2,2'-azinobis(3-ethylbenzothiazoline-6-sulfonate) (ABTS) (Tsujimura et al., 2000; Barton et al., 2004). For the FAD-dependent anodic enzymes (e.g., GOx), the well-studied diffusional mediators include various ferrocene derivatives, N,N,N′,N′-tetramethyl-p-phenylenediamine, benzoquinone, and so on (Bartlett & Whitaker, 1987). Using ABTS as an example, the electron transfer steps in a biocathode catalyzed by laccase *via* MET are shown in Fig. 2.10 B. Despite the fact that the diffusional form of redox mediation is the most efficient approach for MET, the need to integrate semi-permeable membranes or similar technology to keep the mediator close to the electrode imposes limitations on its application in BFCs.

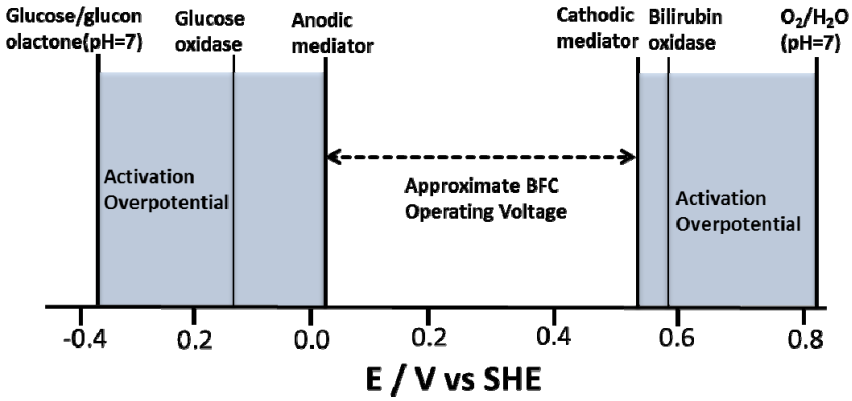

Fig. 2.9. Schematic diagram of the potential components in a MET type BFC. All potentials are specified *vs*. SHE (Barton et al., 2004) (Copyright permission with American Chemical Society)

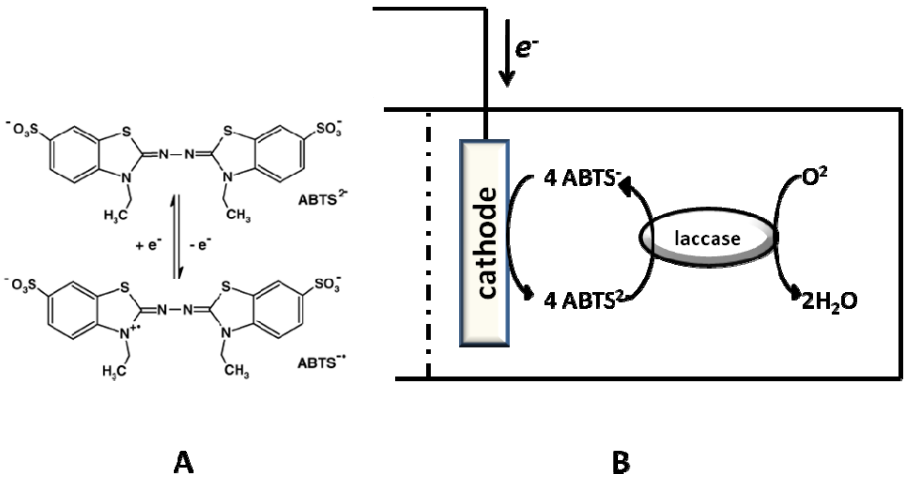

Fig. 2.10. (A) Chemical structure of ABTS; (B) Biocatalysis of laccase on reduction of O_2 mediated by ABTS in biocathode

MET can also be facilitated by immobilizing both enzyme and mediator in the enzyme electrode configuration, which generally requires polymeric materials. Different redox polymers have been used to carry the redox mediating moieties, including ferrocene polymers (Hodak et al., 1997; Deng et al., 2007), Os-polymers (Heller, 2003), and Nafion-N-methyl phenazium (Bartlett & Whitaker, 1987). Among these, the most successful approach for achieving effective biocatalysis is to use a redox hydrogel configuration incorporating the Os-polymers to 'wire' the enzymes. A more detailed discussion of this approach appears in Section 2.5.2.

2.5 Enzyme electrode configuration

The performance of an enzyme electrode is largely governed by the materials and the way they are assembled on the electrode surface (Sarma et al., 2009). The electrical efficiency of an enzyme electrode depends on both the electron transport properties of the mediator (in the case of MET) and the electron transfer steps occurring in the assembly. The immobilization of the enzyme on the electrode surface is crucial in determining the efficiency of the enzyme electrode. Different chemical, biochemical, or physical principles, such as chemical cross-linking using various cross-linkers (Heller, 2003), covalent binding of the enzyme to the functionalized electrode surface, cofactor-apoenzyme affinity (Willner et al., 1996) (Zayats et al., 2008) (Willner et al., 2009), entrapment or encapsulation within polymers (Cooney et al., 2008; Cosnier, 2008), and the formation of paste materials, are exploited to immobilize the enzyme on the electrode surface. Numerous enzyme electrode configurations have been proposed based on these enzyme immobilization strategies involving the integration of novel materials with interesting functionality. Research in materials science related to the development of enzyme electrodes has intensified over the past two decades and there is a large volume of literature on this topic. This section summarizes and classifies the various approaches for constructing enzyme electrodes.

2.5.1 Conducting polymers based enzyme electrode configuration for BFCs

Conducting polymers refer to the conjugated organic polymers that can be made electrically conductive by oxidation (p-doping) or reduction (n-doping) of the polymer

backbone. The conductivity of conducting polymers ranges from 10^{-9} to 10^{+5} S/cm, which bridges the conductivity gap between insulators and metals. Conducting polymers, which combine the properties of polymers and metals, are called 'synthetic metals' (Nobel Prize in Chemistry, 2000). They have a long history as the immobilization matrices for enzymes in biosensor applications, where they perform signal transduction and act as a supporting matrix for enzyme immobilization (Bartlett & Birkin, 1993; Gerard et al., 2002; Vidal et al., 2003; Malhotra, et al., 2006).

Conducting polymers are good candidates as the supporting matrices for the enzyme immobilization, due to their electron-conductive and easily processable properties. They can be synthesized by polymerizing the corresponding monomers, either by chemical polymerization or by electropolymerization. In chemical synthesis, a strong oxidant or reductant is used to polymerize the monomer followed by doping. In electro-chemical synthesis, potential or current is applied to induce the oxidation or reduction of the monomer on the surface of a working electrode, dipped into a solution containing the monomer and the desired dopant ions. Conducting polymer films can be directly fabricated on the working electrode under mild working conditions and the ease of regulating the conducting film characteristics, including film growth over the conductive materials, film morphology, and thickness, is acknowledged. Electropolymerization also permits the entrapment of biological moieties (enzymes, antibodies, and even whole living cells) and other reagents necessary for the relevant biochemical reactions (co-enzymes and mediators) in the polymer structure close to the electrode surface. Moreover, in some cases, the electrical conductivity of conducting polymers allows DET between the electrode surface and the biocatalyst which have been incorporated. The chemical structure of the monomer can be functionalized by introducing functional groups (e.g., –COOH or $–NH_2$); it makes it possible to immobilize enzymes in the conducting polymer through covalent binding.

The conducting polymers which have been extensively studied as matrices for enzyme immobilization include polyaniline (PANi), polypyrrole (PPy), polythiophene, and their amphiphilic derivatives (Gerard et al., 2002; Vidal et al., 2003). In the construction of BFC electrodes, both enzymes and mediators can be entrapped in the conducting polymers during polymerization as dopants or just by physical entrapment. Moreover, $ABTS^{2-}$ can be entrapped as counter ions during the polymerization of PPy *via* enzyme catalysis; this provides a possible approach for co-immobilizing the enzyme and the mediator inside the conducting polymer matrix (Fei et al., 2007). Notably, in PANi films incorporating horseradish peroxidase (Barlett et al., 1998), lactate dehydrogenase (Simon et al., 2002), or CDH (Trashin et al., 2009) and in a PPy film with immobilized quinohemoprotein alcohol dehydrogenase (Schumann et al., 2000), conducting polymers have exhibited electrochemical wiring ability to communicate electron transfer between the enzyme active sites and the electrode surface. In this thesis, electrochemically polymerized poly(3,4-ethylenedioxythiophene) (PEDOT) films, was studied as the enzyme immobilization matrix material due to the interesting properties of PEDOT films, e.g., high electrical conductivity and excellent inherent environmental stability of the oxidized states. The polythiophene derivative PEDOT, developed by Bayer AG research laboratories in Germany in the late 1980s, has a backbone structure (Fig. 2.11). It is reported to exhibit superior conductivity (ca. 300 S/cm) and be one of the most stable conducting polymers available at present (Groenendaal et al., 2000; Kros et al., 2001). It has also been found to promote the DET of GOx in two different enzyme electrode configurations (Kros et al., 2001; Thompson et al., 2010).

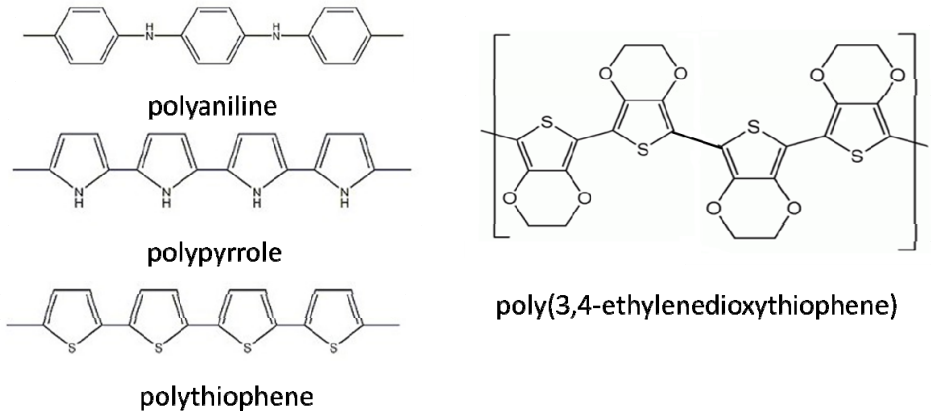

Fig. 2.11. Chemical structure of common conducting polymers

For enzyme electrodes in BFC applications, it is desirable to have a highly porous host matrix containing meso- or micro-pores, which give a large volumetric active surface area. The mass transport of the fuel inside the matrix structure is also a crucial factor determining cell performance. An optimal matrix structure for hosting enzyme molecules in an enzyme electrode configuration should thus achieve a balance between the requirements of two constraints: maximizing the active surface area and ensuring the efficient mass transport of fuel.

2.5.2 'Wired' enzyme redox hydrogel electrodes for BFC applications

The enzyme electrode configuration based on redox hydrogels containing Os^{2+}/Os^{3+} redox-centres is currently the best developed approach for constructing a mediated enzyme electrode. The first design of a 'wired' enzyme in the redox hydrogel configuration was introduced by Heller (Heller, 1990). Over the past two decades, this approach has been widely applied in biosensor and BFC research (Heller, 2003; Mano et al., 2003; Barton et al., 2004; Gao et al., 2010). The enzyme is incorporated into a cross-linked redox polymer hydrogel, producing a catalytic film that is permeable to ions. Redox polymer hydrogels consist of redox-active moieties, which contain coordinated $Os^{2+/3+}$ redox centres and are grafted onto a water-soluble polymer backbone. The electrons can diffuse through collisions between reduced and oxidized Os redox centres present in the hydrogel and then shuttle between the enzyme active sites and the electrode surface. Typically, such a redox hydrogel can be formulated upon complexing water-soluble poly (1-vinylimidazole) (PVI) or polyvinylpyrrolidone (PVP) with Os complexes and then cross-linking with water-soluble poly (ethylene glycol) diglycidyl ether (PEGDGE). When enzyme is integrated into a hydrogel, the electrostatic adducts of some enzymes and the cationic redox polymer can prevent the phase separation to avoid leaching, as opposed to the behavior of the small molecular mediators. When enzyme is immobilized in a redox hydrogel, all enzyme molecules are electroactive, irrespective of their orientation, which dramatically enhances the apparent enzyme activity. Another remarkable characteristic of this enzyme electrode configuration is that the electron transfer properties inside the hydrogel can be tailored by adjusting the synthetic routes. The redox potential of the Os complexes, the key parameter for the mediation of enzymes, can be tuned by engineering the ligands for the coordination of the Os^{2+}/Os^{3+} redox centres, based on the electron donor characteristics of the ligands. A library of Os-based redox mediator complexes has been compiled to provide appropriate mediator for a desired enzyme in the 6^{th} EU framework project BIO-MEDNANO (STRP 017350) (BioMedNano).

The transport of electrons through the redox polymer hydrogel can be measured in terms of the apparent electron diffusion coefficient D_{app}. The rate of electron collisions increases with the mobility of the tethered redox centres: the greater their mobility, the faster the electrons diffuse (Mano et al., 2006). In the construction of an O_2-consuming biocathode, a redox polymer containing eight-atom-long tethers between its redox centres and backbone (polymer I in Fig. 2.12) can form a hydrogel with a larger D_{app}, due to the increasing of the tether length. It is used to 'wire' laccase as the catalyst for the reduction of O_2. The redox hydrogel formed from polymer I has a 100-fold enhanced D_{app} compared to that for the hydrogel formed from the untethered redox polymer. The redox potential of the Os complex in polymer I is 0.55 V *vs*. Ag/AgCl, which brings the redox potential of the redox hydrogel close to that of the T1 Cu site of the high redox potential laccases and minimizes the potential gradient loss caused by the mediation of the biocatalysis (Mano et al., 2006). A miniature compartment-less glucose/O_2 BFC combining a GOx anode 'wired' by Os-redox polymer II (the redox potential is -0.19 V *vs*. Ag/AgCl) and a BOD cathode 'wired' by Os-redox polymer III (the redox potential is 0.34 V *vs*. Ag/AgCl) was reported to be able to operate in a living plant, a grape (> 30 mM glucose; pH 5.4). When the carbon-fiber biocathode was located near the centre of the grape, the power density was 0.47 $\mu W/mm^2$; when the carbon-fiber biocathode was near the skin of the grape, the power density was 2.4 $\mu W/mm^2$ (Mano et al., 2003a).

The 'wired' enzyme redox hydrogel configuration can be applied onto various electrical conductive materials or composites, such as carbon cloth (Barton et al., 2001), carbon fibers (Mano et al., 2006), porous microwires composed of assembled and oriented CNTs (Gao et al., 2010), or three-dimensional carbonaceous electrodes with interconnected hierarchical porosity (Flexer et al., 2010), to maximize the volumetric current output.

In **Paper IV**, six Os-polymers, whose redox potentials range over a broad potential window between +15 and +489 mV *vs.* NHE, were used to 'wire' *Gc*GDH onto spectrographic graphite electrodes for possible applications in biosensors and BFCs.

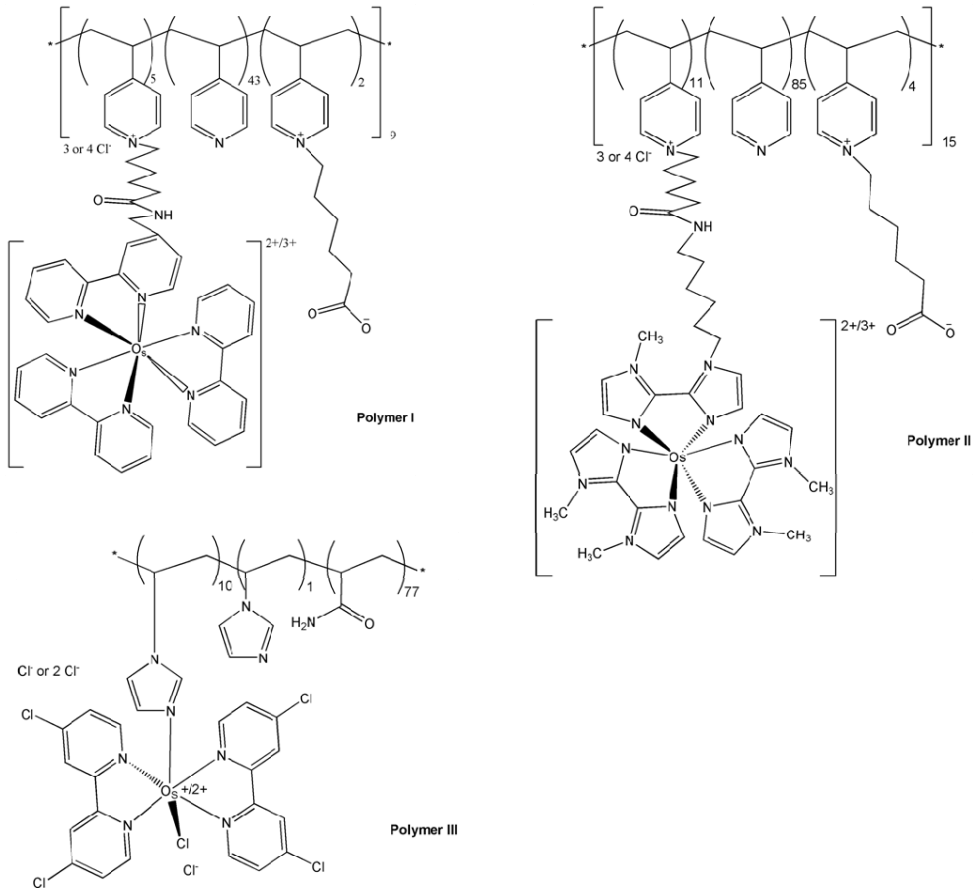

Fig. 2.12. Molecular structure of selected Os-redox polymers used in redox hydrogel enzyme electrode configurations.

2.5.3 Apoenzyme reconstitution approach for constructing enzyme electrodes

For many enzymes, the nondiffusible organic cofactors, such as FAD, haem, or PQQ, can be extracted by chemical methods or by biological manipulation from the active sites of the protein, thus producing the corresponding apoenzyme (Fruk et al., 2009). An intelligent approach to establish electrical contact between enzymes and electrodes is associated with 'apoenzyme reconstitution'. An artificial analogue of the native cofactor is chemically grafted onto the electrode surface to reconstitute the apoenzyme by utilizing the specific affinity between the cofactor and the apoenzyme. Usually, a redox molecular relay or nano-sized promoter (e.g., metallic nanoparticles or CNTs) is incorporated into the electrode configuration to bridge the electron transfer between the cofactor and the electrode surface. The 'apoenzyme reconstitution' approach to construct enzyme electrodes is illustrated in Fig. 2.13. It was first proposed by Willner and co-workers as a method for fabricating electrochemical sensors: the FAD cofactor was stripped from GOx and modified with a redox active ferrocene-containing group, and then the apoenzyme of GOx was reconstituted with these modified cofactors, which allowed site-specific positioning of the electron mediating unit in redox proteins and enhanced the electrical contact between the resulted enzyme and the electrode surface in a controlled and reproducible manner (Riklin et al., 1995). In addition

to the use of ferrocene-tethered molecular relays in enzyme electrode configurations (Katz et al., 1999), Au nanoparticles (AuNPs) (1.4 nm) (Xiao et al., 2003) and CNTs (vertically aligned with shortened length after acid treatment) (Katz & Willner, 2004; Patolsky et al., 2004) were further explored as metallic relays for electron transfer from the FAD in the reconstituted apoenzyme to the electrode surface. The 'apoenzyme reconstitution' paradigm was further extended to electrically 'wire' the PQQ-dependent GDH (Zayats et al., 2005), $NAD(P)^+$-dependent enzymes (e.g., malate dehydrogenase and lactate dehydrogenase) (Zayats et al., 2002), and haem-containing proteins (e.g., horseradish peroxidase) (Zimmermann et al., 2000). Another notable characteristic of this approach is the high electron transfer turnover rate of integrated enzyme electrodes. In the case of ferrocene-tethered molecular relays, the 'reconstituted apoenzyme' is superior to a protein randomly mediated by ferrocene relay units (Riklin et al., 1995); when the AuNPs are used as metallic relays, the electron turnover rate of the reconstituted bioelectrocatalyst is enhanced about seven-fold over the electron transfer rate from the cofactor site to the native O_2 acceptor for GOx (~700 s^{-1}) (Xiao et al., 2003). There are several comprehensive reviews on this topic (Willner et al., 2006; Zayats et al., 2008; Willner et al., 2009; Fruk et al., 2009). At present, the 'apoenzyme reconstitution' approach for constructing enzyme electrodes can be applied only for redox enzymes containing the nondiffusible organic cofactors, and no studies have been reported for the multicopper oxidase family.

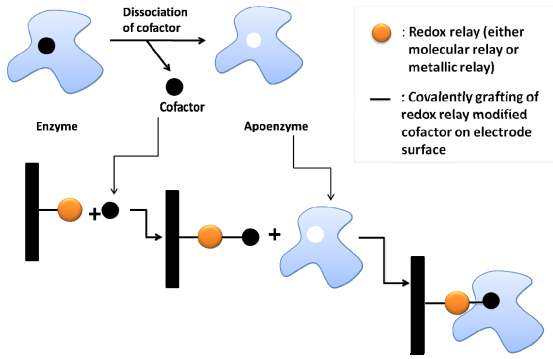

Fig. 2.13. Schematic diagram of the apoenzyme reconstitution strategy (Willner et al., 2006) (Copyright permission with Elsevier).

2.5.4 Nanostructured composite as platform for enzyme immobilization in BFCs

With the rapid advancement of nanotechnology, nanomaterial has taken a vital role in almost all areas of materials science research and applications. The integration of nanomaterial into the enzyme electrode configuration has proved to be successful. They are beneficial regarding several feasible functions, e.g., providing bio-compatible accommodation for the enzymes with extended lifetime of enzymatic catalysis, promoting the DET between enzyme active site and electrode surface, or enlarging the volumetric electroactive surface area to feasibly enhance the biocatalytic current density. The nanomaterials used in the enzyme electrode configurations range widely from nano-scaffolds of functionalized polymeric materials to sol-gel derived nanomaterials, and from carbonaceous materials featured with nanopores to carbon nanotube- or metallic nanoparticles-based composite materials. In the remaining discussion of this chapter, instead of too ambitious to make a complete summary of the present literature on the integration of nanomaterials into enzyme electrode configurations, several case studies are exemplified to illustrate the beneficial functions of nanomaterial on the enzymatic catalysis.

Functionalized polymeric materials with nano-structural features, such as hydrophobically modified chitosan and Nafion, have been explored as the accommodation scaffolds for the immobilization of enzymes. Klotzbach et al. (Klotzbach et al., 2006) reported that both hydrophobically modified nafion using quaternary ammonium bromides and hydrophobically modified chitosan with alkyl chains form micellar aggregates after being resuspended into alcohols; the micellar membranes formed from these polymers can effectively accommodate and stabilize the oxidoreductases. It was observed that the hydrophobic environment of these micellar polymers can increase the enzyme kinetics in the immobilized form than in the free buffer, whilst most immobilization methods (chemically binding enzyme to electrode surface or polymerization around enzyme) decrease enzymatic activity. The lifetime of the immobilized enzymes in the micellar polymer membrane is also greater than in buffers at room temperature (Klotzbach et al., 2006). Three-dimensional scaffolds were created from hydrophobically modified chitosan using a freeze drying approach. They possess a bimodal pore structure: a macropore structure on the order of tens of μm in diameter for fluid transport, and a lawn of amphiphilic mesopores of 10 to 12 nm lining the walls of the larger pores in which enzymes can be entrapped and stabilized. When compared to air-dried thin membrane electrodes made of the same starting material, the three-dimensional scaffold was shown to increase the power density (Klotzbach et al., 2008; Cooney et al., 2008).

It has been proposed that silica-based materials can be used to encapsulate enzyme and mediator simultaneously inside the mesopores of silica gel, which is deposited by a sol-gel process on metallic or carbon-based conductive electrode materials (Nogala et al., 2006; Zawisza et al., 2006). It is believed that the encapsulation process creates fluid microdomains permeable to O_2 and electrolyte, but its porous structure is sufficiently narrow to prevent the enzyme from leaching. Moreover, silica-gel can also protect the protein against denaturation when enzyme molecules are immobilized. Furthermore, the doping of conductive materials (e.g., CNTs) into silica gel, can promote the DET of encapsulated redox enzymes (e.g., BOD) as well as enhance the conductivity of the composite, which improves for enzyme electrode catalytic efficiency (Lim et al., 2007).

Carbonaceous materials featured with nanopores have been used successfully as immobilization platforms in enzyme electrode configurations for BFC applications. These materials, representatively referring to mesoporous carbon particles, functionalized graphite, or carbon fibers, typically offer large electrochemically active surface area and beneficial surface properties for the adsorption and retention of enzymes. Redox enzymes have been immobilized onto/into the carbonaceous structure through physical adsorption and exhibited DET properties in many cases. Ordered mesoporous carbon is synthesized from versatile precursors mainly using template-orientating approaches (Lee et al., 2006) and serves as a high-capacity host material with well-controlled pores for enzyme encapsulation (e.g., GOx) (Lee et al., 2005). In a successful BCF design by Kano and co-workers for a DET type, fructose/O_2 BFC, carbon black particles (Ketjen black particles with an average diameter of 40 nm) strongly adsorb fructose dehydrogenase in the bioanode, and the carbon aerogel particles (with an average pore size of 22 nm) adsorb laccase in the biocathode (Kamitaka et al., 2007). Without mediator, this BFC has an OCV value of 790 mV and a maximum power density of 850 $\mu W/cm^2$ (a current density of 2.8 mA/cm^2 at 410 mV cell voltage with stirring). It is one of the state-of-art designs for the DET type BFC (Kamitaka et al., 2007).

Due to their semiconductive behavior and high porosity, CNTs, the graphite allotropes of carbon, are by far the most widely used nanomaterials for the fabrication of electrodes (Karousis & Tagmatarchis, 2010; Dillon, 2010), and they are also suitable for application in enzyme electrodes (Katz & Willner, 2004; Wang, 2005). Metallic nanoparticles (e.g., AuNPs)

which can be synthesized *via* facile and versatile routes (Daniel & Astruc, 2004; Sardar et al., 2009), are able to promote effective DET from enzyme active sites to the electrode surface, making them attractive components for DET type enzyme electrode configurations (Tel-Vered & Willner, 2010). In fact, CNT- or metallic nanoparticles-based composite materials are the most thoroughly explored platform for enzyme immobilization in BFC applications, so the corresponding literature is extensive (Sarma et al., 2009). The main benefit of integrating CNTs or metallic nanoparticles into the enzyme electrode configuration is that they can promote the DET of redox enzymes. The composite materials can, for example, be formed from CNTs/conducting polymer (Cui et al., 2007), CNTs/polymeric materials (e.g., chitosan, cellulose derivatives, or polyelectrolyte) (Wen et al., 2007; Zhou et al., 2008; Wu et al., 2009), and AuNPs/conducting polymers (Tel-Vered & Willner, 2010). The surface activation possibilities *via* grafting functional groups onto CNTs or AuNPs (e.g., chemical grafting onto CNTs surface or modification by SAM of thiols on AuNPs surface), offer versatile strategies for the integration of redox enzymes into the enzyme electrode configuration *via* covalent binding, cross-linking, or adsorption through site-directed orientation of redox enzymes on the electrode surface (Willner & Katz, 2000). In common, the large surface area of these composite materials offered by their porous feature makes benefits for enlarging the enzyme loading and enhancing the catalytic current density generated by the enzyme electrodes.

3. Methods

This chapter describes the experimental techniques used for the electropolymerization of conducting polymers for enzyme immobilization, the characterizations of the biocatalysis of the enzyme electrodes, the evaluation of the performance of the BFCs incorporating a biocathode and a bioanode, and the structural and morphological characterizations of the materials in the enzyme electrode configuration. The main goal is to provide context for the results by establishing the underlying principles and rules of application of these techniques.

3.1 Electrochemical methods

Electrochemistry is fundamental in many processes including corrosion, battery, electroplating, electrosynthesis and those in biomedical applications. The basic reaction in electrochemistry is described symbolically as follows:

$$O_x + ne^- \rightleftharpoons R_{ed}, \tag{3.1}$$

where O_x and R_{ed} are the oxidized and reduced species, and n is the number of electrons involved. The potential of the electrode surface is then related to the standard potential of the redox reaction and the activities of the species involved in the conversion, as described by the *Nernst Equation* described (Bard & Faulkner, 2001):

$$E = E^{0'} + \frac{RT}{nF} \ln \frac{a_{ox}}{a_{red}}, \tag{3.2}$$

where $E^{0'}$ is the formal potential of the redox couple, R is the universal gas constant (8.313 J/mol·K), T is the absolute temperature (K), n is the number of electrons, F is the Faraday constant (96485 C/mol), and a_{ox} and a_{red} are the chemical activities of the species involved.

There are different approaches and techniques for studying the electrode reactions. The following sections describe the electrochemical methods used in this thesis, including voltammetry, amperometry, methods involving forced convection, and fuel cell performance evaluations.

3.1.1 Voltammetric measurements

Linear sweep voltammetry (LSV) employs a linear potential waveform: the potential is changed as a linear function of time. The rate of change of the potential with respect to time is referred to as the scan rate.

Cyclic voltammetry is one of the most versatile and commonly used electrochemical techniques. Cyclic voltammetry is an extension of LSV in that the direction of the potential scan is reversed at the end of the first scan (the first switching potential), and then the potential range is scanned again in the reverse direction. The experiment can then be stopped at the final potential, or the potential can be scanned past this potential to the second switching potential, where the direction of the scan is again reversed. Typically, CV analysis employs a three-electrode cell configuration, containing a working electrode (WE), a reference electrode (RE), and a counter electrode (CE). The potential is measured between the reference electrode and the working electrode; meanwhile, the current is measured between the working electrode and the counter electrode. A typical representation of cyclic voltammetry is depicted in Fig. 3.1. In the forward scan, the current increases as the potential reaches the oxidation potential of the analyte, but then it falls off as the concentration of the

analyte is depleted close to the electrode surface. A current peak is produced for any analyte which can be oxidized within the chosen potential range. As the applied potential is reversed, it reaches the potential that will reduce the product formed in the first oxidation reaction and produces a current of reverse polarity from the forward scan. Cyclic voltammetry is used to obtain information about the redox potential and electrochemical reaction rates of the compounds of interest.

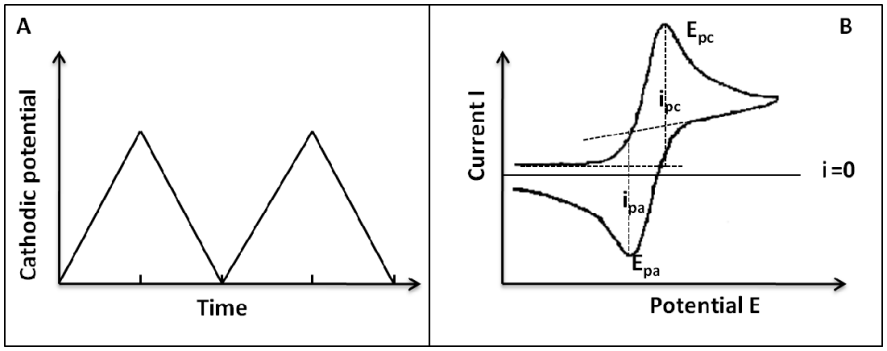

Fig. 3.1. A. Excitation signal: potential *vs*. time in CV; B. Cyclic voltammogram: current *vs*. potential

The important parameters obtained from a cyclic voltammogram are the anodic and cathodic peak potentials (E_{pa} and E_{pc}, respectively) and the anodic and cathodic peak currents (I_{pa} and I_{pc}, respectively). From the peak potentials, it is possible to estimate the degree of electrochemical reversibility of the redox process by analyzing $\Delta E = E_{pa} - E_{pc}$. The formal potential of the redox couple involved in the reaction can also be determined:

$$E^{0'} = \frac{E_{pa} + E_{pc}}{2} \quad . \tag{3.3}$$

In the case of a diffusion-controlled and reversible electron transfer process, the peak height is dependent on the analyte concentration C as expressed by the *Randles-Sevcik Equation*:

$$I_p = 0.4463\, nFAC \left(\frac{nFvD}{RT}\right)^{1/2} \quad , \tag{3.4}$$

where A is the area of the working electrode (cm^2), C is the analyte concentration (mol/cm^3), v is the scan rate (V/s), D is the diffusion coefficient of the analyte (cm^2/s), and *n, F, R, T* have their usual significance as described above for the *Nernst Equation* (3.2). The *Randle-Sevcik Equation* implies that the peak current should be linearly dependent on the square root of the scan rate.

In the case where the redox species are confined at the electrode surface, either by physical adsorption or by covalent bonding, the transport to or from the bulk of the solution for the electrochemical reaction to take place is omitted, so the diffusion dependence disappears. In the simplest case of *Langmuir* adsorption, the shape of the voltammogram is completely symmetric, with identical areas under the two waves, and the peak potentials satisfy $E_{pa} = E_{pc} = E^{0'}$. In this case, the peak current is proportional to v rather than to $v^{1/2}$.

In bioelectrochemistry, voltammetry is commonly used to detect the redox transformation of the redox sites on the electrode surface in the absence of enzyme substrate or to demonstrate the catalytic current response in the presence of enzyme substrate. In this thesis, CV was used in **Papers II** and **III** to detect the catalytic current response with O_2 as substrate in the biocathode. In **Paper IV**, CV was used to determine the redox potential of the immobilized (surface-confined) $Os^{2+/3+}$ centres in different PVI/or PVP-based redox polymers. In **Paper V**, CV was used to determine the redox potential of the haem moiety in *Ct*CDH in the absence of substrate and also the anodic catalytic current response of the immobilized *Ct*CDH on the oxidization of sugars (lactose or glucose); LSV was used to obtain the polarization curves for bioanodes and biocathodes and plots of power density *vs*. operating voltage for BFCs in different buffer solutions and physiological fluids.

3.1.2 Potentiometric measurements

Potentiometric measurements are made using a potentiometer to determine the difference in potential between a working (an indicator) electrode and a counter (a reference) electrode. Potentiometric measurement was used to determine half cell potentials of bioanode and biocathode.

3.1.3 Chronoamperometric measurements

Chronoamperometry (CA) is a simple electrochemical technique that is widely used in electropolymerization and electroanalysis. In CA, with a time-varying model potential, the current on the working electrode is recorded *vs*. time. Compared with CV, which measures the current response in a dynamic mode with scanning over a potential window, CA measures the transient current response under a specific potential until it reaches an equilibrium state. The current measured in this equibirium state is a net value which reflects all the oxidization and reduction processes occurring on the working electrode; hence, it is dependent on both the active surface area (number of active sites) and the diffusion rate of reactant to these sites or of reaction product from these sites. The polarization curves for bioanodes and biocathodes (*j*-*E* curves) were obtained by plotting the steady-state current recorded at each chronoamperometric step *vs*. the applied potential. In **Papers I to III**, single-step CA was used to electropolymerize the conducting polymer onto the supporting material to immobilize the enzyme, and multi-step CA was applied to evaluate the catalytic current density on the reduction of O_2, generated by laccase-based enzyme electrodes.

3.1.4 Hydrodynamic electrochemical measurements

To control the mass transfer to or from the working electrode surface, two main strategies can be applied: moving the electrode surface with respect to the solution, or moving the solution with respect to the electrode surface. Hydrodynamic methods are those which involve the convective mass transport of reactants and products, such as hydrodynamic amperometry and voltammetry.

A rotating disk electrode (RDE) is a hydrodynamic working electrode used in a three-electrode system, which rotates with inducing a flux of analyte to the electrode. The electrode, which includes a conductive disk embedded in an inert non-conductive polymer or resin, is attached to an electric motor that permits fine control of the rotation rate. This type of electrode is used in electrochemical studies investigating the reaction mechanisms related to redox chemistry. Ideally, a laminar flow of the solution is created by the rotation; then transported towards and across the electrode surface (Fig. 3.2). The flow rate can be controlled by adjusting the angular velocity of the electrode and modelled mathematically.

Thus, a reproducible mass transfer can be delivered by the convective flow, and a steady state is quickly established. The steady-state current is controlled by the solution flow rather than diffusion. In contrast, under still, unstirred experimental conditions, the steady-state current is limited by the diffusion of substrate.

The RDE is one of the few convective electrode systems for which the hydrodynamic equation and the convection-diffusion equation have been solved rigorously for the steady state (Bard & Faulkner, 2001). The *Levich Equation* (Eq. 3.5) applies to the mass transfer limited conditions at the RDE and predicts that $i_{l,c}$ is proportional to C_o^* and $\omega^{1/2}$.

$$i_{l,c} = 0.62\, nFAD_0^{2/3}\, \omega^{1/2}\, \upsilon^{-1/6} C_0^*, \tag{3.5}$$

where $i_{l,c}$ is the *Levich* current, A the electrode area, D_0 the diffusion coefficient, ω the angular rotation rate of the electrode, υ the kinematic viscosity, and C_0 the reactant concentration. Under non-limiting current-condition, the *Koutecký-Levich Equation* can be used to describe the current through the RDE (Eq. 3.6).

$$\frac{1}{i} = \frac{1}{i_K} + \frac{1}{i_{l,c}} = \frac{1}{i_K} + \frac{1}{0.62\, nFAD_0^{2/3}\, \omega^{1/2}\, \upsilon^{-1/6} C_0^*}, \tag{3.6}$$

where i_K denotes the current in the absence of any mass transfer effects. When i_K is very large, $i/\omega^{1/2}C$ is a constant. The graph of i *vs.* $\omega^{1/2}$ will be curved and tend towards the limit $i = i_K$ as $\omega^{1/2} \rightarrow \infty$. A plot of i^{-1} *vs.* $\omega^{-1/2}$ should be linear and can be extrapolated to $\omega^{-1/2} = 0$ to yield i_K^{-1}.

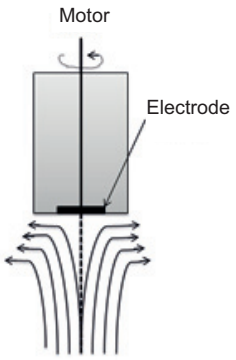

Fig. 3.2. Schematic diagram of the flow near an RDE under ideal conditions.

The equations above are valid for a two-dimensional, smooth electrode surface. In this situation, a laminar flow of the electrolyte can be created and transported towards the electrode surface by rotation, and theoretically the mass transfer to each active site is identical. When the electrode surface has a three-dimensional porous structure, the presence of micro cavities causes disturbances to the flow pattern, which then deviates from ideal laminar flow. The reactant does not have even access into reactive sites in the electrode structure, so a reactant concentration gradient is produced along the thickness of the electrode structure. Accordingly, the *Koutecký-Levich Equation* has limited validity for three-dimensional porous electrodes.

Flow injection analysis (FIA) using a wall-jet cell is another technique involving convective mass transport of reactants and products onto and across the electrode surface. An inert electrolyte solution is transported towards the surface of the WE using a peristaltic pump with a controllable flow rate, and the analyte of interest is injected into the flow stream and carried towards the electrode. The term flow injection analysis was introduced in 1975 by Ruzicka and Hansen (Ruzicka & Hansen, 1975; Ruzicka & Stewart, 1975), and, since then, this approach has been widely used in applications ranging across agriculture, food industry, and biochemical, clinical, and environmental analysis (Ruzicka & Hansen, 1988; Ruzicka & Hansen, 2008).

In this work, an FIA system with amperometric detection was used (**Papers IV and V)** to detect the catalytic current at the bioanodes from the oxidation of sugars (lactose or glucose). The convenience of FIA of being easy to manipulate the analyte concentration is taken advantage to obtain the calibration curves and pH profile for the bioanodes. A typical FIA system with amperometric detection consists of a pump with connection tubing, an injection valve, a flow-through electrochemical cell with electrodes controlled by a potentiostat, and a recorder. Fig. 3.3 is a schematic diagram of such a system, with a wall-jet electrochemical cell is included. Fig. 3.4 describes the construction of the cell, the laminar flow profile at the wall-jet electrode, and the typical response peak from the oxidation or reduction of analyte. The wall-jet cell consists of two counterparts, which can be screwed together. The upper counterpart contains the WE. The lower counterpart has a Pt wire that acts as a CE and a small chamber below the end of the inlet nozzle, which contains the RE (Ag/AgCl/KCl (0.1 M KCl)). The chamber communicates with the sample stream through four small holes situated around the inlet. The carrier solution passes through the injector at an optimal combination of the flow rate and the distance between the inlet nozzle and the WE, forming a laminar flow profile parallel to the surface of the WE (Fig. 3.4.b). A typical FIA system response is an asymmetric peak, with the height dependent on the analyte concentration. The shape of the peak is determined by the dispersion of the sample in the carrier solution during transport from the injection valve detector (Ruzicka & Hansen, 1988).

According to Yamada and Matsuda (Yamada & Matsuda, 1973), the limiting current in a wall-jet cell can be described by Eq. 3.7.

$$I_{lim} = 1.60\, knFD^{2/3} C_0\, v^{-5/12} a^{-1/2} r^{3/4} V_f^{3/4}, \tag{3.7}$$

where k is the cell constant, C_0 the concentration of the reacting species, v the kinetic viscosity of the solution, a the radius of the inlet capillary, r the radius of the disk electrode, and V_f the volume flow rate of the electrolyte; n, F, D are defined as above.

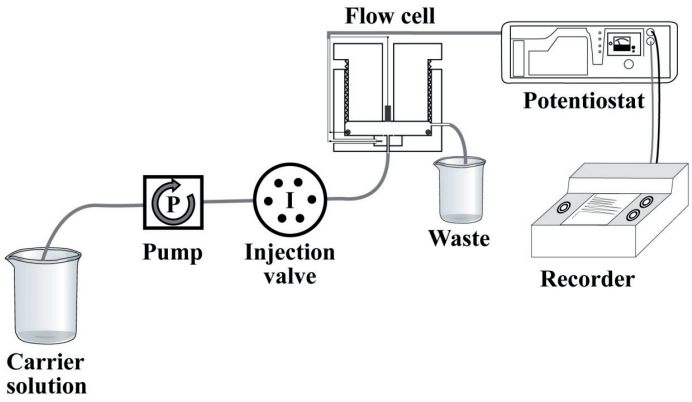

Fig. 3.3. Flow injection analysis set-up using a wall-jet amperometric electrochemical cell (Coman, 2009)

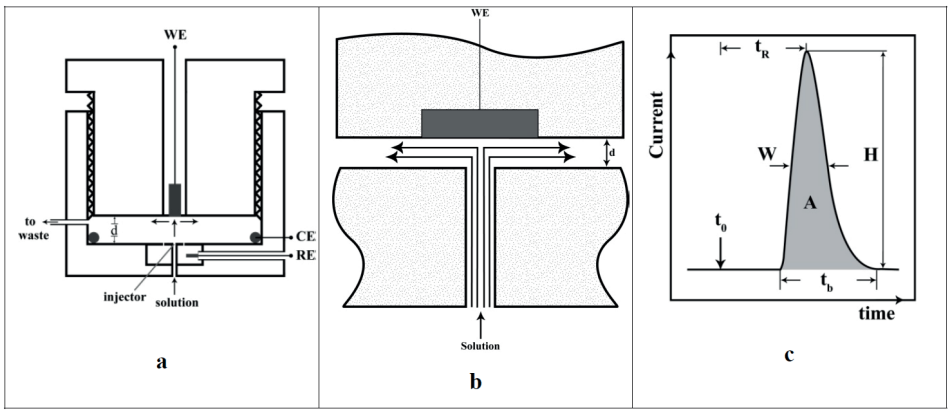

Fig. 3.4. a. Amperometric wall-jet cell: WE (working electrode), RE (reference electrode), CE (counter electrode), and d (distance of injector to WE); b. Laminar flow profile at the wall-jet electrode; c. Amperometric peak response: t_0 (injection time), t_R (residence time), t_b (peak width at the baseline), W (peak width at a selected level), H (peak height), and A (peak area) (Coman, 2009)

3.1.5 Electrochemical evaluation on BFC performance

In a three-electrode system, the catalytic performance of enzyme electrodes on the oxidation of sugars or the reduction of O_2 can be evaluated based on the polarization curves obtained with CA measurements (Section 3.1.2). Typical polarization curves for the bioanode and the biocathode are displayed in Fig. 3.5.A. Here, $E_{cathode}^{0}$ or E_{anode}^{0} refers to the initial active potential for the catalysis response of the biocathode or the bioanode, respectively. The potential difference between $E_{cathode}^{0}$ and E_{anode}^{0} determines the OCV of the BFC composed of these two electrodes. In the ideal case, the OCV is determined by the difference between the thermodynamic potentials of the fuel redox couple and the oxidant redox couple. In the case of a BFC, the measured OCV is the difference between the onset potentials for catalysis at the bioanode and biocathode. Once a current is drawn from the cell and work is performed, there is a rapid initial fall in voltage before a steady state is reached. For example, when a current '*a*' is drawn from the cell, the anode voltage drops to E_1, and the cathode voltage drops to E_2. The voltage difference between E_1 and E_2 is called the operating voltage under a specific

current draw. The magnitude of the current draw in BFCs is limited by the electrode with the lower electrocatalytic rate. A typical plot of cell current *vs.* cell voltage is shown in Fig. 3.5.B. The curve exhibits a characteristic shape, with three regions corresponding to the activation loss at low current density governed by the activation overpotential that arises from the kinetics of electron transfer reactions; the ohmic losses that arise from the resistance of the BFC, which depend on the materials used and the interfaces between enzyme and electrodes; and the concentration polarization at high current density, which depends on the mass transport (Cracknell et al., 2008). The cell power output can be calculated as *cell current* × *cell voltage*; the power output plot for BFC can be made by plotting either power density *vs.* cell voltage or power density *vs.* current density. A typical plot of power density *vs.* cell voltage for biofuel cell is shown in Fig. 3.5.C. Useful power is achieved at current and voltage values that are a compromise between the boundary cases of OCV and a short circuit.

Paper V evaluated BFC performance using a two-electrode system of connecting bioanode as the WE and biocathode as the combined RE and CE in a one-compartment electrochemical cell. The OCV value for the BFC was potentiometrically measured using the voltmeter. The cell current was recorded using the LSV approach at a very low scan rate (0.1 mV/s). The power density plot was obtained by plotting the derived power density (*cell current* × *cell voltage*) *vs.* the cell voltage.

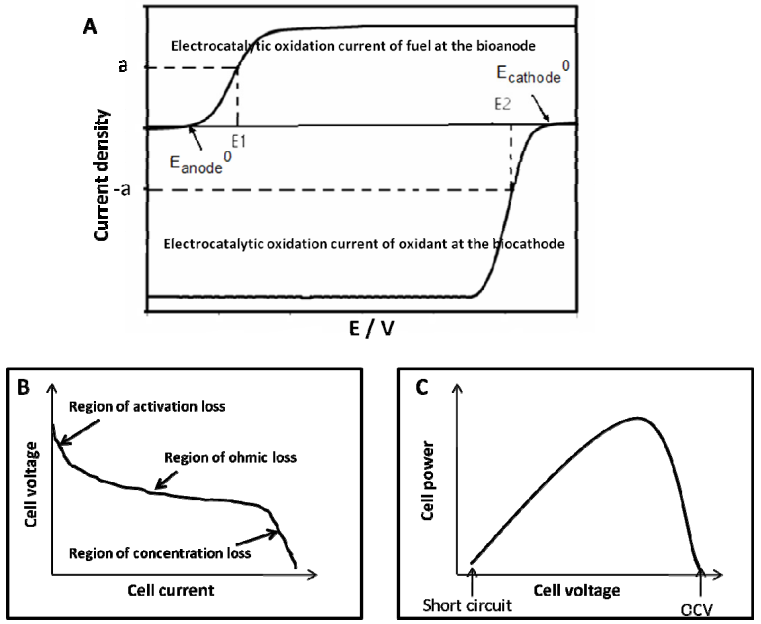

Fig. 3.5. A. Polarization curve for the bioanode or the biocathode (three-electrode system); B. Plot of cell voltage *vs*. current for BFC (two-electrode system); C. Power output plot (cell power *vs.* cell voltage) for BFC (two-electrode system).

3.2 Microscopic characterization

The surface morphology and topography are two key parameters in the characterization of the functional material surface. In **Papers I**, **II** and **III**, the morphology of the PEDOT films growing on the substrate was imaged and an elemental analysis of film was performed via energy dispersive X-ray analysis (EDXA). An SEM (LEO 1530 from LEO Electron

Microscopy Ltd) was connected to an image and X-ray analysis system (Vantage from ThermoNoran). In **Paper I**, the topography of the electrosynthesized PEDOT film was characterized using a Nanofocus μ Surf 3D, confocal white light microscope.

4. Results and discussion

This section discusses the main results of the present work. The thesis has been sub-divided as follows: biocathode construction (Section 4.1: MET type biocathodes and Section 4.2: DET type biocathodes), bioanode construction (Section 4.3: MET type bioanodes and Section 4.4: DET type bioanodes), and an implantable BFC demonstration project (Section 4.5).

4.1 MET type biocathodes

4.1.1 Screening accommodation matrices for *Th*L immobilization: tunable electro-polymerization of PEDOT on porous carbon-based substrates

Effect of counter ions on the morphology of PEDOT films

When the monomer 3,4-ethylenedioxythiophene (EDOT) is oxidized on the electrode surface by electropolymerization, the resulting PEDOT chains acquire positive charges, and the migration of counter ions from the electrolyte into the PEDOT film maintains the electroneutrality of the polymer. Variations in counterion species affect the structural features and morphology of the conducting polymers. Chloride (Cl^-) and nitrate (NO_3^-) were tested as representatives of small mobile anions and then compared with polystyrene sulfonate (PSS^-), a large immobile polyanion. In addition, CNTs were functionalized with carboxylic groups in an acid reflux treatment, and the negatively charged CNTs were introduced into the PEDOT film as dopant.

The SEM images in Fig. 4.1 show the influence of the dopant on the surface morphology of the PEDOT films. The PEDOT-Cl film possesses a looser and more open structure, compared with the denser PEDOT-NO_3 film and more compact PEDOT-PSS film. The fine structure of PEDOT-Cl exhibits flower-like morphology, consisting of numerous thin flakes (Fig. 4.1b). The fine structure of PEDOT-NO_3 exhibits fibrillar morphology (Fig. 4.1d). In contrast, the PEDOT-PSS film has a dense grain-like appearance (Fig. 4.1f). The SEM images of PEDOT-CNT in Fig. 4.2 show the presence of CNTs as dopant in the PEDOT film. The PEDOT-CNT film has an extremely rough, porous structure due to the incorporation of CNT.

Enzymes can be possibly immobilized into conducting polymer films by *in situ* entrapment during electropolymerization or by cross-linking. The open, porous structure observed for PEDOT-Cl and PEDOT-NO_3 should allow efficient fuel diffusion into the inner structure when these films are used for the construction of enzyme electrodes for BFCs. The structural features of PEDOT-CNT make it an attractive candidate since it meets the requirements for maximizing enzyme loading because of its large surface area and also benefits cell performance by improving the electronic conductivity of the film remarkably.

Morphology of PEDOT films on different carbon-based substrates

The morphology of an electrosynthesized PEDOT film on a solid substrate is also affected by the chemical and surface properties of the substrate. As an investigated example, PEDOT-Cl films were electropolymerized on a series of carbon-based substrates ranging from paper-like structures (e.g., carbon ink paper, carbon papers, and carbon felt) to a more three dimensional sponge-like structure (e.g., RVC foam). This was followed by an evaluation of the use of these substrates with PEDOT coating for the construction of enzyme electrodes for BFCs. More detailed results and discussion are presented in **Paper I.**

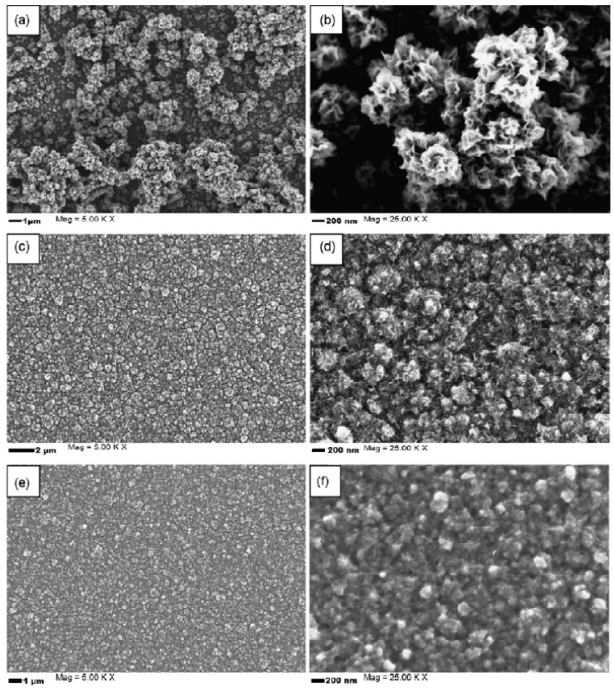

Fig. 4.1. SEM images of PEDOT-Cl (**a**, **b**), PEDOT-NO_3 (**c**, **d**), and PEDOT-PSS (**e**, **f**) films galvanostatically electropolymerized on indium-tin-oxide (ITO) glass. Magnification: × 5k (**a**, **c**, **e**); × 25k (**b**, **d**, **f**)

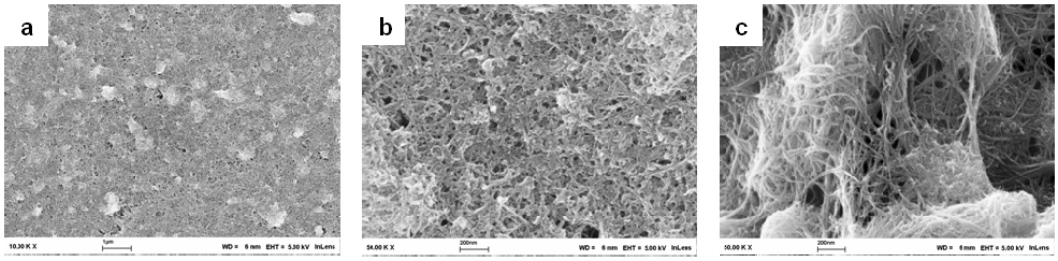

Fig. 4.2. SEM images of PEDOT-SWCNT film galvanostatically electropolymerized on ITO-glass. Magnification: × 10k (**a**); × 50k (**b**, **c**).

Electropolymerization in a pulse mode: for evenly distributed PEDOT deposition through a 3D porous structure

When electropolymerization of PEDOT-Cl was conducted potentiostatically at 0.95 V on a slice of RVC100ppi with a thickness of 2 mm, the SEM images from the cross section of the PEDOT-Cl/RVC 100ppi sample revealed that PEDOT grew mainly on the outermost skeleton. As shown in the EDXA elemental distribution mapping of the cross section, the characteristic elements S and Cl of PEDOT-Cl were located mainly on the outermost skeleton surface of the RVC foam (Fig. 4.3a). Apparently, the diffusion of monomer into the inner voids was so limiting that the monomer was polymerized on the outermost surface of the foam structure before it can diffuse into the inner structure. However, for enzyme electrode construction, a film evenly distributed over the entire porous structure would be preferable

since the motivation for using RVC foam as a substrate material is to exploit its large surface area/volume ratio.

To obtain a more even polymerization, electropolymerization was conducted in a pulse mode. The open circuit potential was applied for a shorter time between every two electropolymerization steps. The purpose of was to even out any monomer concentration gradient formed by allowing the monomer solution to diffuse into the foam voids during the rest period, subsequently followed by a period of potentiostatic electropolymerization. A relatively low polymerization potential (0.915 V) was applied to obtain a low polymerization rate; that made it possible to achieve a balance between the oxidation of the monomer on the outermost surface and its migration into the inner voids. The EDXA elemental mapping of the cross section of the sample obtained in a pulse mode showed a substantially enhanced polymer growth in the inner foam voids, as confirmed by the even distribution of the characteristic elements S and Cl (Fig. 4.3b).

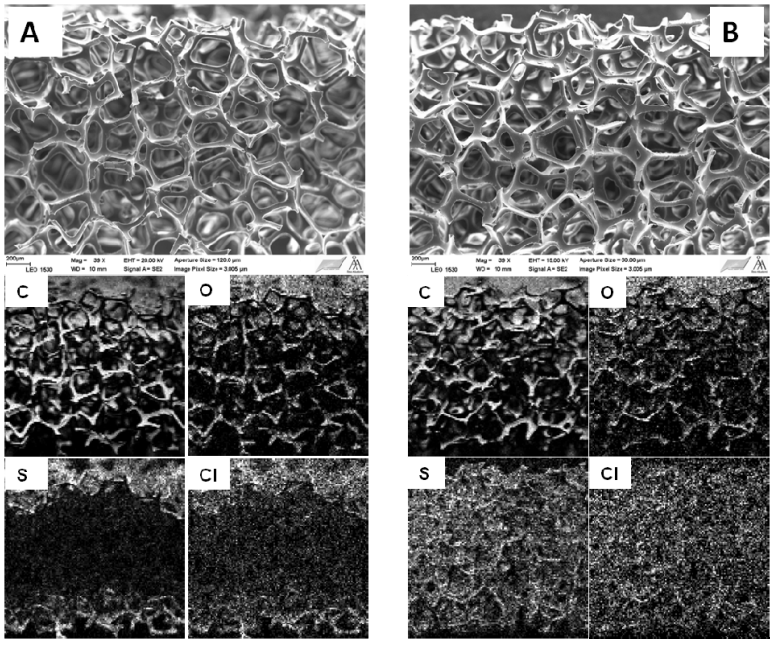

Fig. 4.3. SEM images of a cross section of PEDOT-Cl/RVC 100ppi and EDXA elemental distribution mappings for a cross section of RVC 100ppi coated with PEDOT-Cl film generated by potentiostatic electropolymerization (A) and by pulse mode electropolymerization (B)

4.1.2 Biocathodes manufactured by *in situ* entrapment of *Th*L in PEDOT films generated on RVC foams

Enzymes can be immobilized into conducting polymer films by *in situ* entrapment during electropolymerization. To maximize enzyme loading on the electrode surface, it is desirable to use a highly porous host matrix containing mesopores or macropores for the electrodeposition of conducting polymer; this type of matrix provides a large ratio of active surface area per unit-cross section. The mass transport of fuel inside the matrix structure is also a crucial determinant of the cell performance. Accordingly, an optimal matrix structure

for hosting enzyme molecules should thus balance the requirements of two constraints: maximizing the active surface area and ensuring the efficient mass transport of fuel or oxidant. The strategy presented in **Paper II** is based on fine-tuning the PEDOT film structure generated on porous RVC foam to create a composite structure with pores on different size scales: the mesoporous structure of CP films, and the macroporous structure of the carbon-based substrate.

In situ entrapment of *Th*L in a PEDOT film during electropolymerization: biocatalysis on the reduction of O_2 via a MET pathway

In situ entrapment of *Th*L in PEDOT films is used to immobilize enzyme in the construction of biocathodes. For electropolymerization, a pH = 6 buffer solution was employed as the electrolyte to keep *Th*L negatively charged (the PI value of *Th*L is around pH = 4.7), and 0.05 M KNO_3 was added as a supporting electrolyte to increase the ionic conductivity, since the concentrations of *Th*L were comparatively low. However, to prevent the total replacement of nitrate by *Th*L as counter ions in the PEDOT film, high concentrations of KNO_3 were avoided.

The immobilized *Th*L exhibited catalytic activity for the reduction of O_2, as suggested by the CVs shown in Fig. 4.4a. When *Th*L was present in the electropolymerization electrolyte, in the potential range of 0-0.4 V, a larger cathodic current was obtained, compared with the plain PEDOT film. Since *Th*L is entrapped as a dopant in the polymer film, the amount of entrapped *Th*L is dependent on the amount of PEDOT polymer generated on the support. This was verified by CVs of PEDOT films with entrapped *Th*L, generated using varying amounts of charge in the electropolymerization (Fig. 4.4b). Increasing the amount of charge increased the cathodic current, suggesting that more *Th*L is entrapped in the PEDOT films when more polymers are produced. These films also demonstrated larger catalytic capacities for the reduction of O_2.

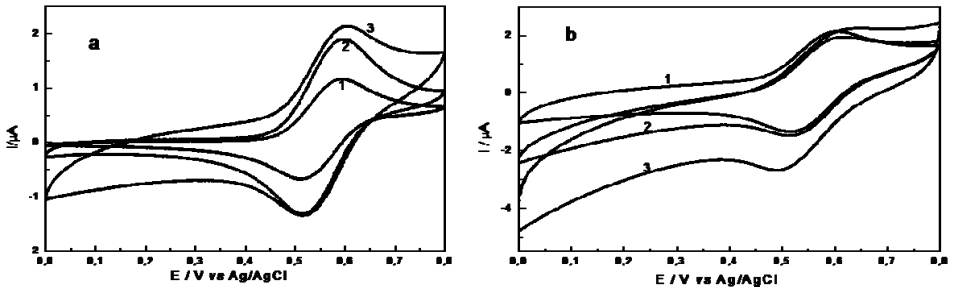

Fig. 4.4. a. CVs of (1) a glassy carbon (GC) electrode; (2) PEDOT film (1 mC) on a GC electrode; and (3) PEDOT film (1 mC) with *Th*L entrapment on a GC electrode. B. CVs of PEDOT film with *Th*L entrapment generated on a GC electrode: (1) 1 mC; (2) 2.5 mC; (3) 5 mC. Electrolyte: 0.05 M, pH = 4.5 succinate buffer containing 0.2 mM ABTS. Scan rate: 25 mV/s.

Biocathode RVC 100ppi/ PEDOT-NO_3/*Th*L: fine-tuning the electrochemical performance

The amount of polymer generated and the concentration of enzyme in the electropolymerization electrolyte are the dominant parameters affecting the performance of a biocathode using entrapped *Th*L as the biocatalyst.

Biocathodes were manufactured by electrochemically depositing 100 mC·cm^{-3} PEDOT film on RVC 100ppi with varying *Th*L concentration in the electrolyte solution. The catalytic performance of the resulting biocathodes for the reduction of O_2 was examined using CA measurements. Fig. 4.5a shows the polarization curves for the different biocathodes. In the absence of enzyme (curve 1), no distinct reduction current was observed, except that from the reduction of $ABTS^{2-}$. In curves 2, 3, and 4, which correspond to varying concentrations of *Th*L, apparent cathodic currents were detected, resulting from the reduction of O_2 catalyzed by *Th*L. The reduction of O_2 occurred at a potential of 0.66 V and levelled off at 0.45 V. In addition, the plateau value of the cathodic current density increased gradually with increasing enzyme concentration in the electrolyte. With 19.5 µg/ml of *Th*L, the highest concentration used in the experiments, the biocathode produced a steady current density, reaching above 1 mA·cm^{-3} at 0.45 V. The current density is here reported *vs*. the volume of RVC foam electrode.

The charge used for the electropolymerization was varied during the manufacture of the biocathode, while the concentration of *Th*L (7.8 µg/ml) in the electrolyte was kept constant. The amount of charge used in the electropolymerization is a parameter which directly reflects the PEDOT film thickness. Fig. 4.5b displays polarization curves for films produced with different amounts of charge. When the charge density was less than 110 mC/cm^3, the biocathodic current density increased gradually as more polymers were generated on the RVC foam. However, the current density did not change notably when the charge density exceeded 110 mC/cm^3. Hence, the thickness corresponding to a deposition charge density of 110 mC/cm^3 can be considered a critical point; within this thickness, O_2 can successfully diffuse into the film and interact with the active centre of the *Th*L immobilized in the PEDOT film.

The working pH profile and storage stability tests for the biocathode RVC 100ppi/ PEDOT-NO_3/*Th*L were determined by CA measurements. The catalytic performance of the biocathode was extremely sensitive to variations in pH, and the optimal working pH was around 4.2. The biocathode retained 80%, 50%, and 30% of its catalytic activity after storage in a +4°C buffer solution for 1 day, 1 week, and 1 month, respectively.

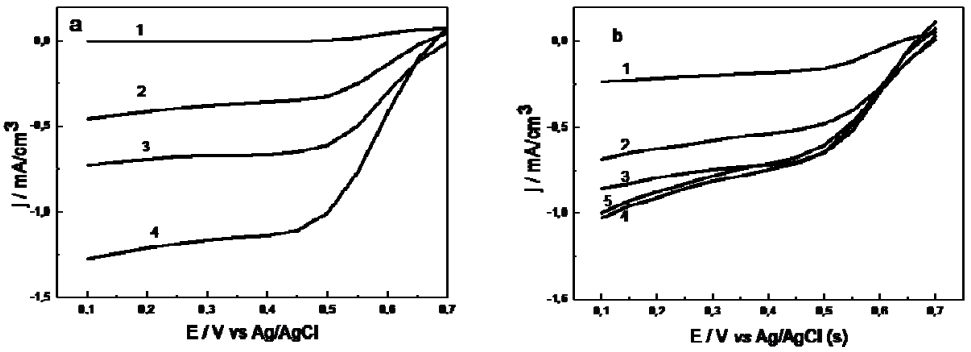

Fig. 4.5. a. Polarization curves for biocathodes manufactured on RVC 100ppi. *Th*L concentration in the electropolymerization electrolyte: (1) 0 µg/ml; (2) 3.9 µg/ml; (3) 7.8 µg/ml; and (4) 19.5 µg/ml. Charge used during the electropolymerization: 100 mC/cm^3. Electrolyte: pH = 4.5, 0.05 M succinate buffer containing 0.2 mM $ABTS^{2-}$. b. Polarization curves for biocathodes manufactured on RVC 100ppi. Charge used during the electropolymerization of PEDOT films: (1) 55 mC/cm^3; (2) 83 mC/cm^3; (3) 110 mC/cm^3; (4) 167 mC/cm^3; and (5) 550 mC/cm^3. The *Th*L concentration in the electropolymerization

electrolyte was 7.8 µg/ml. Electrolyte: pH = 4.5, 0.05 M succinate buffer containing 0.2 mM $ABTS^{2-}$.

4.1.3 Evaluation of the suitability of *Th*L catalyzed PANI inks for use in biocathodes

PANI-based ink was chosen as another matrix material for *Th*L immobilization, as *in situ* entrapment of *Th*L in a PANI matrix can be achieved during the laccase activated polymerization of aniline using a chemical batch reactor method. The ability of laccase to catalyze the chemical synthesis of water-soluble conducting PANI has been reported (Karamsshev et al., 2003; Streltsov et al., 2009). This enzymatic approach is an environmentally friendly alternative for the synthesis of PANI, because it operates under much milder conditions than traditional chemical polymerization, which uses high concentrations of strong acids. The predominat advantages of *Th*L-containing PANI ink are its printability, ease of scalability, and mass processability on paper or cardboard-based template materials. In this work, *Th*L-containing PANI inks were initially evaluated in terms of their suitability for the construction of BFC biocathodes. The integration of these PANI inks into the printed BFC assembly as a printed biocatalytic layer, which was independently tested by our collaborators in the Finnish-Tekes project Tekes-PEPSic (1681/31/07), is beyond the scope of this thesis.

Electrochemical evaluation and characterization of biocathodes made of PANI ink containing *Th*L

Two PANI inks with different *Th*L dosages in the synthesis bath were tested for use as biocatalysts for O_2 reduction. The biocathodes were manufactured by applying PANI ink containing *Th*L (PANI ink 1 or 2) to a carbon paper template disk (GDL35 AA). The current density generated by the biocathode was greater for PANI ink 2 than for PANI ink 1 due to the larger dosage of *Th*L in PANI ink 2. Different amounts of PANI ink 2 were applied to the carbon paper template, and the response of the resulting biocathodes was measured. As shown in Fig. 4.6, the current density generated by the biocathodes increased as the amount of PANI ink 2 applied to the GDL35 AA disk was increased.

Furthermore, *Th*L immobilized into PANI ink retains its catalytic activity for the reduction of O_2 into water, as suggested by the CVs for such a biocathode under an Ar or O_2 atmosphere (Fig. 4.7). The current density of the resulting *Th*L-containing biocathode can be controlled by adjusting the *Th*L concentration in the PANI ink and the amount of PANI ink used. It can be concluded that *Th*L activated polymerization of PANI can be used to immobilize laccase in the construction of biocathodes. However, partial dissolution of PANI ink from the electrode surface into the aqueous phase of the electrolyte was observed during the measurements. So its applications in large volume BFCs would be limited; it is more suitable for the printable thin-layer BFC design proposed in the Finnish-Tekes project PEPSic (1681/31/07).

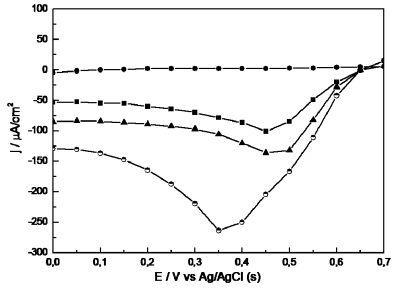

Fig. 4.6. Polarization curves for biocathodes manufactured on carbon paper GDL35 AA (disk diameter 5 mm) by applying different amounts of PANI ink 2 to the carbon paper template. The amount of PANI ink 2 applied was (●) 0 µl; (■) 2.5 µl; (▲) 7.5 µl; and (◓) 10.0 µl. Electrolyte: pH = 4.5, 0.05 M succinate buffer containing 0.2 mM $ABTS^{2-}$.

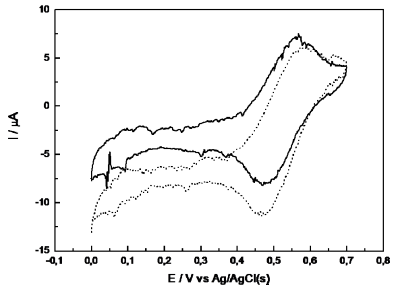

Fig. 4.7. CVs for a biocathode manufactured on carbon paper GDL35 AA (disk diameter 5 mm) by applying 2.5 µL PANi ink 2. Electrolyte: pH = 4.5, 0.05 M succinate buffer containing 0.2 mM $ABTS^{2-}$. The CVs were obtained under an Ar (solid line) or O_2 (dashed line) atmosphere.

4.2 DET type biocathodes

4.2.1 DET of *Th*L adsorbed on CNT-modified electrodes

Integration of nano-sized constructive components into enzyme electrode construction is a widely applied strategy for promoting DET between the enzyme and the current collector. CNT is a remarkable one, which has been reported in numerous cases functioning as the promoter for the pronounced DET between the enzyme and the electrode surface. The ability of CNT-modified electrodes to promote electron transfer has been documented in connect with the bridging effect of CNTs between the enzyme active centres and the electrode surface (Ivnitski et al., 2007). The DET of laccase via CNTs has been investigated in a few studies (Zheng et al., 2006; Zheng et al., 2008). In the present work, DET type biocatalysis of *Th*L was achieved on a GC electrode, promoted by multi-walled CNTs (MWCNs), and an electrode design based on the adsorption of *Th*L on MWCNTs was evaluated for use as an oxygen-consuming biocathode.

Chemical oxidation and fuctionalization can dramatically increase the stability of MWCNTs suspension. Nitric acid reflux treatment is well-adapted approach for the purification and chemical modification of CNTs (Tchoul et al., 2007; Datsyuk et al., 2008). When MWCNTs were treated in 3 M HNO_3 by refluxing, the defect sites, which are normally located at the tube ends and occasionally on the sidewalls, were primarily attacked. The carbon atoms were oxidized mainly into oxygen-containing functional groups, like carboxylic, hydroxyl and carbonyl moieties, which improve the solubilization of the nanotubes. In the reflux treatment, CNTs may also be cut when active sites on the sidewall are attacked by the oxidizer; shortened tubes are terminated with carboxylic acid groups at the ends. The presence of carboxylic groups on MWCNTs was confirmed by FT-IR, which detected stretching bands of –C=O at 1710 cm^{-1} in the spectrum (data not shown).

*Th*L-MWCNT/GC and Nafion/*Th*L-MWCNT/GC enzyme electrodes were prepared as follows: 1.2 mg MWCNT sample was dispersed into 450 µl Milli-Q water to form a homogenous suspension using ultrasonication. Then, 450 µl MWCNT dispersion was mixed with 50 µl 3.9 mg/ml *Th*L stock solution (the enzyme activity of *Th*L in stock solution is 421 U/ml on ABTS at pH 4.5), and this black suspension was stirred using a magnet for 3 h and kept overnight at +4°C to achieve equilibrium for the adsorption of *Th*L onto MWCNTs. Next, 10 µl of MWCNT/*Th*L was placed on top of a GC electrode and kept in ambient atmosphere until it was dried. This electrode was called *Th*L-MWCNT/GC. The active unit of laccase on such an enzyme electrode is 0.42 U. After that, a 1:4 Nafion solution was prepared by mixing 1 volume of 5 wt% Nafion ethanol solution and 4 volumes of Milli-Q water. A1:8 Nafion solution and a 1:16 Nafion solution were prepared in the same manner. Then, 10 µl of the diluted Nafion solution was placed on top of the *Th*L-MWCNT/GC electrode and dried to form a capping layer. The enzyme electrode capped with Nafion film was called Nafion/*Th*L-MWCNT/GC

O_2 reduction catalyzed by *Th*L adsorbed on MWCNTs via DET.

For an MWCNT/GC electrode, the CV under O_2 almost coincided with the CV under Ar, which implies that no reduction of O_2 occurred on the MWCNT-modified electrode surface in the absence of laccase (Fig. 4.8.a). The wide redox peaks observed around 100 mV could be attributed to the redox process of the oxygen-containing groups on MWCNTs.

For a *Th*L-MWCNT/GC electrode, no redox peaks corresponding to the redox transition of Cu sites in *Th*L were found on the CV under anaerobic conditions (dashed line in Fig. 4.8.b). Zheng et al.(Zheng et al., 2006) observed a pair of well-defined voltammetric peaks for the T1 Cu site of *Tv*L on a CNT-modified GC electrode, with a formal potential of +0.53 V *vs*. SCE; this constitutes direct proof that CNTs promote the DET of laccase. In this thesis, failure to observe the redox transition peaks for the Cu sites of *Th*L was probably due to interference from the large capacitive current from the MWCNTs in the enzyme electrodes. As shown in the voltammogram performed under an O_2 atmosphere (solid line in Fig. 4.8.b), an apparent cathodic shift was initiated at 0.70 V *vs*. Ag/AgCl (s). Hence, MWCNTs promote the DET of *Th*L on an MWCNT modified GC electrode by orienting the *Th*L in a DET-preferable manner on the MWCNT surface (Fig. 2.7.B).

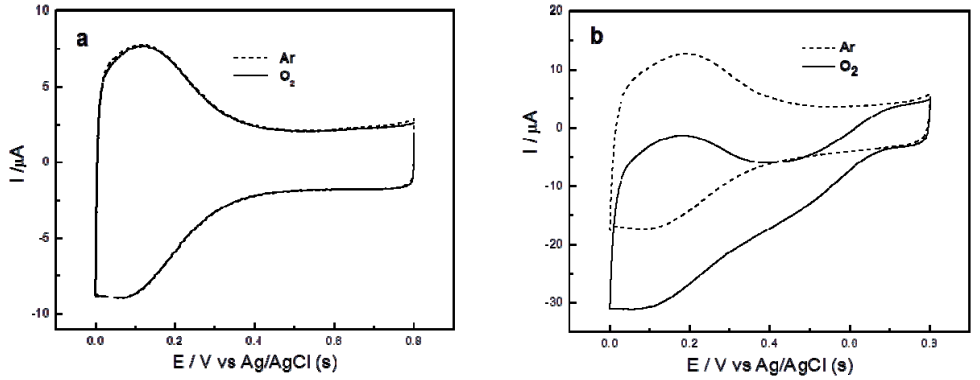

Fig. 4.8. CVs for enzyme electrode a. MWCNT/GC: 10 µl 2.5 mg/ml MWCNTs on a GC electrode; b. *Th*L-MWCNT/GC: 10 µl mixture of 2.5 mg/ml MWCNTs and 0.39 mg/ml *Th*L on a GC electrode. Measurements were performed under an Ar atmosphere (dashed lines) and under an O_2 atmosphere (solid lines). The electrolyte for all the measurements was 0.05 M, pH = 4.5 succinate buffer and the scan rate was 10 mV/s.

Electrochemical characterization of Nafion/*Th*L-MWCNT/GC enzyme electrodes

Nafion film was introduced as a capping layer to strengthen the binding of MWCNTs and to diminish the leakage of *Th*L from the electrode structure. Nafion films with varying thickness resulting from different concentrations of Nafion solution were evaluated to determine their effect on the catalytic performance of the enzyme electrode, as characterized by the *j-E* curves in Fig. 4.9.a. When the capping layer from 1:4 Nafion solution or 1:8 Nafion solution was formed on the enzyme electrodes, the catalytic current from the reduction of O_2 decayed completely (curves 3 or 4 compared with curve 1 in Fig. 4.9.a). Probably, this was the denaturing or inhibition caused by the alcohol concentration variations in casting solution. The use of Nafion film from 1:16 Nafion solution made it possible to achieve a compromise, causing only partial loss of apparent *Th*L activity while preventing enzyme leakage. Under a potential of 0.1 V *vs.* Ag/AgCl (s), *Th*L-MWCNT/GC and Nafion/*Th*L-MWCNT/GC produced current densities of 140 µA/cm^2 or 40 µA/cm^2, respectively.

With 1:16 Nafion film as a capping layer, concentrations of 0.195 mg/ml, 0.39 mg/ml, 0.585 mg/ml, or 0.78 mg/ml *Th*L, were used to test the effect of *Th*L concentration on the catalytic performance of the Nafion/*Th*L-MWCNT/GC enzyme electrode. Greater catalytic reduction current was observed in the CA response with increasing *Th*L concentration as shown in Fig. 4.9.b. It reached a plateau when the *Th*L concentration was above 0.585 mg/ml. This might be attributed to the adsorption mechanism of *Th*L on MWCNTs or to the limited proportion of MWCNTs which have the orientation appropriate for facilitating the DET.

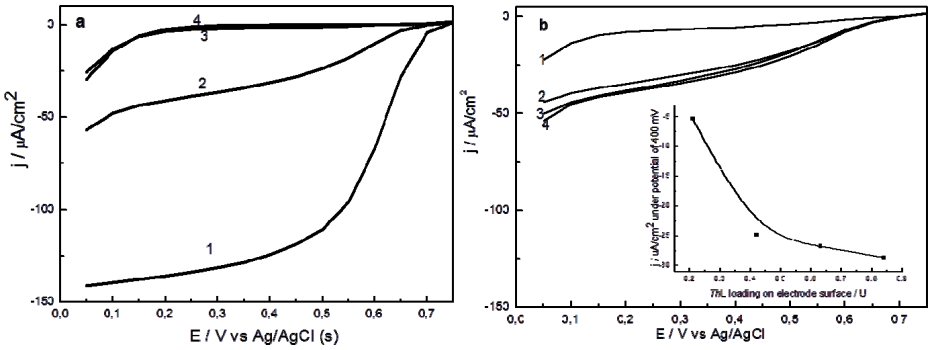

Fig. 4.9. a) *j-E* curves for the O_2 reduction catalyzed by *Th*L via DET in Nafion/*Th*L-MWCNT/GC electrodes with Nafion film of different thicknesses. (1) *Th*L-MWCNT/GC; (2) Nafion(1:16)/*Th*L-MWCNT/GC; (3) Nafion(1:8)/*Th*L-MWCNT/GC; (4) Nafion(1:4)/*Th*L-MWCNT/GC. b) *j-E* curves from O_2 reduction catalyzed by *Th*L via DET in Nafion(1:16)/*Th*L-MWCNT/GC electrodes with different amounts of *Th*L. *Th*L: (1) 0.21 U; (2) 0.42 U; (3) 0.63 U; (4) 0.84 U. Insert: Catalytic current density generated by Nafion(1:16)/*Th*L-MWCNT/GC electrodes under a potential of 400 mV *vs.* *Th*L loading on the electrode surface. The electrolyte for all measurements was 0.05 M, pH = 4.5 succinate buffer, which was thoroughly purged with O_2 before the measurements.

4.2.2 DET of *Th*L confined in a dual-layer-architecture of PEDOT films

DET type biocatalysis of *Th*L was also accomplished in a conducting polymer-based enzyme electrode configuration: confinement of *Th*L in a well-designed dual-layer-architecture of PEDOT films. A PEDOT film with NO_3^- as the counter ions (PEDOT-NO_3) was deposited as an accommodation layer on a GC electrode *via* electropolymerization, enzyme (*ThL*) was cast on top of this layer, and then PEDOT film with PSS^- as the counter ions (PEDOT-PSS) was subsequently electrodeposited as a capping layer to entrap *Th*L between the PEDOT layers. The resulting enzyme electrode promotes DET between *Th*L and the current collector and catalyzes the reduction of O_2 into water. Fig. 4.10 is a schematic diagram of this dual-layer-architecture enzyme electrode, which is called PEDOT-NO_3/*Th*L/PEDOT-PSS.

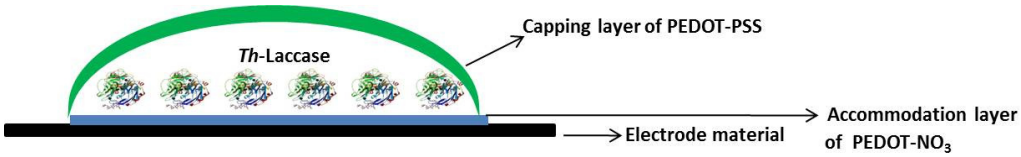

Fig. 4.10. Schematic diagram of the dual-layer-architecture enzyme electrode PEDOT-NO_3/*Th*L/PEDOT-PSS.

Oxygen reduction catalyzed by *Th*L via a DET pathway through conducting polymer PEDOT chains

The unique capability of PEDOT-NO_3/*Th*L/PEDOT-PSS fabricated on a GC electrode (d = 6 mm) to promote DET type catalysis of *Th*L was verified (**Paper III**). As shown in Fig. 4.11b, when a PEDOT-NO_3/*Th*L/PEDOT-PSS enzyme electrode was examined using cyclic voltammetry in the absence of any redox mediator, a distinct shift in the reduction wave caused by the oxygen reduction was observed under aerobic ambient conditions compared to that under anaerobic ambient conditions. In contrast, in the control sample without *Th*L (Fig. 4.11a), no cathodic shift was observed below a potential of 0.2 V *vs*. Ag/AgCl (s), at which point O_2 reduction on the PEDOT film structure is initiated as a bulk electrode reaction without enzymatic catalysis. For the PEDOT-NO_3/*Th*L/PEDOT-PSS enzyme electrode, the catalytic reduction of O_2 is initiated at a potential of around 0.55 V *vs.* Ag/AgCl (s) (0.75 V *vs.* NHE), which is in the vicinity of the redox potential of the T1 Cu of *Th*L (0.78 V *vs.* NHE). Therefore, the participation of *Th*L biocatalysis enables O_2 reduction at a lower overpotential. This is convincing evidence for the role of the T1 Cu site as the primary electron acceptor in the electron transfer process. In Fig. 4.11c, the CA response of the enzyme electrode at a potential of 0.35 V *vs.* Ag/AgCl (s) with varying O_2 concentrations in the electrolyte supports the conclusion that the reduction current is produced by the bioelectrocatalytic reduction of O_2.

The fabrication of such a dual-layer-architecture was optimized on a GC electrode and the parameters investigated included the *Th*L loading and the thickness of both the PEDOT-NO_3 layer and the PEDOT-PSS layer (**Paper III**). For a specific dual-layer-architecture, the catalytic current density has a linear dependence on the *Th*L loading inside the architecture. For a certain quantity of enzyme, the thicknesses of the PEDOT-NO_3 layer and the PEDOT-PSS layer determine the DET promoting capability on the biocatalysis of O_2 reduction. The dual-layer-architecture enzyme electrode PEDOT-NO_3/*Th*L/PEDOT-PSS exhibited fairly good reproducibility and operational stability. Its pH profile has a bell shape, with an optimal pH in the range of 3.0-3.5.

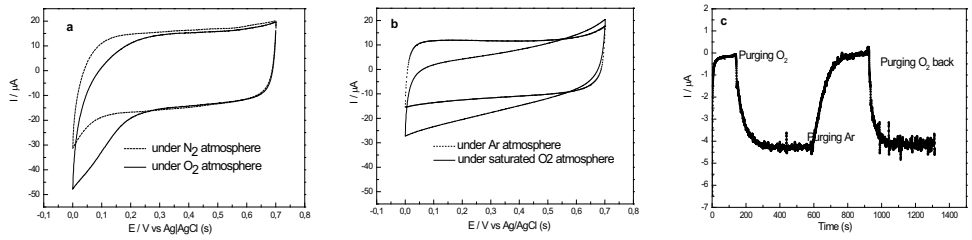

Fig. 4.11. a. CVs of dual-layer-architecture electrode PEDOT-NO_3 (56 mC) /PEDOT-PSS (14 mC) under anaerobic ambient conditions (dashed line) and aerobic ambient conditions (solid line). B. CVs of dual-layer-architecture enzyme electrode PEDOT-NO_3 (56 mC) /*Th*L/PEDOT-PSS (14 mC) under anaerobic ambient conditions (dashed line) and aerobic ambient conditions (solid line). Electrolyte: 50 mM, pH = 4.5 succinate buffer. Scan rate: 5 mV/s. c. CA response (at 0.35 V *vs*. Ag/AgCl (s)) of dual-layer-architecture enzyme electrode PEDOT-NO_3 (56 mC) /*Th*L (1.26 U) /PEDOT-PSS (14 mC), when the electrolyte (50 mM, pH = 4.5 succinate buffer) was purged Ar or O_2: t = 0, Ar saturated solution; t = 135 s, O_2 purging; t = 592 s, Ar purging; t = 919 s, O_2 purging.

ET pathway between *Th*L and the current collector *via* PEDOT chains in the dual-layer-architecture enzyme electrode PEDOT-NO_3/*Th*L/PEDOT-PSS

The DET of *Th*L was not observed when *Th*L was immobilized into the PEDOT-NO_3 film through *in situ* entrapment, as discussed in Section 4.1.2. Moreover, failure to observe DET in both the GC/PEDOT-NO_3/*Th*L/PEDOT-NO_3 and GC/PEDOT-PSS/*Th*L/PEDOT-PSS combinations underlines the critical role of the GC/PEDOT-NO_3/*Th*L/PEDOT-PSS combination in accomplishing DET (Fig. 4.12a). In the case of GC/PEDOT-PSS/*Th*L/PEDOT-PSS, the failure to accomplish DET may be due to the compact and dense micro-structure of PEDOT-PSS, whose grain-like morphology makes it unsuitable for capturing enzyme clusters after the drop-casting of *Th*L and for retaining them from diffusing off during the synthesis of the capping layer. In constrast, the pore structure of PEDOT-NO_3, which is on the order of several tens of nm, provides adequate accommodation to a single *Th*L molecule or enzyme cluster of agglomerated *Th*L molecules since the *Th*L molecule theoretically has a crystalline dimension close to that of *Tv*L (65×55×45 Å) (Piontek et al., 2002). Most striking, there is no DET observed with the combination GC/PEDOT-NO_3/*Th*L/PEDOT-NO_3, which strongly suggests that the PEDOT-PSS capping layer plays a decisive role in promoting the DET in enzyme electrode PEDOT-NO_3/*Th*L/PEDOT-PSS.

A non-ionic surfactant, Tween-20, was added to the succinate buffer to evaluate its effect on the bioelectrocatalytic performance of the dual-layer-architecture enzyme electrode. The catalytic current density decayed dramatically when Tween-20 was present in the electrolyte (Fig. 4.12.b). Increasing the concentration of Tween-20 degraded the electrode performance even further. Based on this observation, it is believed that Tween-20 is adsorbed onto the dual-layer-architecture and perturbs the enzyme electrode by altering its micro-structure. This supports the proposed electron transfer mechanism in the dual-layer-architecture enzyme electrode: the interaction between PSS^- and the hydrophobic substrate-binding pocket close to the T1 Cu is probably responsible for resulting in the favorable location of the conducting polymer chains close to the T1 Cu site. This interaction is also the main driving force for the DET in this system, an explanation similar to that offered by Blandford *et al*. (Blanford et al., 2008) for achieving DET of laccase via an enhanced adsorption method. When PEDOT-PSS film was electrosynthesized to create the capping layer, PEDOT-PSS chains preferably grew preferentially towards the vicinity of the substrate-binding pocket most likely due to the π-π interaction between the aromatic benzene rings of PSS^- and the hydrophobic substrate-binding pocket; thus, the polymer chain is brought close to the T1 Cu site of *Th*L. In this manner, the PEDOT-PSS chain provides an electron transfer pathway from the electrode surface to the T1 Cu site. The electron is transferred through an internal electron transfer mechanism to the T2/T3 cluster (a distance of 12-13 Å), where oxygen is reduced to water. Fig. 4.13 presents a schematic diagram of the dual-layer-architecture enzyme electrode, illustrating the proposed electron transfer pathway.

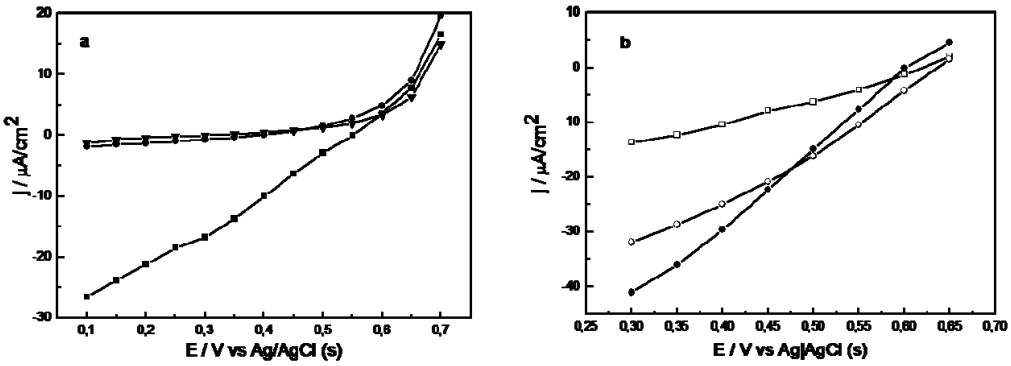

Fig. 4.12. a. *j*-E curves of dual-layer-architecture enzyme electrodes with different combinations of dual layers: PEDOT-NO_3 (56 mC) /*Th*L (1.26 U) /PEDOT-PSS (14 mC) (-■-); PEDOT-PSS (56 mC) /*Th*L (1.26 U) /PEDOT-PSS (14 mC) (-●-); PEDOT-NO_3 (56 mC) /*Th*L (1.26 U) /PEDOT-NO_3 (14 mC) (-▼-). Electrolyte: 50 mM pH = 4.5 succinate buffer; b. *j*-E curves of dual-layer-architecture enzyme electrode PEDOT-NO_3 (28 mC) /*Th*L (1.26 U) /PEDOT-PSS (3.5 mC) in buffer solutions with or without Tween 20: 50 mM, pH = 4.5 succinate buffer (-●-); 50 mM, pH = 4.5 succinate buffer containing 0.5 % Tween 20 (-○-); 50 mM, pH = 4.5 succinate buffer containing 2.5 % Tween 20 (- -)

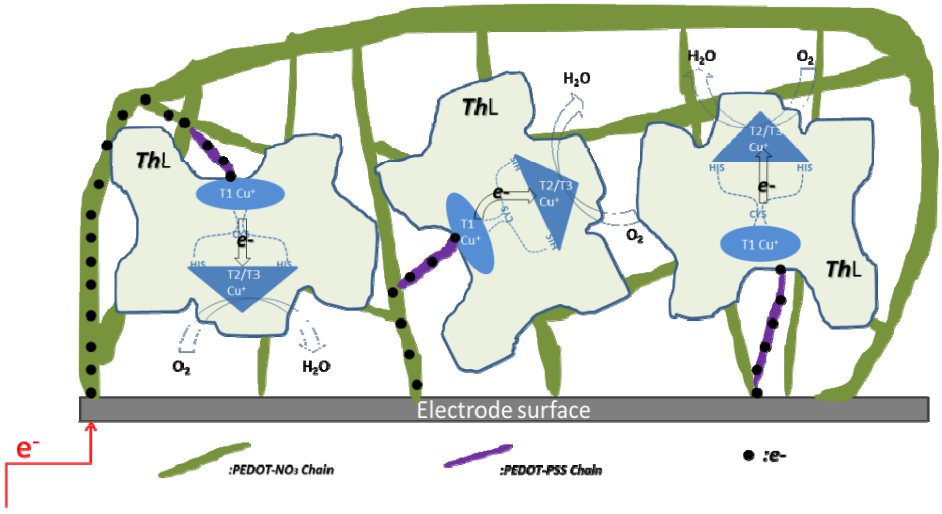

Fig. 4.13. Schematic diagram of the electron transfer pathway in the dual-layer-architecture enzyme electrode PEDOT-NO_3/*Th*L/PEDOT-PSS.

Initial RDE kinetics measurements on the O_2 reduction catalyzed by PEDOT-NO_3/*Th*L/PEDOT-PSS biocathode

Initially, RDE measurements for the PEDOT-NO_3/*Th*L/PEDOT-PSS enzyme electrode were initially conducted as an attempt to understand the kinetics limitations on the biocatalysis of *Th*L for O_2 reduction in the dual-layer-architecture enzyme electrode.

Fig 4.14a shows the *Koutecky-Levich* plots for the RDE measurements of a PEDOT-NO_3/*Th*L/PEDOT-PSS enzyme electrode under varying O_2 concentrations in the buffer electrolyte. The *Koutecky-Levich* plots exhibit good linearity, as the I^{-1} *vs.* $\omega^{-1/2}$ plots in Fig. 4.14b. With increasing of O_2 gradient present in the pH = 4.5 succinate buffer, PEDOT-NO_3/*Th*L/PEDOT-PSS electrode produced larger catalytic reduction currents. However, for each O_2 concentration ranging from that of an air saturated buffer (C_{O2} around 5.6 mg/l) to that of an O_2 saturated buffer (C_{O2} around 26 mg/l), the *I vs.* $\omega^{1/2}$ plot for the PEDOT-NO_3/*Th*L/PEDOT-PSS enzyme electrode deviated from a straight line and tended toward the limit $I = I_K$ as the rotational speed increased to $\omega^{1/2} \rightarrow \infty$. Here, I_K represents the current in the absence of any mass transfer effect, that is, the current that would flow under the kinetics limitations if the mass transfer is efficient enough to maintain the concentration at the electrode surface equal to the bulk value, regardless of the electrode reaction. The curved *I vs.* $\omega^{1/2}$ plots imply that a kinetics limitation is involved in the electron transfer reaction and that the enzymatic catalysis occurring in the PEDOT-NO_3/*Th*L/PEDOT-PSS enzyme electrode has slow kinetics.

The electrobiocatalysis of O_2 reduction in the PEDOT-NO_3/*Th*L/PEDOT enzyme electrode involves the following sequence of kinetics-related steps: (i) electron transfer from the current collector through the conducting polymer chain to the electron acceptor of *Th*L, the T1 Cu^+ site; (ii) intra-molecular electron transfer from the T1 Cu^+ to the T2/T3 Cu^+ cluster; and (iii) reduction of O_2 to H_2O. It remains to be decided which of these steps is the rate-determining step that limits the kinetics of the enzyme reaction.

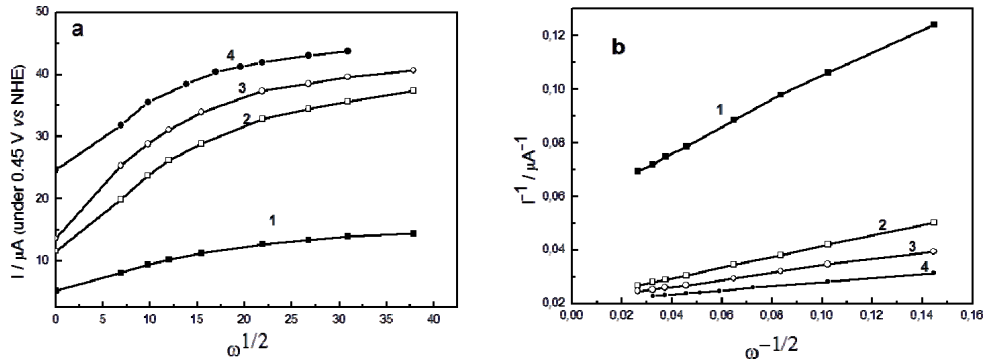

Fig. 4.14. a. RDE chronoamperometric measurements of the enzyme electrode PEDOT-NO_3 (56 mC) /*Th*L (1.26 U) /PEDOT-PSS (14 mC). The current was recorded under the potential of 0.45 V *vs.* NHE in a 50 mM, pH = 4.5 succinate buffer. The O_2 bulk concentration was (1) 5.6 mg/l; (2) 12 mg/l; (3) 18 mg/l; (4) 26 mg/l. b. *Koutecky-Levich* plots for RDE measurements of PEDOT-NO_3 (56 mC) /*Th*L (1.26 U) /PEDOT-PSS (14 mC) in (a).

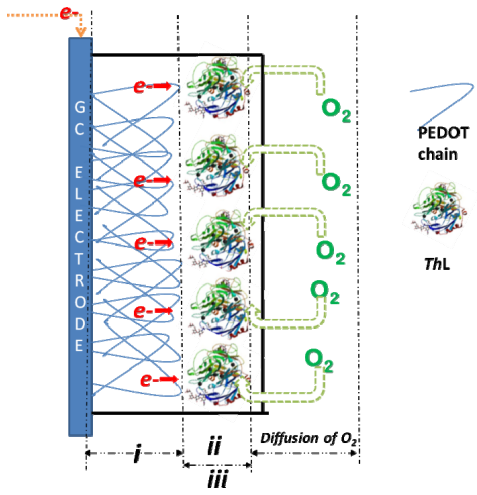

Fig. 4.15. Kinetics-related steps involved in the electrobiocatalysis of the O_2 reduction occurring in the enzyme electrode PEDOT-NO_3/*Th*L/PEDOT-PSS.

4.3 MET type bioanode: 'wiring' *Gc*GDH using Os-polymers on graphite electrodes

A new extracellular redox enzyme, FAD-dependent GDH from *Glomerella cingulata (Gc*GDH) was electrochemically investigated in terms of its ability to catalyze the oxidation of glucose on a spectrographic graphite electrode. Six Os-polymers, whose redox potentials ranged across the broad potential window between +15 and +489 mV *vs*. NHE, were used to 'wire' the *Gc*GDH onto spectrographic graphite electrodes for possible applications in biosensors and BFCs. The *Gc*GDH/Os-polymer modified electrodes were evaluated in a CA mode using FIA. The current response was investigated across a step-wise increasing potential window. Among the six PVI or PVP polymers with $Os^{2+/3+}$ redox centres, polymer *c* ([Os (4,4′-dimethyl-2,2′-bipyridine)$_2$ (PVI)Cl]$^+$) and polymer *d* ([Os (2,2'-bipyridine)$_2$ (PVI)Cl]$^+$) gave the best results for 'wiring' *Gc*GDH to catalyze the oxidation of glucose. In addition, the ratio of *Gc*GDH to Os-polymer in the overall loading of the enzyme electrode significantly affects its ability to catalyze glucose oxidation. The *Gc*GDH:Os-polymer ratio for the solution cast dosage was optimized to achieve a large catalytic current.

Cyclic voltammetry of Os-polymers

The electrochemical behavior of a series of Os-polymers was characterized using cyclic voltammetry. Fig. 4.16 shows typical CVs for the different Os-polymers adsorbed on the surface of a spectrographic graphite electrode in a pH = 7.4, 50 mM phosphate buffer. All Os-polymers displayed a pair of well-defined, chemically reversible redox peaks for the $Os^{2+/3+}$ redox centres in the polymer. Because different ligands coordinate the $Os^{2+/3+}$ redox centres, the formal redox potentials of the redox polymers vary substantially covering the entire potential range from +15 to + 489 mV (*vs*. NHE). The redox potentials of the polymers depend, as expected, on their intrinsic chemistry, as discussed in **Paper IV**.

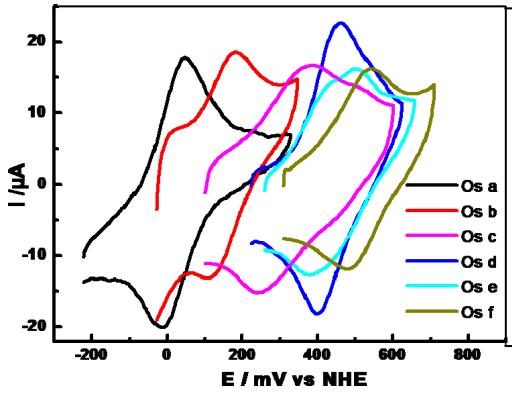

Polymer sequence	Os polymer	$E^{0\prime}$ vs. NHE
Os a	PVP-[Os(N,N′-methylated-2,2′-biimidazole)$_3$]$^{2+/3+}$	15 mV
Os b	[Os(4,4′-dimethoxy-2,2′-bipyridine)$_2$(PVI)Cl]$^+$(1:9)	140 mV
Os c	[Os(4,4′-dimethyl-2,2′-bipyridine)$_2$(PVI)Cl]$^+$(1:9)	309 mV
Os d	[Os(2,2′-bipyridine)$_2$(PVI)Cl]$^+$(1:9)	420 mV
Os e	[Os(4,4′-dimethyl-2,2′-bipyridine)$_2$(PVI)Cl]$^+$(1:11)	444 mV
Os f	[Os(4,4′-dichloro-2,2′-bipyridine)$_2$(PVI)Cl]$^+$(1:9)	489 mV

Fig. 4.16. CVs of *Gc*GDH/Os-polymers on spectrographic graphite electrodes (2 µl of *Gc*GDH, 4 µl of Os redox polymers, and 1 µl of PEGDGE) measured at a scan rate of 10 mV/s in the absence of substrate. Measurements were performed in a pH = 7.4, 50 mM phosphate buffer.

'Wiring' *Gc*GDH using Os-polymers on graphite electrodes

For *Gc*GDH, the redox potential of the FAD cofactor remains undetermined. The current response of the *Gc*GDH/Os-polymer modified electrode was recorded within a step-wise increasing potential window ranging from 65 mV to 790 mV (*vs*. NHE) in a pH = 7.4, 50 mM phosphate buffer containing 5 mM glucose (Fig. 4.17.a). The activation potential for the catalytic oxidation current shifts more positively from polymer *a* to polymer *f*, in line with the shifting direction of the redox potential of the $Os^{2+/3+}$ redox centres in these polymers. As discussed in Section 2.4.3, the reversible potential of a mediated biocatalytic electrode is a mixed potential dominated by the mediator couple. Among the six Os-polymers, polymers *a* and *b* were the least efficient mediators for *Gc*GDH, yielding lower currents. This is likely because the redox potentials of polymers *a* (15 mV *vs*. NHE) and *b* (140 mV *vs*. NHE) are too low with respect to the potential of the FAD cofactor of *Gc*GDH, so the electron transfer step from the FAD cofactor to the Os redox centre is thermodynamically uphill. In contrast, when polymer *c* and polymer *d* were used to 'wire' *Gc*GDH, much higher response currents were obtained from the glucose oxidization, and the steady-state currents were achieved at around 370 mV *vs*. NHE. For polymer *e* and polymer *f*, steady-state catalytic currents were observed at more positive potentials, demonstrating 'wiring' performance intermediate between that of polymer *a*, *b* and that of polymer *c*, *d*. Referring to the 'wiring' performance of the six Os-polymers, it is anticipated that the $E^{o\prime}$ value of the FAD cofactor of *Gc*GDH will be in the vicinity of the redox potentials of $Os^{2+/3+}$ redox centres in polymer *c* and *d*.

The ratio of *Gc*GDH to Os-polymer (*c* or *d*) for the solution cast dosage was optimized to achieve a higher catalytic current for glucose oxidation on the enzyme electrode. The *Gc*GDH/Os *c* modified electrode produced the highest current density: 493 µA/cm^2 for 30 mM glucose. Thus it is applicable as the bioanode for glucose-fueled BFCs. Its desirable features also include insensitivity to O_2 and catalytic efficiency comparable to that of commercial GOx from *Aspergillus niger* (Fig. 4.17.b).

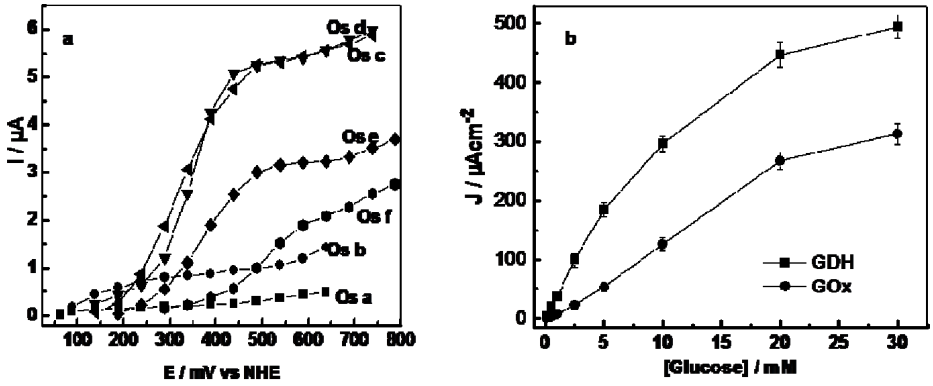

Fig. 4.17. a. Dependence of catalytic current of *Gc*GDH/osmium redox polymer modified graphite electrodes (5 µl of *Gc*GDH, 2 µl of Os redox polymer, and 1 µl of PEGDGE) on the applied potential. The experiments were performed in a pH = 7.4, 50 mM phosphate buffer, with a flow rate of 0.5 ml/min and a glucose concentration of 5 mM. b. Calibration curves (current density) of GOx/Os *c* and *Gc*GDH/Os *c* modified graphite electrodes (1 µl of *Gc*GDH or GOx (equivalent activity unit), 2 µl of Os *c*, and 1 µl of PEGDGE) with glucose as substrate. The experiments were performed in a pH = 7.4, 50 mM phosphate buffer with a flow rate of 0.5 ml/min. The working potential was 465 mV *vs*. NHE.

4.4 DET type, CDH-based bioanode

DET biocatalysis of *Ct*CDH for sugar oxidation on an AuNP-structured electrode

Using glutaraldehyde as a cross-linker, *Ct*CDH was covalently immobilized on a thiol-modified AuNP surface. The immobilization strategy is shown schematically in Fig. 4.18. An AuNP dispersion was cast onto an Au-disk electrode, which resulted in a meso-porous Au structure. The electrode was electrochemically treated to obtain a clean Au surface, followed by the formation of a self-assembled monolayer (SAM) of thiols on it. Covalent binding between the -NH_2 group on *Ct*CDH and the -NH_2 group on the SAM is realized in the reactant drop formed by mixing the CDH enzyme solution and glutaraldehyde on the electrode surface. A more detailed description of the fabrication of the enzyme electrode *Ct*CDH/AuNP/Au is included in **Paper V**.

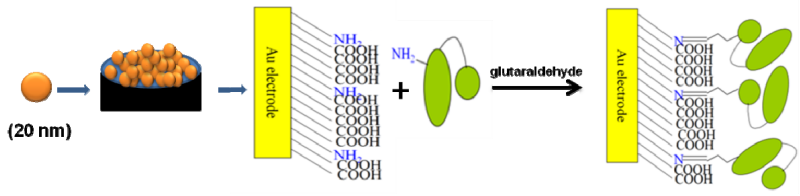

Fig. 4.18. Schematic diagram of the preparation of the enzyme electrode *Ct*CDH/AuNP/Au

The CVs for the bioanode *Ct*CDH/AuNP/Au with or without lactose/glucose in the buffer solution are displayed in Fig. 4.19.A. In the absence of substrate (curve *a*), a pair of well-defined, nearly symmetric redox peaks was observed at $E_{1/2}$ = -122 mV *vs*. Ag/AgCl/KCl (s) (75 mV *vs*. NHE). The CVs in Fig. 4.19.B show that both the peak separation (24 mV) involved in the redox reaction does not vary when the scan rate increases from 2 mV/s to 100

mV/s and that the cathodic/anodic peak current (I_{pc}/or I_{pa}) is linearly proportional to the scan rate (see the insert in Fig. 4.19.C). Those observations indicate that this redox reaction is a fully reversible and surface-confined process. This pair of redox peaks is attributed to the redox oxidation/reduction of the haem (1 e^- process) of *Ct*CDH. In the presence of substrate, an apparent anodic shift was observed in both curve *b* (5 mM lactose) and curve *c* (100 mM glucose) due to the oxidation of the sugars catalyzed by *Ct*CDH via DET. The catalytic current onsets at a potential around -150 mV and reaches a plateau at -50 mV for the oxidation of both lactose and glucose. Based on the integrated redox peak area for the redox response of the haem and the plateau value of the catalytic current produced from lactose oxidation, an active enzyme surface coverage of 0.65 pmol/cm^2 (against electrochemical active surface area) was calculated for *Ct*CDH, and a turnover number of 0.5 s^{-1} was estimated for the *Ct*CDH immobilized on the AuNP surface on lactose oxidation *via* DET.

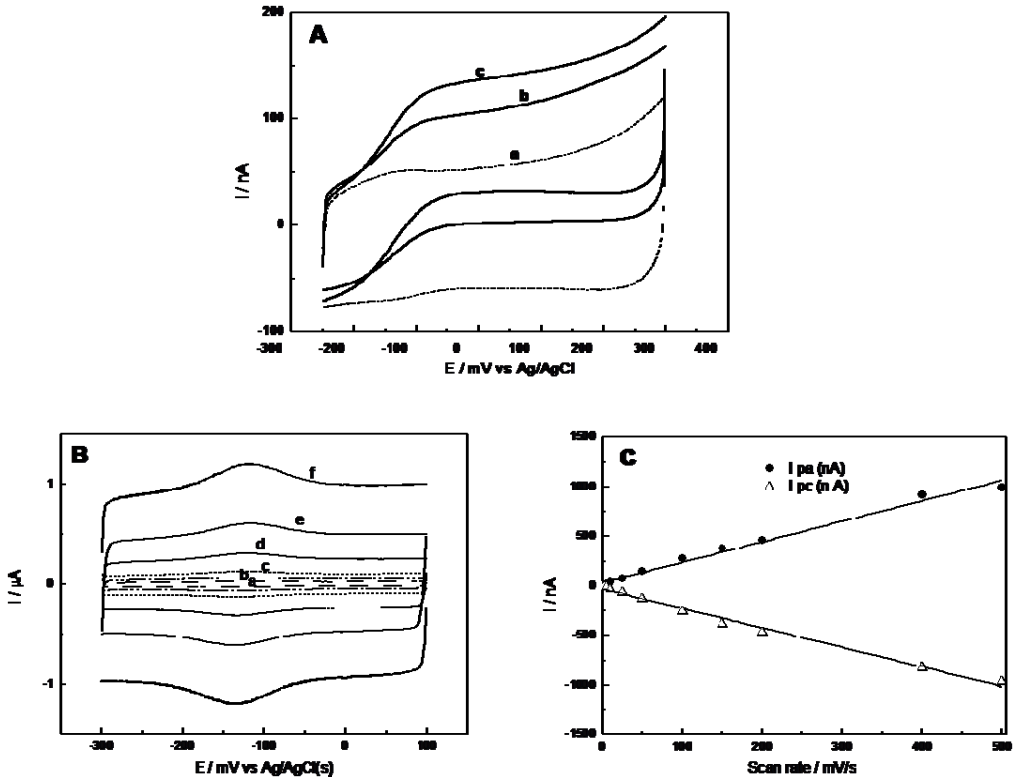

Fig. 4.19. A. CVs for the *Ct*CDH/AuNP/Au bioanode in (a) a pH = 7.4, 50 mM phosphate buffer (solid line); (b) in a pH = 7.4, 50 mM phosphate buffer containing 100 mM glucose (dotted line); and (c) in a pH = 7.4, 50 mM phosphate buffer containing 5 mM lactose (dashed line). The electrolyte was purged with Ar for 15 mins before each measurement. Scan rate: 2 mV/s. B. CVs for the *Ct*CDH/AuNP/Au bioanode in a pH = 7.4, 50 mM phosphate buffer in the potential range from -300 mV to 100 mV. Scan rate: (a) 2 mV/s; (b) 5 mV/s; (c) 10 mV/s; (d) 25 mV/s; (e) 50 mV/s; (f) 100 mV/s. C. Linear plot of the cathodic/anodic peak current (I_{pc}/or I_{pa}) *vs*. scan rate

Enhanced performance of the *Ct*CDH/AuNP/Au bioanode achieved by optimizing the fabrication parameters

The cross-linker concentration in the reactant drop for *Ct*CDH immobilization was varied to investigate the influence of the strength of cross-linking on the activity of the immobilized *Ct*CDH. For a reactant drop with a total volume of 3 µl, 1 µl 2% glutaraldehyde was optimal dosage for 2 µl *Ct*CDH solution. With these dosages, the cast number of the concentrated AuNP was increased from 3 to 20 to enlarge the active surface area available for *Ct*CDH immobilization. The electroactive surface area of the AuNP structure on the Au-disk electrode was estimated from the CVs obtained during electrochemical cleaning (CV scans from -100 mV to 1700 mV) by normalizing the charge under the stripping peak of the gold surface oxide against a specific charge density of 386 µC/cm^2 (Woods, 1980). As the electroactive surface area involved in the bioanode fabrication increased, the catalytic current increased, reaching a plateau when the surface area of the AuNPs was above 12 cm^2 on the 0.02 cm^2 Au-disk electrode (Fig. 4.20). It can be inferred that more *Ct*CDH was immobilized from the reactant drop onto the AuNP surface and exhibited a higher apparent catalytic activity on the oxidation of sugars. However, even more cast can be applied to achieve a larger active surface area, *Ct*CDH perhaps cannot access into the inner structure of the AuNPs in the immobilization due to the diffusion barrier created by the meso-porous structure of the AuNPs packed during solvent evaporation (Murata et al., 2010).

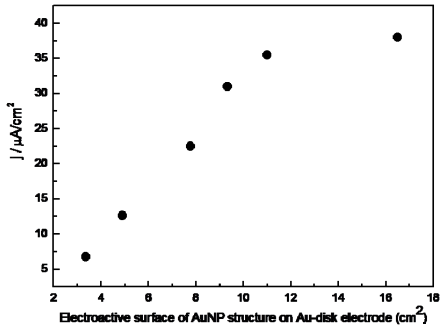

Fig. 4.20. The catalytic current generated by the *Ct*CDH/AuNP/Au bianode *vs*. the electroactive surface area of AuNPs on a 0.02 cm^2 Au-disk electrode

Calibration curves and pH profile of the *Ct*CDH/AuNP/Au bioanode

The calibration curves for the *Ct*CDH/AuNP/Au bioanode on lactose and glucose are displayed in Fig. 4.21.A and B, respectively. The kinetics parameters of the enzymatic reactions, K_m (the Michaelis-Menten constant) and I_{max} (the maximum current response), were calculated using non-linear least squares regression, fitting the calibration curves to the *Michaelis-Menten Equation*. The values of K_m and I_{max} were, for lactose, 0.155±0.024 (mM) and 43.3±1.52 (µA/cm^2), respectively, and, for glucose, 27.5±6.42 (mM) and 31.2±2.3 (µA/cm^2), respectively. The value of I_{max}/K_m, which can be interpreted as the catalytic efficiency, is 250 times lower for glucose oxidation than for lactose oxidation.

The current response of the bioanode *Ct*CDH/AuNP/Au at a potential of 0 mV *vs.* Ag/AgCl/KCl$_{sat}$, was recorded for 5 mM lactose in buffer carriers with different pH. The pH profile is presented in Fig. 4.21.C. The *Ct*CDH on *Ct*CDH/AuNP/Au bioanode was most efficient in terms of high catalytic current response in the neutral pH range (pH 7.0 to 8.5),

which makes *Ct*CDH an attractive biocatalyst for the fabrication of implantable glucose/O_2 BFCs.

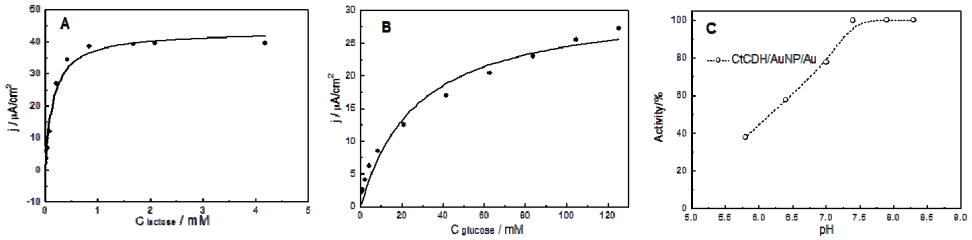

Fig. 4.21. A and B: Calibration curves for the *Ct*CDH/AuNP/Au bioanode in a pH = 7.4, 50 mM phosphate buffer determined by means of FIA for lactose and glucose, respectively; C. pH profile for the *Ct*CDH/AuNP/Au bioanode

4.5 An implantable BFC demonstration unit: AuNP-based, DET type, sugar/O_2 BFC operating in physiological fluids

The bioanode *Ct*CDH/AuNP/Au was coupled with a *Myrothecium verrucaria* bilirubin oxidase *(Mv*BOD)-based, AuNP-structured Au disk electrode as the biocathode to construct a sugar/O_2 BFC. In the *Mv*BOD/AuNP/Au biocathode configuration, *Mv*BOD was immobilized on AuNPs by physical adsorption; the resulting device was able to catalyze the reduction of O_2 into water via DET. The fabrication details are given in **Paper V**. The catalytic current generated by the biocathodes in the air-saturated and quiescent buffer solution showed a clear limitation by O_2 diffusion with a maximal current density of 110 μA/cm^2. The DET type biocatalysis is facilitated for *Ct*CDH and *Mv*BOD in the bioanode and the biocathode, respectively, which makes possible a membrane-less design for a one-compartment BFC (Fig. 4.22). This BFC generates power output when operating in physiological fluids by utilizing the glucose and dissolved O_2 as the fuel and the oxidant at the anode and the cathode, respectively.

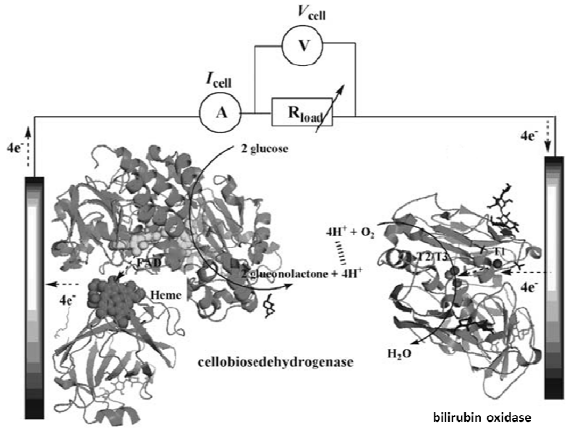

Fig. 4.22. Schematic diagram of the configuration of a one-compartment sugar/O_2 BFC (Coman et al., 2008) (Copyright permission with RSC publishing).

When this BFC operates in a lactose- (5 mM) or glucose- (100 mM) containing phosphate buffer (pH = 7.4), the potential difference between the onsets of biocatalysis at the biocathode

(500 mV *vs*. SCE) and at the bioanode (-180 mV *vs*. SCE) determines the OCV of the BFC, which is 0.68 V for the BFC operating in either a lactose- or a glucose-containing buffer. The anodic catalytic currents are around 1-2 times less than the cathodic ones, which makes the anode the limiting side for overall BFC performance. The maximal power density of 14.9 or 10.3 $\mu W/cm^2$ was achieved at an operating voltage of 0.52 V with 5 mM lactose or 100 mM glucose as the fuel (**Paper V**).

A one-compartment *Ct*CDH/AuNP/Au|*Mv*BOD/AuNP/Au BFC was also evaluated in terms of their operation in complex biological fluids, i.e., human blood and plasma. The glucose concentration in blood from a healthy individual is known to vary from 3.9 mM to 5.6 mM (around 13 % higher in plasma), with variation dependant on the time at which the sample was taken (Lind et al., 1972). The oxygen concentration in air-saturated fluids is around 0.25 mM at room temperature (Truesdale & Downing, 1954). As a reference media for these biological fluids, the BFC performance was evaluated in a pH = 7.4 phosphate buffer containing 5 mM glucose and 150 mM NaCl, which is a simplified mimic of the physiological fluids. Fig. 4.23.A shows the LSV curves for both the bioanode *Ct*CDH/AuNP/Au and the biocathode *Mv*BOD/AuNP/Au in human blood and plasma. The bioanode *Ct*CDH/AuNP/Au displayed almost the same behavior in the blood and plasma as in the reference media in the potential window -0.2 V to 0.16 V (*vs.* SCE). The biocathode *Mv*BOD/AuNP/Au had slightly poorer performance in the blood and plasma than in the reference media: in each case, the potential onset for O_2 reduction shifted more positively, and lower catalytic activity of *Mv*BOD on the reduction of $O_2$was observed. Fig. 4.23.B shows power density plots for the BFC operating in different media. The performance parameters are summarized in Table 4.1. In blood and plasma, the BFC gives power density profiles quite similar to those for the reference physiological buffer. The power generated by the BFC in physiological fluids is well correlated with the value for the physiological buffer, which is to be expected considering that the glucose concentrations are similar.

Another important aspect of the BFC is its operational stability since an implantable BFC is required to have a long lifetime operating under the physiological conditions. The operational stability of the *Ct*CDH/AuNP/Au|*Mv*BOD/AuNP/Au BFC in physiological media was assessed. When the BFC operated in the physiological buffer, a 20% drop in power density was observed during continuous operation for 10 h; in plasma and blood, the BFC had estimated half-lifetimes of about 8 h and 2 h, respectively. It is difficult to predict the exact cause of the deactivation of the BFC in plasma and blood due to the presence of so many different compounds. Physiological fluids contain many different organic and inorganic compounds that can affect the catalytic activity of enzymes. A more detailed discussion of this issue is included in **Paper V**.

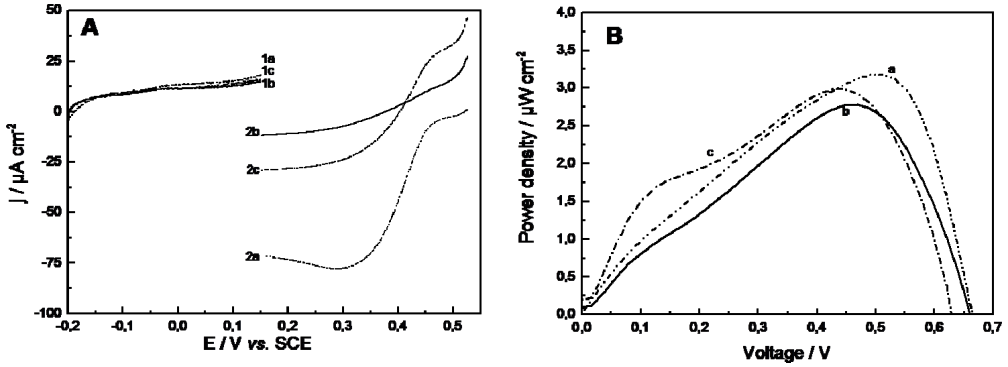

Fig. 4.23. A. LSVs of CDH-modified electrodes (curves 1) and BOD-modified electrodes (curves 2) in (a) a pH = 7.4, 50 mM phosphate buffer containing 5 mM glucose and 150 mM NaCl (dash-dot-dot line); (b) human blood (solid line); (c) plasma (dash-dotted line). Scan rate: 2 mV/s; B. Dependence of power density on operating voltage for the BFC under air-saturated and quiescent conditions. (a) a pH = 7.4, 50 mM phosphate buffer containing 5 mM glucose and 150 mM NaCl (dash-dot-dot line); (b) human blood (solid line); (c) plasma (dash-dotted line). Scan rate: 0.1 mV/s

Table 4.1. Performance parameters for the *Ct*CDH/AuNP/Au|*Mv*BOD/AuNP/Au BFC operating in different media.

media type	OCV of BFC	maximum power-output at operating voltage	operational stability
pH = 7.4, 50 mM phosphate buffer containing 5 mM glucose and 150 mM NaCl	0.664V	3.3 µW/cm^2 at 0.52 V	20% drop in power density during continuous operation for 10 h
blood	0.660 V	2.8 µW/cm^2 at 0.45 V	Half-lifetime: 2 h
plasma	0.63V	3 µW/cm^2 at 0.47 V	Half-lifetime: 8 h

5. Conclusions

The counter ions for the conducting polymer PEDOT, significantly affect the structural features and morphology of the polymer film resulting from the electropolymerization process. The morphological variations of PEDOT films caused by the counterion species offer unique possibilities for tailoring the fine structure of the host matrix for the purpose of maximizing enzyme loading in the enzyme electrode design. Electropolymerization in a pulse mode is beneficial for obtaining evenly distributed PEDOT deposition through a 3D macro-porous structure in the supporting material.

In situ entrapment of enzyme as a dopant during the electropolymerization of PEDOT was successfully used to immobilize *Th*L as the catalyst in the construction of an O_2-consuming cathode. RVC foam is a good template material for PEDOT deposition. Biocathodes manufactured by *in situ* entrapment of *Th*L in PEDOT film polymerized on RVC foam, produced a high current density, reaching 1 mA/cm^3 at 0.45 V in the presence of the mediator of $ABTS^{2-}$.

MWCNT functions as the DET promoter for the biocatalysis of *Th*L. A DET type catalytic current density of 40 μA/cm^2 is generated by the *Th*L-MWCNTs/ Nafion/GC biocathode. DET type biocatalysis is also accomplished for *Th*L by immobilizing *Th*L into a fine-tuned dual-layer-architecture of PEDOT films. This enzyme electrode PEDOT-NO_3/*Th*L/PEDOT-PSS is able to promote DET between *Th*L and the GC electrode. The reduction of oxygen in water was catalyzed with the T1 Cu^+ site as the primary electron acceptor. The enzyme electrode PEDOT-NO_3/*Th*L/PEDOT-PSS works in an optimal pH range of 3.0-3.5. It is proposed that the π-π interaction between the PSS^- and the hydrophobic substrate-binding pocket in the vicinity of the T1 Cu site causes the PEDOT-PSS chain to grow close to the T1 Cu site, thus facilitating the DET of *Th*L within this particular architecture. The initial RDE kinetics measurements imply that a kinetics limitation is involved in the electron transfer steps. The enzyme reaction occurring in the PEDOT-NO_3/*Th*L/PEDOT-PSS enzyme electrode has a slow kinetics.

For the new, FAD-dependent *Gc*GDH, among the six PVI or PVP polymers with $Os^{3+/}Os^{2+}$ redox centres, whose redox potentials range between +15 and +489 mV *vs*. NHE, polymer *c* ([Os (4,4′-dimethyl-2,2′-bipyridine)$_2$ (PVI)Cl]$^+$ and polymer *d* ([Os (2,2'-bipyridine)$_2$ (PVI)Cl]$^{+2/+}$) gave the best results for wiring *Gc*GDH to catalyze the oxidation of glucose. The highest current density of 493 μA·cm^2 for 30 mM glucose was produced with a *Gc*GDH/Os *c* modified electrode with an optimized *Gc*GDH:Os *c* ratio. With the desirable features of insensitivity to O_2 and catalytic efficiency comparable to that of commercial GOx from *Aspergillus niger*, it can be used as an anodic biocatalyst for glucose-fueled BFC applications.

CDHs are interesting alternative enzymes for catalyzing sugar oxidation, with the great feature of being insensitive to O_2. The DET type biocatalysis of *Ct*CDH for lactose (and glucose) oxidation was accomplished on an AuNP-structured electrode. The haem site in *Ct*CDH functions as enzyme itself 'built-in' mediator to communicate the electron transfer from the FAD site to the AuNP surface. The redox potential of the haem site in *Ct*CDH was determined to be $E_{1/2}^{'}$ = *-122 mV vs.* Ag/AgCl/KCl(s) (75 mV *vs*. NHE). The *Ct*CDH/AuNP/Au bioanode generates the maximum current response for lactose: I_{max} = 43.3±1.52 (μA/cm^2); for glucose: I_{max} = 31.2±2.3 (μA/cm^2). The *Ct*CDH on *Ct*CDH/AuNP/Au bioanode was most efficient in terms of high catalytic current response in the neutral pH range (pH 7.0 to 8.5), which makes *Ct*CDH a suitable biocatalyst for the fabrication of implantable glucose/O_2 BFCs. A *Ct*CDH enzyme electrode as the bioanode was

coupled with a BOD enzyme electrode as the biocathode to fabricate a one-compartment implantable BFC. The following characteristics of the mediator-, separator-, and membrane-less BFC were obtained: in a pH = 7.4 phosphate buffer containing 5 mM lactose, an OCV of 0.68 V and a maximum power density of 15 $\mu W/cm^2$ at an operating cell voltage of 0.52 V; in human blood, an OCV of 0.65 V and a maximum power density of 3 $\mu W/cm^2$ at an operating cell voltage of 0.45 V.

References

Armstrong, F. A. (2002). Protein film voltammetry: revealing the mechanisms of biological oxidation and reduction. *Russ. J. Electrochem.*, 38, 49-62.

Bak, T. (1967). Studies on glucose dehydrogenase of *Aspergillus oryzae*. II. Purification and physical and chemical properties. *Biochim. Biophys.Acta*, 139, 277-293.

Bard, A. J., & Faulkner, L. R. (2001). *Electrochemical methods: fundamentals and applications (second edition).* Hoboken, New Jersey: John Wiley & Sons, Inc.

Bartlett, P., & Whitaker, R. (1987). Strategies for the development of amperometric enzyme electrodes. *Biosensors*, 3, 359-379.

Bartlett, P., & Birkin, P. (1993). The application of conducting polymer in biosensors. *Synth. Met.*, 61, 15-21.

Barlett, P., Birkin, P., & Wang, J. (1998). An enzyme switch employing direct electrochemical communication between horseradish peroxidase and a poly (aniline) film. *Anal. Chem.*, 70, 3685-3694.

Bartlett, P. (2008). Bioenergetics and biological electron transport. In P. Bartlett, *Bioelectrochemistry. Fundamentals, Experimental Techniques and Applications* (pp. 1-38). Chichester, England: John Wiley & Sons Ltd.

Barton, S. C., Kim, H.-H., Binyamin, G., Zhang, Y., & Heller, A. (2001). The 'wired' laccase cathode: high current density electroreduction of O_2 to water at +0.7 V (NHE) at pH 5. *J. Am. Chem. Soc.*, 123, 5802-5803.

Barton, S. C., Gallaway, J., & Atanassov, P. (2004). Enzymatic biofuel cells for implantable and microscale devices. *Chem. Rev.*, 104, 4867-4886.

Biellli, P., & Calabrese, L. (2002). Structure to function relationships in ceruloplasmin: a 'moonlight' protein. *Cell. Mol. Life Sci.*, 59, 1413-1427.

BioMedNano. (n.d.). Retrieved May 24th, 2011, from Welcome to the BioMedNano Project Website: http://www.nuigalway.ie/biomednano/

Blanford, C. F., Foster, C. E., Heath, R. S., & Armstrong, F. A. (2008). Efficient electrocatalytic oxygen reduction by the 'blue' copper oxidases, laccase, direct attached to chemically modified carbons. *Faraday Discuss.*, 140, 319-335.

Bond, A. M. (1994). Chemical and electrochemical approaches to the investigations of redox reactions of simple electron transfer metaloproteins. *Inorg. Chim. Acta*, 226, 293-340.

Bullen, R., Arnot, T., Lakeman, J., & Walsh, F. (2006). Biofuel cells and their development. *Biosens. Bioelectron.*, 21, 2015-2045.

Butler, J., & Hugh, M. (n.d.). Retrieved from www.teknologiateollisuus.fi/file/4792/2009-FC-Expo-Report2.pdf.html.

Cai, C., & Chen, J. (2004). Direct electron transfer of glucose oxidase promoted by CNTs. *Anal. Biochem.*, 332, 75-83.

Cinquin, P., Gondran, C., Giroud, F., Mazabrard, S., Pellissier, A., Boucher, F., Alcaraz, J.-P., Gorgy, K., Lenouvel, F., Mathé, S., Porcu, P., & Cosnier, S. (2010). A glucose biofuel cell implanted in rats. *PLoS ONE*, 5, e10467.

Clark Jr., L. C., & Lyons, C. (1962). Electrode systems for continuous monitoring in cardiovascular surgery. *Ann. NY Acad.*, 102, 29-45.

Claus, H. (2004). Laccases: structure, reactions and distributions. *Micron*, 35, 93-96.

Coman, V., Vaz-Domínguez, C., Ludwig, R., Harreither, W., Haltrich, D., De lacey, A. L., Ruzgas, T., Gorton, L., & Shleev, S. (2008). A membrane-, mediator-, cofactor-less glucose/oxygen biofuel cell. *Phys. Chem. Chem. Phys.*, 10, 6093-6096.

Coman, V. (2009). Heterogeneous electron transfer studies with ligninolytic redox enzymes and living bacteria. Ph.D thesis, Lund University, Sweden.

Cooney, M. J., Svoboda, V., Lau, C., Martin, G., & Minteer, S. D. (2008). Enzyme catalysed biofuel cells. *Energy Environ. Sci.*, 1, 320-337.

Cooney, M., Lau, C., Windmeisser, M., Liaw, B., Klotzbach, T., & Minteer, S. (2008). Design of chitosan gel pore structure: towards enzyme catalyzed flow-through electrodes. *J. Mater. Chem.*, 18, 667-674.

Cosnier, S. (2008). Immobilization of biomolecules by electropolymerized film. In R. Marks, *Handbook of biosensors and biochips.* Chichester, UK: John Wiley & Sons Ltd.

Cracknell, J. A., Vincent, K. A., & Armstrong, F. A. (2008). Enzymes as working or inspirational electrocatalysts for fuel cells and electrolysis. *Chem. Rev.*, 108, 2439-2461.

Cracknell, J. A., Vincent, K. A., Ludwig, M., Lenz, O., Friedrich, B., & Armstrong, F. A. (2008). Enzymatic oxidation of H_2 in atmospheric O_2: the electrochemistry of energy generation from trace H_2 by aerobic microorganisms. *J. Am. Chem. Soc.*, 130, 424-425.

Cui, X., Li, C. M., Zang, J., Zhou, Q., Gan, Y., Bao, H., Guo, J., Lee, V. S., & Moochhala S. M. (2007). Biocatalytic generation of Ppy-enzyme-CNT nanocomposite: from nework assembly to film growth. *J. Phys.Chem. C.*, 111, 2025-2031.

Dagys, M., Haberska, K., Shleev, S., Arnebrant, T., & Kulys, J. (2010). Laccase-gold nanoparticle assisted bioelectrocatalytic reduction of oxygen. *Electrochem. Commun.*, 12, 933-935.

Daniel, M.-C., & Astruc, D. (2004). Gold nanoparticles: assebly, supermolecular chemistry, quantum-size-related properties, and applications toward biology, catalysis, and nanotechnology. *Chem. Rev.*, 104, 293-346.

Datsyuk, V., Kalyva, M., Papagelis, K., Parthenios, J., Tasis, D., Siokou, A., Kallitsis, I., & Galiotis, C. (2008). Chemical oxidation of multiwalled CNTs. *Carbon*, 46, 833-840.

Davis, G., Hill, H. O., Aston, W. J., Higgins, I. J., & Turner, A. P. (1983). Bioelectrochemical fuel cell and sensor based on a quinoprotein, alcohol dehydrogenase. *Enzyme Microb. Technol.*, 5, 383-388.

Degani, Y., & Heller, A. (1988). Direct electrical communication between chemically modified enzymes and metal electrodes. 2. Methods for bonding electron-transfer relays to glucose oxidase and d-amino-acid oxidase. *J. Amer. Chem. Soc.*, 111, 2615-20.

Degani, Y., & Heller, A. (1989). Electrical communication between redox centres of glucose oxidase and electrodes via electrostatically and covalently bound redox polymers. *J. Amer. Chem. Soc.*, 111, 2357-2358.

Deng, L., Liu, Y., Yang, G., Shang, L., Wen, D., Wang, F., Xu, Z., & Dong, S. (2007). Molecular "wiring" glucose oxidase in supermolecular architecture. *Biomacromolecules*, 8, 2063-2071.

Dillon, A. C. (2010). CNTs for photoconversion and electrical energy storage. *Chem. Rev.*, 110, 6856-6872.

dos Santos, L., Climent, V., Blandford, C. F., & Armstrong, F. A. (2010). Mechanistic studies of the 'blue' Cu enzyme, bilirubin oxidase, as a highly efficient electrocatalyst for the oxygen reduction reaction. *Phys. Chem. Chem. Phys.*, 12, 13962-13974.

Eddowes, M. J., & Hill, H. A. (1977). Novel method for the investigation of the electrochemistry of metalloproteins: cytochrome c. *J. Chem. Soc. Chem. Commun.*, 771-772.

Fei, J., Song, H.-K., & Palmore, G. (2007). A biopolymer composite that catalyzes the reduction of oxygen to water. *Chem. Mater.*, 19, 1565-1570.

Flexer, V., Brun, N., Backov, R., & Mano, N. (2010). Designing highly efficient enzyme-based carbonaceous foams electrodes for biofuel cells. *Energy Environ. Sci.*, 3, 1302-1306.

Fruk, L., Kuo, C.-H., Torres, E., & Niemeyer, C. (2009). Aopenzyme reconstitution as a chemical tool for structural enzymology and biotechnology. *Angwe. Chem. Int. Ed.*, 48, 1550-1574.

Gao, F., Viry, L., Maugey, M., Poulin, P., & Mano, N. (2010). Engineering hybrid nanotube wires for high-power biofuel cells. *Nature Commun.*, 1:2, 1-7.

Gary, H. B., & Winkler, J. R. (1996). Electron transfer in proteins. *Ann. Rev. Biochem.*, 65, 537-561.

Gerard, M., Chaubey, A., & Malhotra, B. (2002). Application of conducting polymer to biosensors. *Biosens. Bioelectron.*, 17, 345-359.

Gorton, L., Jönsson-Pettersson, G., Csöregi, E., Johansson, K., Dominguez, E., & Marko-Varga, G. (1992). Amperometic biosensors based on an apparent direct electron transfer between electrodes and immobilized peroxidase. Plenary lecture. *Analyst*, 117, 1235-1241.

Gorton, L., Lindgren, A., Larsson, T., Munteanu, F. D., Ruzgas, T., & Gazaryan, I. (1999). Direct electron transfer between haem-containing enzymes and electrodes as basis for third generation biosensors. *Anal. Chim. Acta*, 400, 91-108.

Gray, H. B., & Winkler, J. R. (2001). Electron transfer in metalloproteins. In Balzani, V., *Electron transfer in chemistry* (pp. 3-23). Weinheim, Germany: Wiley-VCH.

Groenendaal, L., Jonas, F., Freitag, D., Pielartzik, H., & Reynolds, J. R. (2000). Poly(3,4-ethylenedioxythiophene) and its derivatives: past, present and future. *Adv. Mater.*, 12, 481-494.

Guo, L.-H., & Hill, H. (1991). Direct electrochemistry of proteins and enzymes. *Adv. Inorg. Chem.*, 36, 341-375.

Gupta, G., Rajendran, V., & Atanassov, P. (2004). Bioelectrocatalysis of oxgen reduction by laccase on gold electrodes. *Electroanalysis*, 16, 1182-1185.

Habrioux, A., Napporn, T., Servat, K., & Kokoh, K. (2010). Electrochemical characterization of adsorbed bilirubin oxidase on Vulcan XC 72 R for the biocathode preparation in a glucose/O_2 biofuel cell. *Electrochim. Acta* , 55, 7701-7705.

Harrieither, W., Coman, V., Ludwig, R., Haltrich, D., & Gorton, L. (2007). Investigation of graphite electrodes modified with cellobiose dehydrogenase from the ascomycete *myriococcum thermophilum*. *Electroanlysis*, 19, 172-180.

Harreither, W., Sygmund, C., Augustin, M., Narciso, M., Rabinovich, M., Gorton, L., Haltrich, D., & Ludwig, R. (2011). Catalytic properties and classification of cellobiose dehydrogenases from ascomycetes. *Appl. Environ. Microbiol.*, 77, 1804-15.

Hauge, J. (1964). Glucose dehydrogenase of Bacterium anitratum: an enzyme with a novel prosthetic group. *J. Bio. Chem.*, 239, 3630-3639.

Hecht, H. J., & Schomburg, D. (1993). The 3D structure of glucose oxidase from *Aspergillus niger.* Implications for the use of GOD as a biosensor enzyme. *Biosens. Bioelectron.*, 8, 197-203.

Heller, A. (1990). Electrical wiring of redox enzymes. *Acc. Chem. Res.*, 23, 123-134.

Heller, A. (2003). Redox hydrogel-based electrochemical biosensors. In Cooper, J. M. & Cass, A. E., *Biosensors- a practical approach (2nd edition)* (pp. 1-18). Oxford: Oxford University Press.

Henriksson, G., Johansson, G., & Pettersson, G. (2000). A critical review of cellobiose dehydrogenases. *J. Biotechnol.*, 78, 93-113.

Hill, H., Guo, L., & McLendon, G. (1996). In Scott, R., & Mauk, A., *Cytochrome c: a multidisciplinary approach.* (pp. 317-333). University Science Books: Sausalito.

Hodak, J., Etchenique, R., Calvo, E. J., Singhal, K., & Bartlett, P. (1997). Layer-by-layer self assembly of glucose oxidase with a poly (allylamine)ferrocene redox mediator. *Langmuir*, 13, 2708-2716.

Ivnitski, D., Branch, B., Atanassov, P., & Apblett, C. (2006). Glucose oxidase anode for biofuel cell based on direct electron transfer. *Electrochem. Commun.*, 8, 1204-1210.

Ivnitski, D., Atanassov, P., & Apblett, C. (2007). Direct bioelectrocatalysis of PQQ-dependent glucose dehydrogenase. *Electroanalysis*, 19, 1562-1568.

Ivnitski, D., Artyushkova, K., Rincon, R., Atanassov, P., Luckarift, H., & Johnson, G. (2008). Entrapment of enzymes and CNTs in biologically synthesized silica: glucose oxidase-catalyzed direct electron transfer. *Small*, 4, 357-364.

Jia, N., Liu, L., Zhou, Q., Wang, L., Yan, M., & Jiang, Z. (2005). Bioelectrochemistry and enzymatic activity of glucose oxidase immobilized onto the bamboo-shaped CN_x nanotubes. *Electrochim. Acta*, 51, 611-618.

Jia, W., Schwamborn, S., Jin, C., Xia, W., Muhler, M., Schuhmann, W., Stoica, L. (2010). Towards a high potential biocathode based on direct bioelectrochemistry between horseradish peroxidase and hierarchically structured CNTs. *Phys. Chem. Chem. Phys.*, 12, 10088-10092.

Jones, A. K., Sillery, E., Albracht, S. J., & Armstrong, F. A. (2002). Direct comparsion of the electrocatalytic oxidation of hydrogen by an enzyme and a platinum catalyst. *Chem. Commun.*, 866-867.

Kamitaka, Y., Tsujimura, S., Setoyama, N., Kajino, T., & Kano, K. (2007). Frutose/dioxygen biofuel cell based on direct electron transfer-type bioelectrocatalysis. *Phys.Chem. Chem. Phys.*, 9, 1793-1801.

Kang, C., Shin, H., & Heller, A. (2006). On the stability of the 'wired' bilirubin oxidase oxygen cathode in serum. *Bioelectrochemistry*, 68, 22-26.

Kang, X., Wang, J., Wu, H., Askay, I., Liu, J., & Lin, Y. (2009). Glucose oxidse-graphene-chitosan modified electrode for diret electrochemistry and glucose sensing. *Biosens. Bioelectron.*, 25, 901-905.

Karamsshev, A. V., Shleev, S. V., Koroleva, O. V., Yaropolov, A. I., & Sakharov, I. Y. (2003). Laccase-catalyzed synthesis of conducting polymers. *Enzyme Microb. Technol.*, 33, 556-564.

Karousis, N., & Tagmatarchis, N. (2010). Current progress on the chemical modification of CNTs. *Chem. Rev.*, 110, 5366-5397.

Karyakin, A. A., Morozov, S. V., Karyakina, E. E., Zorin, N. A., Perelygin, V. V., & Cosnier, S. (2005). Hydrogenase electrodes for fuel cells. *Biochem. Soc. Trans.*, 33, 73-75.

Katz, E., Riklin, A., Heleg-Shabtai, V., Willner, I., & Buckmann, A. (1999). Glucose oxidase electrode via reconstitution of the aop-enzyme: tailoring of novel glucose bisoesnsors. *Anal. Chim. Acta*, 385, 45-85.

Katz, E., Willner, I., & Kotlyar, A. B. (1999). A non-compartmentalized glucose/O_2 biofuel cell by bioengineered electrode surfaces. *J. Electroanal.Chem.*, 479, 64-68.

Katz, E., & Willner, I. (2004). Biimolecule-functionalized CNTs: applications in nanobioelectronics. *Chemphyschem*, 5, 1184-2104.

Kim, J., Jia, H., & Wang, P. (2006). Challenges in biocatalysis for enzyme-based biofuel cells. *Biotech. Adv.*, 24, 296-308.

Klonowska, A., Gaudin, C., Fournel, A., Asso, M., Le Petit, J., Giorgi, M., & Tron, T. (2002). Characterization of a low potential laccase from basidiomycete C30. *Eur. J. Biochem.*, 269, 6119-6125.

Klotzbach, T., Watt, M., Ansari, Y., & Minteer, S. (2006). Effects of hydrophobic modification of chitosan and Nafion on transport properties, ion-exchange capacities, and enzyme immobilization. *J. Membr. Sci.*, 282, 276-283.

Klotzbach, T., Watt, M., Ansari, Y., & Minteer, S. (2008). Improving the microenvironment for enzyme immobilization at electrodes by hydrophobically modifying chitosan and Nafion polymers. *J. Membr. Sci.*, 311, 81-88.

Kosman, D. J. (2010). Multicopper oxidases: a workshop on copper coordination chemistry, electron transfer, and metallophysiology. *J. Bio. Inorg. Chem.*, 15, 15-28.

Kros, A., van Hövell, S., Sommerdijk, N., & Nolte, R. (2001). Poly(3,4-ethylenedioxythiophene)-based glucose biosensors. *Adv. Mater.*, 13, 1555-1557.

Kuznetsov, A. M., & Ulstrup, J. (1999). Elements of charge transfer in biological systems. In Kuznetsov, A. M., & Ulstrup, J., *Electron transfer in chemistry and biology. An introduction to the theroy* (pp. 301-322). Chichester, England: John Wiley & Sons Ltd.

Langen, R., Chang, I. J., Germannas, J. P., Richards, J. H., Winkler, J. R., & Gary, H. B. (1995). Electron tunneling in proteins: coupling through a beta strand. *Science*, 402, 47-52.

Larsson, T., Lindgren, A., Ruzgas, T., Lindquist, S.-E., & Gorton, L. (2000). Bioelectrochemical characterisation of cellobiose dehydrogenase modifed graphite electrodes:ionic strength and pH dependences. *J. Electroana. Chem.*, 482, 1-10.

Lee, D., Lee, J., Kim, J., Na, H. B., Kim, J., Kim, B., Shin, C.-H., Dohnalkova, A., Grate, J. W., Hyeon, T., & Kim, H.-S. (2005). Simple fabrication of a highly sensitive and fast glucose biosensor using enzyme immobilization in mesocellular carbon foam. *Adv. Mater.*, 17, 2828-2833.

Lee, J., Kim, J., & Hyeon, T. (2006). Recent process in the synthesis of porous carbon materials. *Adv. Mater.*, 18, 2073-2094.

Leger, C., & Bertrand, P. (2008). Direct electrochemistry of redox enzymes as a tool for mechanistic studies. *Chem. Rev.*, 108, 2379-2438.

Lim, J., Cirigliano, N., Wang, J., & Dunn, B. (2007). Direct electron transfer in nanostructured sol-gel electrodes containing bilirubin oxidase. *Phys. Chem. Chem. Phys.*, 9, 1890-1814.

Lind, T., de Groot, H., Brown, G., & Cheyne, G. (1972). Observations on blood glucose and insulin determinations. *Brit. Med. J.*, 3, 320-322.

Lindgren, A., Larsson, T., Ruzgas, T., & Gorton, L. (2000). Direct electron transfer between the haem of celllobiose hydrogenase and thiol modifed gold electrodes. *J. Electroanal. Chem.*, 494, 105-113.

Lindgren, A., Ruzgas, T., & Gorton, L. (2001). Direct electron transfer of native and modified peroxidase. *Curr. Top. Anal. Chem.*, 2, 71-94.

Liu, Y., Wang, M., Zhao, F., Xu, Z., & Dong, S. (2005). The direct electron transfer of glucose oxidase and glucose biosensor based on CNTs/chitosan matrix. *Biosens. Bioelectron.*, 21, 984-988.

Ludwig, R., Harreither, W., Tasca, F., & Gorton, L. (2010). Cellobiose dehydrogenase: a versatile catalyst for electrochemical applications. *Chemphyschem*, 11, 2674-2697.

Malhotra, B., Chaubey, A., & Singh, S. (2006). Prospects of conducting polymers in biosensors. *Anal. Chim. Acta*, 578, 59-74.

Mano, N., Mao, F., & Heller, A. (2002). A minature biofuel cell operating in a physiological buffer. *J. Am. Chem. Soc.*, 124, 12962-12963.

Mano, N., Mao, F., & Heller, A. (2003). Characterisitic of a minature compartment-less glucose-O_2 biofuel cell and its operation in a living plant. *J. Am. Chem. Soc.*,125, 6588-6594.

Mano, N., Mao, F., Shin, W., Chen, W., & Heller, A. (2003). A minature biofuel cell operating at 0.78 V. *Chem. Commun.*, 518-519.

Mano, N., Mao, F., & Heller, A. (2005). On the parameters affecting the characteristics of the 'wired' glucose oxidase anode. *J. Electroanal. Chem.*, 574, 347-357.

Mano, N., Soukharev, V., & Heller, A. (2006). A laccase-wiring redox hydrogel for efficient catalysis of O2 electroreduction. *J. Phy. Chem. B*, 110, 11180-11187.

Marcus, R. A. (1956). Electrostatic free energy and other properties of states having noequilibrium polarization. *J. Chem. Phys.*, 24, 979-989.

Marcus, R. A. (1956). On the theory of ixudatuib-reduction reactions involving electron transfer. *J. Chem. Phys.*, 24, 979-989.

Marcus, R. A. (1964). Chemical and electrochemical electron-transfer reactions. *Annu. Rev. Phys. Chem.*, 15, 155-196.

Marcus, R. A. (1965). On the theroy of electron-transfer reactions.VI. Unified treatment for homogeneous and electrode reactions. *J. Phys. Chem.*, 43, 679-701.

Marcus, R. A., & Sutin, N. (1985). Electron transfers in chemsitry and biology. *Biochim. Biophys. Acta*, 811, 265-322.

Marcus, R. A. (1993). Electron-transfer reactions in chemistry-theory and experiment (Nobel Lecture). *Angew. Chem. Int. Ed.*, 32, 1111-1112.

Martin Hallberg, B., Henriksson, G., Peterrsson, G., & Divne, C. (2002). Crystal structure of the flavoprotein domain of the extracellular flavocytochrome cellobiose dehydrogenase. *J. Mol. Biol.*, 315, 421-434.

Matsushita, K., Ohno, Y., Shinagawa, E., Adachi, O., & Ameyama, M. (1980). Membrane-bound D-Glucose dehydrogenase from *Pseudomonas sp.*: solubilization, purification and characterization. *Agric. Biol. Chem.*, 44, 1505-1512.

Michaelis, L., & Menten, M. L. (1913). Die Kinetik der Invertinwirkung. *Biochem. Z.*, 49, 333-369.

Minteer, S. D., Liaw, B. Y., & Cooney, M. J. (2007). Enzyme-based biofuel cells. *Curre. Opin. Biotechnol.*, 18, 1-7.

Miyake, T., Oike, M., Yoshino, S., Yatagawa, Y., Haneda, K., Kaji, H., & Nishizawa, M. (2009). Biofuel cell anode: NAD^+/glucose dehydrogenase-coimmoilized ketjenblack electrode. *Chem. Phys. Lett.*, 480, 123-126.

Mizutani, K., Toyada, M., Sagara, K., Takahashi, N., Sato, A., Kamitaka, Y., Tsujimura, S., Nakanishi, Y., Sugiura T., Yamaguchi, S., Kano, K., & Mikami, B. (2010). X-ray analysis of bilirubin oxidase from *Myrothecium verrucaria* at 2.3 Å resolution using a twinned crystal. *Acta Cryst.* F66, 765-770.

Moore, C. M., Akers, N. L., Hill, A. D., Johnson, Z. C., & Minteer, S. D. (2004). Improving the environment for immobilized dehydrogenase enzymes by modifying nafion with tetraalkylammonium bromides. *Biomacromolecules*, 5, 1241-1247.

Moser, C. C., Keske, J. M., Warncke, K., Farid, R. S., & Dutton, P. L. (1992). Nature of biological electron transfer. *Nature*, 355, 796-802.

Murata, K., Kajiya, K., Nakamura, N., & Ohno, H. (2009). Direct electrochemistry of bilirubin-oxidase on three-dimensional gold nanoparticle electordes and its application in a biofuel cell. *Energy Enviorn. Sci.*, 2, 1280-1285.

Murata, K., Kajiya, K., Nukaga, M., Suga, Y., Watanabe, T., Nakamura, N., & Ohno H. (2010). A simple fabrication method for three-dimensional gold nanoparticle electrodes and their application to the study of the direct electrochemistry of Cytochrome c. *Electroanalysis*, 22, 185-190.

Nakabayashi, Y., & Yoshikawa, H. (2000). Amperometric biosensors for sensing of hydrogen peroxide based on electron transfer between horseradish peroxidase and ferrocene as a mediator. *Anal. Sci.*, 16, 609-613.

Nakamura, K., & Go, N. (2005). Function and molecular evolution of multicopper blue proteins. *Cell. Mol. Life. Sci.*, 62, 2050-2066.

Nogala, W., Celebanska, A., Szot, K., Wittstock, G., & Opallo, M. (2010). Bioelectrocatalytic mediatorless dioxygen reduction at carbon ceramic electrodes modified with bilirubin oxidase. *Electrochim. Acta*, 55, 5719-5729.

Nogala, W., Rozniecka, E., & Opallo, M. (2006). Immobilization of ABTS-laccase system in silica based electrode for bioelectrocatalytic reduction of dioxygen. *Electrochem. Commun.*, 8, 1850-1854.

Odaci, D., Telefoncu, A., & Timur, S. (2008). Pyranose oxidase bisensor based on carbon nanotube (CNT)-modified carbon paste electrodes. *Sens. Actuators B*, 159-165.

Page, C. C., Moser, C. C., & Dutton, P. L. (2003). Mechanism for electron transfer within and between protein. *Curr. Opin. Chem. Biol.*, 7, 551-556.

Patolsky, F., Weizmann, Y., & Willner, I. (2004). Long-range electical contacting of redox enzymes by SWCNT connectors. *Angew. Chem. Int. Ed.*, 43, 2113-2117.

Piontek, K., Antorini, M., & Choinowski, T. (2002). Crystal structure of a laccase from the fungus Trametes versicolor at 1.9-A resolution containing a full complement of coppers. *J. Biol. Chem.*, 277, 37663-37669.

Pita, M., Shleev, S., Ruzgas, T., Fernandez, V., Yaropolov, A., & Gorton, L. (2008). Direct heterogeneous electron transfer reactions of fungal laccases at bare and thiol modified gold electrodes. *Electrochem. Commun.*, 8, 747-753.

Polyakov, K. M., Fedorova, T. V., Stepanova, E. V., Cherkashin, E. A., Kurzeev, S. A., Strokopytov, B. V., Lamzin, V. S., & Koroleva, O. V. (2009). Structure of native laccase from *Trametes hirsuta* at 1.8 Å resolution. *Acta Cryst.*, D65, 611-617.

Potter, M. C. (1912). Electrical effects accompanying the deposition of organic compounds. *Pro. R. Soc. London Ser. B,*, 260-276.

Rahman, M. A., Noh, H.-B., & Shim, Y.-B. (2008). Direct electrochemistry of laccase immobilized on Au nanoparticles encapsulated-dendrimer bonded conducting polymer: application for a catechin sensor. *Anal. Chem.*, 80, 8020-8027.

Ramasamy, R., Luckarift, H., Ivnitski, D., Atanassov, P., & Johnson, G. (2010). High electrocatalytic activity of tethered multicopper oxidase-carbon nanotube conjugates. *Chem. Comm.*, 46, 6045-6047.

Ramirez, P., Mano, N., Andreu, R., Ruzgas, T., Heller, A., Gorton, L., & Shleev, S. (2008). Direct electron transfer from graphite and functionalized gold electrodes to T1 and T2/T3 copper centres of bilirubin oxidase. *Biochim. Biophys. Acta*, 1777, 1364-1369.

Reinhammar, B. (1972). Oxidation-reduction potentials of the electron acceptors in laccases and stellacyanin. *Biochim. Biophys. Acta*, 275, 245-259.

Reinhammar, B., & Vänngård, T. (1971). Electron-accepting sites in *Rhusvernicifera* laccase as studied by anaerobic oxidation-reduction titration. *Eur. J. Biochem.*, 18, 463-468.

Riklin, A., Katz, E., Willner, I., Stocker, A., & Buckmann, A. (1995). Improving enzyme-electrode contacts by redox modification of cofactos. *Nature*, 376, 672-675.

Rodgers, C. J., Blanford, C. F., Giddens, S. R., Skamnioti, P., Armstrong, F. A., & Gurr, S. J. (2009). Designer laccases: a vogue for high-potential fungal enzymes. *Trends Biotechnol.*, 28, 63-72.

Rubenwolf, S., Strohmeier, O., Kloke, A., Kerzenmacher, S., Zengerle, R., & Stetten, F. (2010). carbon electrodes for direct electront transfer type laccase cathodes investigated by current-density-cathode potential behavior. *Biosens. Bioelectron.*, 26, 841-845.

Rusling, J. F., & Zhang, Z. (2003). Designing functional biomolecurlar films on electrode. In Rusling, J. F., *Biomolecular films* (pp. 1-64). N. Y.: Marcel Dekker.

Ruzgas, T., Gsöregi, E., Emneus, J., Gorton, L., & Marko-Varga, G. (1996). Peroxidase-modified electrodes: fundatmentals and application. *Anal. Chim. Acta*, 330, 123-138.

Ruzicka, J., & Hansen, E. H. (1975). Flow injection analyses. I. New concept of fast continuous flow analysis. *Anal. Chim. Acta.*, 78, 145-157.

Ruzicka, J., & Hansen, E. H. (1988). *Flow injection analysis, 2nd ed.* Hoboken, New Jersey: John Wiley & Sons, Inc.

Ruzicka, J., & Hansen, E. H. (2008). Retro-review of flow-injection analysis. *TrAC, Trends Anal. Chem.*, 27, 390-393.

Ruzicka, J., & Stewart, J. W. (1975). Flow injection analysis. II. Ultrafast determination of phosphorus in plant materials by continuous flow spectrophotometry. *Anal. Chim. Acta.*, 79, 79-91.

Sakai, H., Nakagawa, T., Mita, H., Kumita, H., & Tokita, Y. (2010). Evolution of Sony's biofuel cell. *217th ECS meeting*, Vancouver.

Sardar, R., Funston, A. M., Mulvaney, P., & Murray, R. W. (2009). Gold nanoparticles: past, present, and future. *Langmuir*, 25 (24), 13840-13851.

Sarma, A., Vatsyayan, P., Goswami, P., & Minteer, S. (2009). Recent advances in materiall science for developing enzyme electrodes. *Biosens. Bioelectron.*, 24, 2313-2322.

Schneider, P., Caspersen, M., Mondorf, K., Halkier, T., Skov, L. K., Østergaard, P. R., Brown, K. M., Brown, S. H., & Xu, F. (1999). Characterisation of a Coprinus cinereus laccase. *Enzyme Microb. Tech.*, 25, 502-508.

Schumann, W., Zimmermann, H., Habermuller, K., & Laurinavicius, V. (2000). Electron-transfer pathways between redox enzymes and electrode surface: Reagentless biosensors based on thiol-monolayer-bound and polypyrrole-entrapped enzymes. *Faraday Discuss.*, 116, 245-255.

Serra, B., Reviejo, A., & Pingarron, J. (2003). Composite multienzyme amperometric biosensors for an improved detection of phenolic compounds. *Electroanalysis*, 15, 1737-1744.

Shimizu, A., Kwon, J.-H., Sasaki, T., Satoh, T., Sakurai, N., Sakurai, T., Yamaguchi, S., & Samejima, T. (1999). *Myrothecium verrucaria* bilirubin oxidase and its mutants for potential copper ligands. *Biochemistry*, 38, 3034-3042.

Shleev, S., Christenson, A., Serezhenkov, V., Burbaev, D., Yaropolov, A., Gorton, L., & Ruzgas, T., (2004). Electrochemical redox transformations of T1 and T2 copper sites in native *Trametes hirsuta* laccase at gold electrode. *Biochem. J.*, 385, 745-754.

Shleev, S., Jarosz-Wilkolazka, A., Khalunina, A., Morozova, O., Yaropolov, A., Ruzgas, T., & Gorton, L. (2005). Direct electron transfer reactions of laccases from different origins on carbon electrodes. *Bioelectrochemistry*, 67, 115-124.

Shleev, S., Tkac, J., Christenson, A., Ruzgas, T., Yaropolov, A. I., Whittaker, W., Gorton L. (2005). Direct electron transfer between copper-containing proteins and electrodes. *Biosens. Bioelectron.*, 20, 2517-2554.

Shleev, S., Pita, M., Yaropolov, A. I., Ruzgas, T., & Gorton, L. (2006). Direct heterogeneous electron transfer reactions of *Trametes hirsuta* laccase at bare and thiol-modified gold electrodes. *Electroanalysis*, 18, 1901-1908.

Simon, E., Halliwell, C., Toh, C., Cass, A., & Bartlett, P. (2002). Immobilisation of enzymes on poly (aniline)-poly (anion) composite films: preparation of bioanodes for biofuel cell applications. *Bioelectrochemsitry*, 55, 13-15.

Smolander, M., Vaari, A., Tuurala, S., Valkiainen, M., Koivula, A., Keskinen, J., Kaukoniemi, O.-V., Uotila, J., & Bergelin, M. (2010). Biofuel cell based on printed bioelectrocatalytic layers. *217th ECS meeting,* Vancouver.

Sode, K., Tsugawa, W., Yamazaki, T., Watanabe, M., Ogasawara, N., & Tanaka, M. (1996). A novel thermostable glucose dehydrogenase varying temperature properties by altering its quaternary structures. *Enzyme Microb. Technol.*, 19, 82-85.

Solomon, E. I., Sundaram, U. M., & Machonkin, T. E. (1996). Multicopper oxidases and oxygenases. *Chem. Rev.*,7, 2563-2605.

Song, H., & Palmore, G. (2005). Conductive polypprrole via enzyme catalysis. *J. Phys. Chem. B*, 109, 19278-19287.

Sony Globe. (2011, 02 16). Retrieved from Sony Globe-Technology-Bio Battery: http://www.sony.net/SonyInfo/technology/technology/thaem/bio_01.html

Stoica, L., Dimcheva, N., Haltrich, D., Ruzgas, T., & Gorton, L. (2005). Electrochemical investigation of cellobiose dehydrogenase from new fungal sources on Au electrodes. *Biosens. Bioelectron.*, 20, 2010-2018.

Stoica, L., Ruzgas, T., Ludwig, R., Haltrich, D., & Gorton, L. (2006). Direct electron transfer-a favorite electron route for cellobiose dehydrogenase (CDH) from *Trametes villosa*. Comparsion with CDH from *Phanerochaete chrysosporium*. *Langmuir*, 22, 10801-10806.

Stracha, T., & Read, A. P. (1999). *Human molecular genetics. 2nd edition.* New York: Wiley-Liss: Bios Scientific Publishers.

Streltsov, A. V., Morozova, O. V., Arkharova, N. A., Klechkovskaya, V. V., Staroverova, I. N., Shumakovich, G. P., & Yaropolov, A. I. (2009). Sythesis and characterization of conducting polyaniline prepared by laccase-catalyzed method in sodium dodecylbenzenesulfonate micellar solutions. *J. Appl. Polym. Sci.*, 114, 928-934.

Tanne, C., Göbel, G., & Lisdat, F. (2010). Development of a (PQQ)-GDH-anode based on MWCNT-modified gold and its application in a glucose/O_2-biofuel cell. *Biosens. Bioelectron.*, 26, 530-535.

Tarasevich, M. R., Yaropolov, A. I., Bogdanovskaya, V. A., & Varfolomeev, S. D. (1979). Electrocatalysis of a cathodic oxygen reduction by laccase. *Bioelectrochem. Bioenerg.*, 6, 393-403.

Tasca, F., Gorton, L., Harreither, W., Haltrich, D., Ludwig, R., & Nöll, G. (2008). Direct electron transfer at cellobiose dehydrogenase modified anodes for biofuel cells. *J. Phys. Chem. C.*, 112, 9956-9961.

Tasca, F., Gorton, L., Harreither, W., Haltrich, D., Ludwig, R., & Nöll, G. (2009). Comparision of diect and mediated electron transfer for cellobiose hydrogenase from *Phanerochaete sordida*. *Anal. Chem.*, 81, 2797-2798.

Tasca, F., Gorton, L., Kujawa, M., Patel, I., Harreither, W., Peterbauer, C. K., Lundwig, R., & Nöll, G. (2010). Increasing the coulombic efficiency of glucose biofuel cell anodes by combination of redox enzymes. *Biosens. Bioelectron.*, 25, 1710-1716.

Taube, H., Myers, H., & Rich, R. (1953). Observation of the mechanism of electron transfer in solution. *J.Am. Chem. Soc.*, 75, 4118-4119.

Tchoul, M. N., Ford, W. T., Lolli, G., Resasco, D. E., & Arepalli, S. (2007). Effect of mild nitric acid oxidation on dispersability, size and structure of single-wallled CNTs. *Chem. Mater.*, 19, 5765-5772.

Tel-Vered, R., & Willner, I. (2010). Bis-aniline-crosslinked enzyme-metal nanoparticle composites on electrode for bioelectronics applications. *Isr. J. Chem.*, 50, 321-332.

Tessema, M., Csöregi, E., Ruzgas, T., Kenausis, G., Solomon, T., & Gorton, L. (1997). Oligosaccharide dehydrogenase-modified graphite electrodes for the amperometric determination of sugars in a flow injection system. *Anal. Chem.*, 69, 4039-4044.

The Nobel Prize in Chemistry 2000. (2000). Retrieved March 25th, 2011, from Nobelprize.org: http://nobelprize.org/nobel_prizes/chemistry/laureates/2000/.

Thompson, B., Winther-Jensen, O., Vongsvivut, J., Winther-Jensen, B., & MacFarlane, D. (2010). Conducting polymer enzyme alloys:electromaterials exhibiting direct electron transfer. *Macromol. Rapid. Commun.*, 31, 1293-1297.

Thorum, M. S., Anderson, C. A., Hatch, J. J., Campbell, A. S., Marshall, N. M., Zimmerman, S. C., Lu Y., & Gewirth, A. A. (2010). Direct, electrocatalytic oxygen reduction by laccase on anthracene-2-methanethiol-modified gold. *J. Phys. Chem. Lett.*, 1, 2251-2254.

Trashin, S., Haltrich, D., Ludwig, R., Gorton, L., & Karyakin, A. (2009). Improvement of direct bioelectrocatalysis by cellobiose dehydrogenase on screen printed graphite electrodes using polyaniline modification. *Bioelectrochemistry*, 76, 87-92.

Truesdale, G., & Downing, A. (1954). Solubility of oxygen in water. *Nature*, 173, 1236.

Tsujimura, S., Tatsumi, H., Ogawa, J., Shimizu, S., Kano, K., & Ikeda, T. (2000). Bioelectrocatalytic reduction of dioxygen to water at neatral pH using bilirubin oxidase as an enzyme and 2,2'-azinobis (3-ethylbenzothiazolin-6-sulfonate) as an electron transfer mediator. *J. Electroanal.Chem.*, 496, 69-75.

Tsujimura, S., Kojima, S., Kano, K., Ikeda, T., Sato, M., Sanada, H., & Omura, H. (2006). Novel FAD-dependent glucose dehydrogenase for a dioxygen-insensitive glucose biosensor. *Biosci. Biotechnol. Biochem.*, 70, 654-659.

Vidal, J.-C., Garcia-Ruiz, E., & Castillo, J.-R. (2003). Recent advances in electropolymerized conducting polymers in amperometric biosensors. *Microchim. Acta*, 143, 93-111.

Vincent, K. A., Cracknell, J. A., Clark, J. R., Ludwig, M., Lenz, O., Friedrich, B., & Armstrong, F. A. (2006). Electricity from low-level H_2 in still air-an ultimate test for an oxygen tolerant hydrogenase. *Chem. Commun.*, 48, 5033-5035.

Wang, J. (2005). Carbon-nanotube based electrochemical biosensors: a review. *Electroanalysis*, 17, 7-14.

Wang, J. (2008). Electrochemical glucose biosensors. *Chem. Rev.*, 108, 814-825.

Wen, D., Liu, Y., Yang, G., & Dong, S. (2007). Electrochemistry of glucose oxidase immobilized on the carbon nanotube wrapped by polyelectrolyte. *Electrochim. Acta*, 52, 5312-5317.

Willner, B., Katz, E., & Willner, I. (2006). Electrical contacting of redox proteins by nanotechnological means. *Curr. Opin. Biotechnol.*, 17, 589-596.

Willner, I., Heleg-Shabtai, V., Blonder, R., Katz, E., Tao, G., Bückmann, A. F., Heller, A. (1996). Electrical wiring of glucose oxidase by reconstitution of FAD modified monolayers assembled onto Au electrodes. *J. Am. Chem. Soc.*, 118, 10321-10322.

Willner, I., & Katz, E. (2000). Integration of layered redox protein and conductive supports for bioelectronic application. *Angew. Chem. Int. Ed.*, 39, 1180-1218.

Willner, I., Yan, Y.-M., Willner, B., & Tel-Vered, R. (2009). Integrated enzyme-based biofuel cells-a review. *Fuel cells*, 9, 7-24.

Wilson, G. S., & Hu, Y. (2000). Enzyme-based biosensors for in vivo measurments. *Chem. Rev.*, 100, 2693-2704.

Wohlfahrt, G., Witt, S., Hendle, J., Schomburg, D., Kalisz, H., & Hecht, H.-J. (1999). 1.8 and 1.9 Å resolution structures of the *Penicillium amagasakiens*e and *Aspergillus niger* glucose oxidases as a basis for modelling substrate complexes. *Acta Cryst.*, D55, 969-977.

Woods, R. (1980). In Bard, A., *Electroanalytical chemistry: a series of advances.* New York: Marcel Dekker.

Wu, X., Zhao, F., Varcoe, J., Thumser, A., Avignone-Rossa, C., & Slade, R. (2009). Direct electront transfer of glucose oxidase immobilized in an ionic liquid reconstituted cellulose-carbon nanotube matrix. *Bioelectrochemistry*, 77, 64-68.

Xiao, Y., Patolsky, F., Katz, E., Hainfeld, J., & Willner, I. (2003). 'Plugging into enzymes': nanowiring of redox enzymes by a gold nanoparticle. *Science*, 299,1877-1881.

Xu, F., Shin, W., Brown, S. H., Wahleithner, J., Sundaram, U., & Solomon, E. I. (1996). A study of a series of recombinant fungal laccases and bilirubin oxidases that exhibit significant differences in redox potential, substrate specificity and stability. *Biochim. Biophys. Acta*, 1292, 303-311.

Yahiro, A. T., Lee, S. M., & Kimble, D. O. (1964). Bioelectrochemistry I. enzyme utilizing bio-fuel cell studies. *Biochim. Biophys. Acta*, 88, 375-383.

Yamada, J., & Matsuda, H. (1973). Limiting diffusion currents in hydrodynamic voltammetry. III. Wall jet electrodes. *J. Electroanal. Chem. Interfacial Electrochem.*, 44, 189-198.

Yaropolov, A. I., Malovik, V., Varfolomeev, S. D., & Berezin, I. V. (1979). Electroreduction of hydrogen peroxide on an electrode with immobilized peroxidase. *Dokl. Akad. Nauk.*, SSSR 249, 1399-1401.

Yaropolov, A. I., Skorobogat'ko, O. V., Vartanov, S. S., & Varfolomeyev, S. D. (1994). Laccase. Properties, catalytic mechanism, and applicability. *Appl. Biochem. Biotechnol.*, 49, 257-280.

Yeh, P., & Kuwana, T. (1977). Reversible electrode reaction of *cytochrome c*. *Chem. Lett.*, 1145-1148.

Zafar, M. N., Tasca, F., Boland, S., Kujawa, M., Patel, I., Peterbauer, C. K., Leech, D., & Gorton, L. (2010). Wiring of pyranose dehydrogenase with Os-polymers of different rodox potential. *Bioelectrochemistry*, 80, 38-42.

Zamocky, R., Ludwig, R., Peterbauer, C., Hallberg, B., Divne, C., Nicholls, P., & Haltrich, D. (2006). Cellobiose hydrogenase-a flavochytochrome from wood-degrading, phytopathogenic and saprotropic fungi. *Curr. Protein Pept. Sci.*, 7, 255-280.

Zawisza, I., Rogalski, J., & Opallo, M. (2006). Electrocatalytic reduction of dioxygen by redox mediator and laccase immobilized in silica thin film. *J. Electroanal. Chem.*, 588, 244-252.

Zayats, M., Katz, E., & Willner, I. (2002). Electrical contacting of flavoenzymes and NAD $(P)^{+}$-dependent enzymes by reconstitution and affinity interactions on phenylboronic acid monolayers associated with Au-Electrodes. *J. Am. Chem. Soc.*, 124, 14724-14735.

Zayats, M., Katz, E., Baron, R., & Willner, I. (2005). Reconstitution of aop-glucose dehydrogenase on pyroloquinoline quinone-functionalized Au nanoparticles yiels an electrically contacted biocatalyst. *J. Am. Chem. Soc* , 127, 12400-12406.

Zayats, M., Willner, B., & Willner, I. (2008). Design of amperometric biosensors and biofuel cells by the reconstitution of electrically contacted enzyme electrodes. *Electroanalysis*, 6, 583-601.

Zhang, Q., Wu, S., Zhang, L., Lu, J., Verproot, F., Liu, Y., Xing, Z., Li, J., & Song, X. M. (2011). Fabrication of polymeric ionic liquid/graphene nanocomposite for glucose oxidase immobilization and direct electrochemistry. *Biosens. Bioelectron.*, 26, 2632-2637.

Zhao, S., Zhang, K., Bai, Y., Yang, W., & Sun, C. (2006). Glucose oxidse/colloidal gold nanoparticles immobilized in Nafion film on glassy carbon electrode: direct electron transfer and electrocatalysis. *Bioelectrochemistry*, 69, 158-163.

Zheng, W., Li, Q., Su, L., Yan, Y., Zhang, J., & Mao, L. (2006). Direct electrochemistry of multi-copper oxidases at CNTs noncovalently functionalized with cellulose derivatives. *Electroanalysis*, 18, 587-594.

Zheng, W., Zhou, H., Zheng, Y., & Wang, N. (2008). A comparatively study on electrochemistry of laccase at two kinds of CNTs and its application for biofuel cell. *Chem. Phys. Lett.*, 457, 381-385.

Zheng, W., Zhao, H., Zhang, J., Zhou, H., Xu, X., Zheng, Y., Wang, Y., Cheng, Y., & Jang, B. (2010). A glucose/O_2 biofuel cell based on nanographene platelet-modified electrodes. *Electrochem. Commun.*, 12, 869-871.

Zhou, Y., Yang, H., & Chen, H.-Y. (2008). Direct electrochemistry and reagentless biosensing of glucose oxidase immobilized on chitosan wrapped single-walled CNTs. *Talanta*, 76, 419-423.

Zimmermann, H., Lindgren, A., Schuhmann, W., & Gorton, L. (2000). Anisotropic orientation of horseradish peroxidase by reconstitution on a thiol-modified gold electrode. *Chem. Eur. J.*, 6, 592-599.

RECENT REPORTS FROM THE COMBUSTION AND MATERIALS CHEMISTRY GROUP OF THE ÅBO AKADEMI PROCESS CHEMISTRY CENTRE:

04-01	Jatta Partanen	Chemistry of HCl and Limestone in Fluidised Bed Combustion
04-02	Nici Bergroth	Char Bed Processes in a Kraft Recovery Boiler - A CFD Based Study
04-03	Veikko Niiniskorpi	Development of Phases and Structures during Pelletizing of Kiruna Magnetite Ore
04-04	Nikolai DeMartini	Conversion Kinetics for Smelt Anions: Cyanate and Sulfide
05-01	Edgardo Coda Zabetta, Mikko Hupa	Gas-Born Carbon Particles Generated by Combustion: A Review on the Formation And Relevance
05-02	Jukka Konttinen, Rainer Backman, Mikko Hupa, Antero Moilanen, Esa Kurkela	Trace Element Behaviour in the Fluidized Bed Gasification of Solid Recovered Fuels –a Thermodynamic Study
05-03	Edgardo Coda Zabetta, Clifford Ekholm, Mikko Hupa, Tommi Paanu, Mika Laurén, Seppo Niemi	TEKES FINE-BioPM "Dieselmoottorin nanohiukkaspäästöt biopohjaisia öljyjä poltettaessa" (Nanoparticles from Diesel Engines Operated with Bio-Derived Oils) -Project Report
05-04	Vesna Barišić	Morphology and Composition of Bed-Material Particles from Combustion of Biomass Fuels and Wastes in CFB Boilers
06-01	Edgardo Coda Zabetta	Gas-Phase Detailed Chemistry Kinetic Mechanism "ÅA". A Mechanism for Simulating Biomass Conversion Including Methanol and Nitrogen Pollutants -Validation, Verification and Parametric Tests
06-02	Mischa Theis	Interaction of Biomass Fly Ashes with Different Fouling Tendencies
06-03	Michal Glazer	TGA-Investigation of KCl-Kaolinite Interaction
07-01	Vesna Barišić	Catalytic Reactions of N2O and NO over Bed Materials from Multi-fuel Circulating Fluidized Bed Combustion
07-02	Andrius Gudzinskas Johan Lindholm Patrik Yrjas	Sulphation of Solid KCl
07-03	Daniel Lindberg	Thermochemistry and Melting Properties of Alkali Salt Mixtures in Black Liquor Conversion Processes
07-04	Linda Fröberg	Factors Affecting Raw Glaze Properties
07-05	Tor Laurén	Methods and Instruments for Characterizing Deposit Buildup on Heat Exchangers in Combustion Plants

RECENT REPORTS FROM THE COMBUSTION AND MATERIALS CHEMISTRY GROUP OF THE ÅBO AKADEMI PROCESS CHEMISTRY CENTRE:

08-01	Erik Vedel	Predicting the Properties of Bioactive Glasses
08-02	Tarja Talonen	Chemical Equilibria of Heavy Metals in Waste Incineration -Comparison of Thermodynamic Databases-
08-03	Micaela Westén-Karlsson	Assessment of a Laboratory Method for Studying High Temperature Corrosion Caused by Alkali Salts
08-04	Zhang Di	*In vitro* Characterization of Bioactive Glass
08-05	Maria Zevenhoven, Mikko Hupa	The Environmental Impact and Cost Efficiency of Combustible Waste Utilisation - The Potential and Difficulties of Ongoing Technology Developments-
08-06	Johan Werkelin	Ash-forming Elements and their Chemical Forms in Woody Biomass Fuels
08-07	Hanna Arstila	Crystallization Characteristics of Bioactive Glasses
10-01	Markus Engblom	Modelling and Field Observations of Char Bed Processes in Black Liquor Recovery Boilers
11-01	Leena Varila *et al.*	Fyrtio år oorganisk kemi vid Åbo Akademi
11-02	Johan Lindholm	On Experimental Techniques for Testing Flame Retardants in Polymers
11-03	Minna Piispanen	Characterization of Functional Coatings on Ceramic Surfaces
11-04	Sonja Enestam	Corrosivity of hot flue gases in the fluidized bed combustion of recovered waste wood

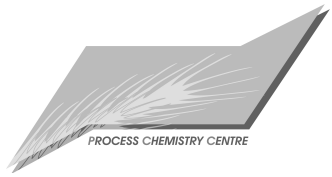

ISSN 159-8205
ISBN 978-952-12-2703-5 (hard copy)
ISBN 978-952-12-2704-2 (pdf)
Painosalama Oy
Åbo, Finland, 2012